Computational Modelling of Immune Interaction and Epidermal Homeostasis in Psoriasis

Dinika Paramalingam

School of Computing

Newcastle University

A thesis submitted for the degree of

Doctor of Philosophy

August 2024

Acknowledgement

I would like to express my deepest gratitude for the people who have contributed and supported me throughout my time doing this research.

Firstly, my supervisors, Dr. Paolo Zuliani and Prof. Nick J. Reynolds, for their time and effort in giving me valuable advice, continued support and guidance throughout my PhD journey. This journey has helped me gain more knowledge and insights to computational modelling and its application to medicine.

My colleagues and friends in ICOS for the everyday conversations and encouragement. Dr. Bowen Li, for the many discussions and ideas on modelling with NUFEB. Dr. Fedor Shmarov, for the discussions on our psoriasis models and how we could incorporate ideas from each other's work. Yiming Huang, Dr. Xue Chen, Dr. Nishant Sinha, Jack Jennings, and Lewis Grozinger for all the nights we stayed in the office working, supper and night outs, and keeping positive especially after the COVID lockdown ended.

ICOS and PGR admins, Andrew Lawson, Hannah Hoare, Catherine McAndrew and Emma Thompson for always being prompt in resolving any issues and answering questions. Also, for helping with the paperwork whenever booking to travel.

My husband, Jacky Cheung, for the encouragement, support and patience throughout the process. My family, for the emotional and physical support for the many and constantly changing decisions I make in life - from changing my profession and moving to another country to doing a PhD.

Abstract

Psoriasis is an incurable chronic inflammatory skin disease characterised by immune cytokine-stimulated epidermal hyperproliferation. This results in the skin becoming red with scaly plaques that can appear anywhere on the body, decreasing the quality of life for patients. Previous modelling studies of psoriatic skin have been limited to 2D models and lacked cell-cell interactions. I have developed a 3D agent-based model of epidermal cell dynamics to gain insights into how immune cytokine stimuli induces hyperproliferation in psoriasis to better understand disease formation and structural changes.

The model takes into account the main cell types - stem, transit-amplifying (TA), differentiated and T cells with the growth and division of stem and TA cells governed by extracellular calcium, endogenous growth factors and immune cytokines in line with known experimental data. Each cell has a set of attributes (growth rate, division probability, position, etc) whose values are governed by processes such as monod-based cellular growth model, probability-based division based on calcium and cytokine concentration and various forces to form the epidermal layers. Different scenarios can be simulated including delineating how psoriasis developed in response to immune stimuli concentration and duration and changing the rate of division of proliferative cells to capture how it changes from normal to diseased state.

The model has 2 steady states, healthy (non-lesional) and psoriatic (lesional) skin. Transition from healthy to psoriatic state is triggered by a temporary cytokine stimulus which causes hyperproliferation to occur, a hallmark of psoriasis. This results in the deepening of rete ridges and thickening of the epidermal structure. The model has been validated against population ratios of stem, TA, differentiated, and T cells, cell cycle and turnover times *in vivo*. The model simulates the structural properties of epidermis, including layer stratification, formation of wave-like rete ridges, change in epidermal height and length of rete ridges from normal to psoriatic.

The model has helped gain some insights on the complex spatio-temporal changes when transitioning between the 2 steady states and how a shot of temporary cytokine stimulus can induce different severity of psoriasis and how proliferation is altered between healthy and psoriatic skin in line with known literature. This provides the basis to study different cytokine simulation variations of psoriasis development and tracking of cell proliferation in the lab. In

addition, it provides a base to model the effects of psoriasis treatments such as UVB or biologics and predict potential treatment outcomes for patients.

Contents

List of Tables

List of Figures

Chapter 1

Introduction

Psoriasis is a chronic and disabling inflammatory skin disease that affects about 25 million people in North America and Europe [3], and approximately 2-3% of the UK population, affecting both genders equally. The disease can occur at any age and reduces the quality of life both physically and mentally [4]. Patients may experience a lower self-esteem and feeling shame and embarrassment for having such a disease. In addition, there may be pain and itching associated depending which area of the body is affected by psoriasis. Other impact to patients' quality of life could also be due to the fact that they may have to be absent from work for treatment which could lead to financial burdens if they are unable to work if the patient undergoes phototherapy treatments [5, 6]. There is no cure for psoriasis, however, it is a treatable condition with various types of treatment options available depending on the severity of the disease - ranging from topical treatment, such as topical corticosteroids to systemic therapies, such as methotrexate, to phototherapy treatments, such as Narrow-band Ultraviolet B (NB-UVB)[4], [7]. The mechanism of action for each type of treatment varies, and one of the most commonly used treatment is phototherapy, NB-UVB, in particular for moderate to severe psoriasis [7, 8, 9, 10]. NB-UVB works by various mechanisms of actions such as altering the cytokine profile, apoptosis of keratinocytes for clearance, promotion of immunosuppression and other mechanisms like cell-cycle arrest [8].

There are various ways for measuring the severity of psoriasis. One of the commonly used scoring guide is the Psoriasis Area Severity Index (PASI). It measures the average redness, thickness and scaliness of lesions, weighted by the area of involvement and calculated by visual inspection by clinicians. The grading scores range from 0 to 4 and the final result ranges from 0 to 72 [11]. In most clinical studies, a reduction of $\geq$75% from baseline PASI (PASI 75) is

considered the benchmark endpoint in assessing how well the therapy is going.

Phototherapy treatments usually follow a generalised form of NB-UVB which is given to all patients under a dosing regime that partially depends on the skin's reaction to NB-UVB light. An assessment is made to determine what the Minimal Erythema Dose (MED), the amount of UV that will produce minimal erythema (i.e. redness) following long exposure to UV [8, 12], before the therapy is given. This may not benefit all patients the same way. NB-UVB treatments also require patients to come into the hospital for outpatient treatment. Depending on their regime, patients may have to come in either 2-, 3- or 5-times weekly until the therapy induces a period of remission, which could approximately take 7-13 weeks [13, 14]. This may cause the patient distress if after going through weeks of therapy, the treatment has little effect.

Personalising treatments is one way of helping patients. If medical practitioners are able to find out that the treatment has minimal effect ahead of time, this gives them the ability to decide on changing the type of treatment without the patient having to go through the entire treatment course. On top of that, it will also reduce cost and stress on the patients, healthcare providers [10, 15, 16] and the NHS. In 2008, the estimated annual UVB treatment cost per patient that the NHS pays are as follows [10] :

- Treatment succeeds: £694
- Relapse at 6 months: £2,045
- Treatment fails [1]: £3,394

Computational models may provide an attractive solution to this challenge. They can provide better ways for scientists and medical practitioners in understanding the structure and dynamics of the processes and be able to formulate better predictions [17] in managing patients, for example. My research seeks to explore how computational models, in particular, stochastic agent-based modelling techniques, can be introduced as a platform in managing psoriasis through NB-UVB treatments and develop a framework to simulate normal epidermal and psoriasis formation in 3D. The 3D model looks to explore how psoriasis is activated and developed by cytokine immune stimulus and how the transition from normal to psoriatic epidermis changes certain mechanisms, such as how stem and transit-amplifying (TA) cells divide.

[1] Treatment fails if the patient is unable to reach remission (i.e. PASI 75, where there is a reduction of plaques by 75% from baseline) [13, 14].

1.1 Aims and Objectives

The overall aim of my research project is to develop a 3D computational model of epidermal homeostasis in psoriasis based on various immune interactions to explore disease development and treatment. For this aim to be achieved, the research questions to explore are as follows:

1. What are the necessary considerations to take into account when modelling epidermal formation and homeostasis and the key differences when transitioning to psoriatic state?
2. How cytokine immune stimulus activates psoriasis and how psoriasis affects the proliferative cells, stem and TA cells?
3. How do the different mechanisms of action caused by NB-UVB treatment affect epidermal remodelling?
4. How can spatial models and the personalisation of NB-UVB treatments benefit researchers and medical practitioners in better understanding the disease?

The project looks into how a new computational model can be developed that is able to simulate the normal epidermis and how it transitions to psoriasis. The approach is to first understand and replicate the results of a previously developed 2D model which was developed by our partners [18] which will be explained in detail in Chapter 3. The original model [18] was developed to simulate how psoriasis occurs and how clearance occurs with a high dose of NB-UVB. However, in reality, such high doses are not given to patients as they will cause burning of the skin. Hence, modifications to the model were done to simulate NB-UVB doses that were given to patients in clinic. I also looked into exploring the different mechanisms of action that NB-UVB induces to better understand what is necessary in remodelling the epidermis. In addition, I looked into exploring how computational model outputs can be used to simulate real patients and their accuracy to personalise treatment by clustering the model outputs using a clustering algorithm developed by [19].

Initial work on the 2D model informed me a better grasp of some of the basic concepts of how psoriasis develops and the mechanisms behind NB-UVB. However, the software the model was developed on was not ideal in adding complexity and stochasticity to it. Some of the limitations to support the development of a new 3D model includes improving the simulation time, removal of some fixed parameters to allow the behaviours of cells to be more stochastic rather than deterministic and adding signalling chemicals such as immune cytokines to trigger psoriasis rather than artificially altering the cell cycle time of proliferating cells. Chapter 4

describes the new model developed and which new features have been added as compared to the 2D model to solve some of these limitations and methods used to develop the model in 3D to answer the above research questions.

1.2 Thesis Outline

This section briefly describes the chapters in this thesis.

- Chapter 1 introduces the research topic and what are the aims and objectives of my project.
- Chapter 2 describes the background and related work done in the related field.
- Chapter 3 introduces a 2D model which was previously developed and extended to model a lower NB-UVB treatment dose, different treatment frequencies and fed into a clustering algorithm to validate the simulation outputs against patient data.
- Chapter 4 describes the 3D model developed and introduces the modelling software, mechanical, biological and chemical processes involved as an overview and a steady state model of how the normal epidermis is developed and formed and validation done against literature and clinical studies.
- Chapter 5 describes how the normal epidermis transitions to a diseased state with the onset of psoriasis and the changes made to the biological and physical processes. The simulation results are then validated with known literature and clinical studies similar to the normal epidermis.
- Chapter 6 introduces how psoriasis alters the way proliferative cells, stem and TA cell, divide from the normal state. The simulation results show how some mechanisms in the epidermis may cause changes and can be proposed for future experimental studies.
- Chapter 7 gives an overview of the conclusions drawn and final remarks for future work to be done.

1.3 Publications

- ESDR 2022, Poster Presentation: D. Paramalingam, B. Li, N. J. Reynolds, and P. Zuliani, "089 3D Computational Modelling of Immune Interaction and Epidermal Homeostasis in

Psoriasis," J Invest Dermatol, vol. 142, p. S195, Dec. 2022.

- ISID 2023, Poster Presentation: D. Paramalingam, B. Li, N. J. Reynolds, and P. Zuliani, "730 3D Modelling altered cell proliferation and differentiation in psoriasis," J Invest Dermatol, vol. 143, p. S126, May 2022.

- Manuscript in progress: D. Paramalingam, B. Li, N. J. Reynolds, and P. Zuliani, Computational Modelling of Immune Interaction and Epidermal Homeostasis in Psoriasis," Feb. 2023.

Chapter 2

Background & Related Work

2.1 The Epidermis

The skin is the largest organ in the body and is structurally made of 2 components, the epidermis and the dermis. The epidermis is the upper layer of the skin and is typically made up of 4 to 5 layers of epithelial cells while the dermis is the lower layer of the skin as seen in Figure 2.1. The epidermis consists mostly of keratinocytes (at approximately 80%) and are either proliferative or non-proliferative (Figure 2.2) [20, 21]. Proliferative keratinocytes consists of cells that are able to divide such as stem (SC) and transit-amplifying (TA) cells while the non-proliferative keratinocytes are terminally differentiated cells. Other cells that reside in the epidermis include melanocytes, T cells, Langerhans' cell and monocytes. The epidermal structure can be further divided into four main layers as follows:

- Stratum basale (SB) is the bottom most layer of the epidermis closest to the dermis where stem cells mostly reside and has the strongest attachment to the basement membrane and this layer.
- Stratum spinosum (SS) is the layer above the SB which holds mostly proliferative cells that will terminally differentiate. The cells that reside here are mostly TA cells.
- Stratum granulosum (SG) is the layer above the SS layer which comprises mostly of differentiated cells. It is here that the morphology of the cells changes and where calcium is secreted out and cells start to flatten from their spherical shape. This is also the layer where the calcium concentration is at its highest [23, 24].
- Stratum corneum (SC) is the top most layer which comprises of differentiated cells which

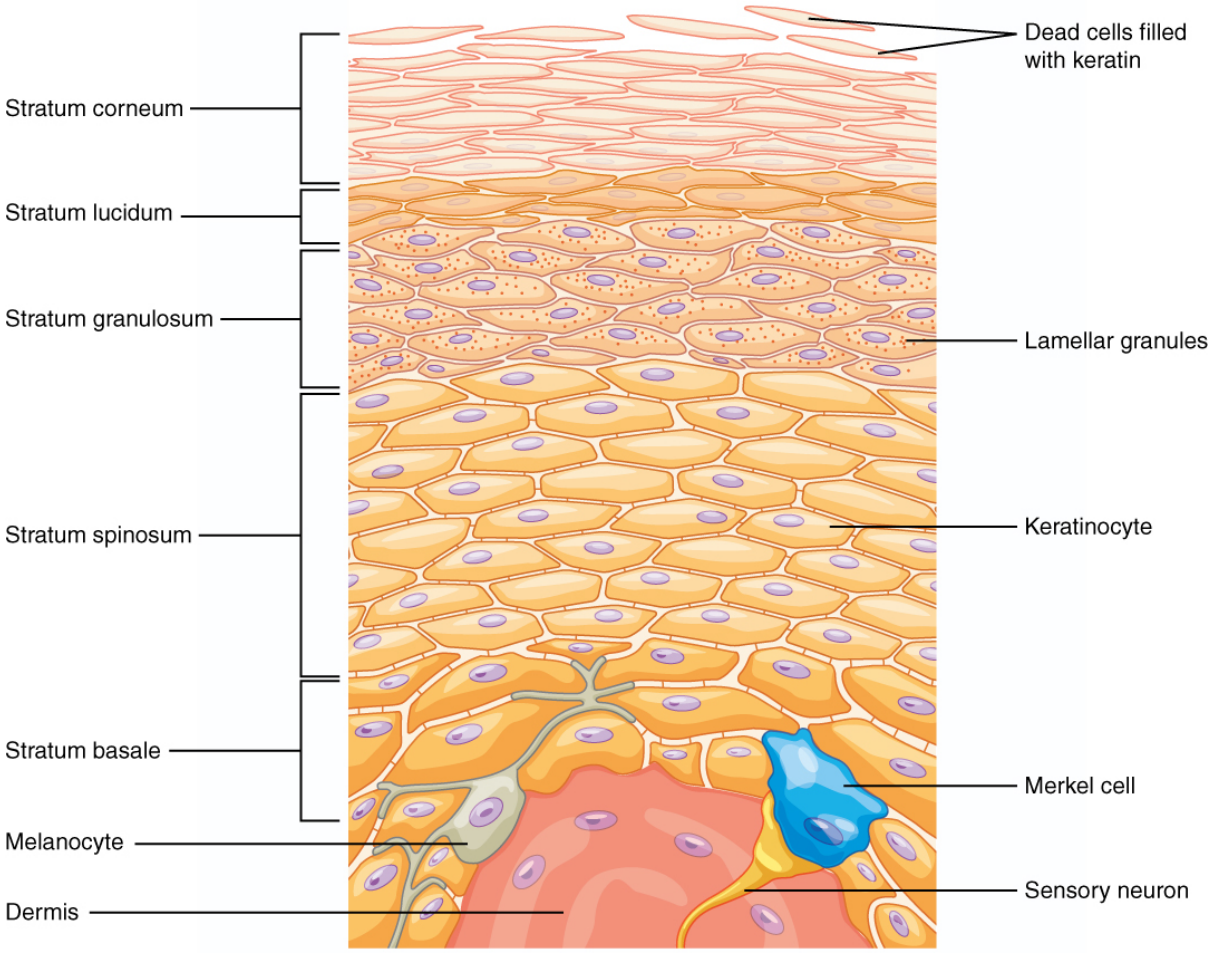

Figure 2.1: Figure adapted from [22]. Schematics of the different epidermal layers and types of cells that reside. On the left, the label shows 5 different layers of the epidermis, from the bottom, stratum basale, stratum spinosum, stratum granulosum, stratum lucidum, stratum corneum. The top three layers consists of differentiated cells and the stratum lucidum layer is not always prominent in all areas of the skin. The bottom layers, stratum basale and stratum spinosum, consists of mostly proliferative keratinocytes, stem and TA cells. The figure also shows addition cells melanocyte and merkel cells which are not considered in the model.

are due to be desquamated out of the system. The differentiated cells here are of a flat shape.

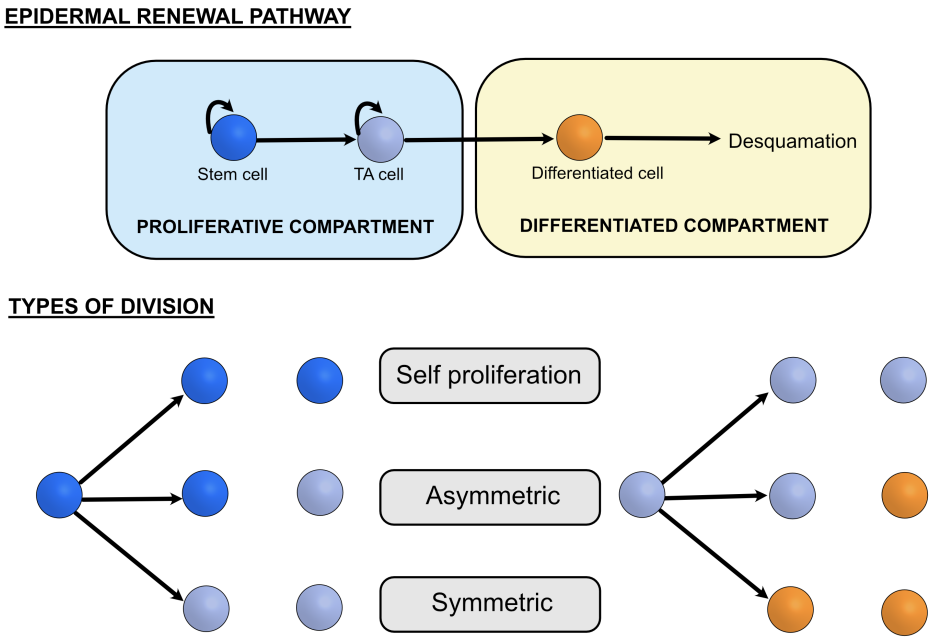

Figure 2.2: (Top) Schematic of the epidermal renewal pathway. There are two main functional compartments found in the epidermis - proliferative and differentiated. The proliferative compartment consists of stem and TA cells which can divide in three different ways. Only TA cells will terminally differentiate and migrate up the epidermis. (Bottom) Stem and TA cells can divide to produce daughter cells of the same type or of a different type. Self proliferation occurs when both daughter cells are of the same kind. Asymmetric division is the type of division that occurs mostly and occurs when one daughter cell is of the same type and the other being a different type while symmetric division occurs when both daughter cells are of a different type from the parent cell.

2.1.1 Types of cells in epidermis

The main type of cell in the epidermis are keratinocytes, which can be further subdivided in stem, TA and differentiated cells [20, 25] and this subdivision of cells can help in identifying and creating layer stratification. Each cell type plays a different role in proliferation and/or differentiation and are described below.

Stem cells

Stem cells are the located on the basement membrane which is right on top of the dermis and are located throughout the basement membrane [26]. Epidermal stem cell location on the rete pegs (or dermal papillae) has been largely debated. The rete pegs are the downward thickenings of the epidermis between the dermal layer which give the epidermis its unique wave-like shape [27].

The location of stem cells can be on the top or bottom edges of the rete pegs and there is still very little data that can be found clinically [8, 20, 25]. Epidermal cells have the potential to divide in three different ways, self proliferation, symmetrically or asymmetrically (Figure 2.2). Self proliferation occurs when a cell divides to two daughter cells of the same type as the parent, while in symmetric division, two daughter cells different from the parent type are produced. In asymmetric division, the cell divides to one daughter cell of the same type and one daughter cell of a different type. For example, a stem cell will produce two daughter stem cells when it self-proliferates. If it divides symmetrically, it produces two TA daughter cells while asymmetric division will produce one stem and one TA daughter cell. Proliferation is driven by various factors such as calcium or keratinocyte growth factors, which are diffused from the dermis or produced by stem and TA cells. The proportion of cycling proliferative cell is estimated to be around 43-66% [28, 26] with stem cells accounting for 3-12% of cycling epidermal cells. Stem cells are thought to have a slower cycling rate as compared to TA cells. It is estimated that stem cells have a cycling time of 100-200 hours [29] and can be as slow as 400 hours [30]. The proportion of stem cells in the epidermis depends on the part of the body [26].

TA cells

TA cells are located in the basal or suprabasal (the layer right above the basal layer) layer and have limited proliferative ability, which has been estimated to be around three to five times [25, 31] before migrating upwards and terminally differentiating. Proliferating TA cells are mostly located close to the basement membrane due to a stronger adhesion and higher concentration of nutrients that are diffused from the basement membrane and the dermis. Division in TA cells is in a similar fashion as stem cells where a cell can divide in three different ways to produce TA or differentiating cells. The rate of TA cells cycling is much faster than stem cells at around 60 hours, ranging from 50-65 hours [21].

Differentiated cells

The epidermis comprises of approximately 40-66% of differentiated cells [31, 28], which continue to migrate upward to the upper layers of the epidermis. As they reach the SG layer, calcium gets secreted and the cells start to flatten, changing their morphology. They continue to migrate to the SC layer and eventually shed off by desquamating out of the epidermis.

Stem and TA cells require certain signalling chemicals to grow, divide and differentiate. Calcium is one of the most commonly studied chemical signals found in the epidermis and plays an important role in the growth and differentiation of keratinocytes [32, 24]. Calcium exists in the lower and upper layers of the epidermis with the highest concentration levels in the SG layer, where differentiated cells mostly reside. Calcium is secreted by differentiated cells as their shape change from a sphere to flat cells, losing most of their contents. In addition, the calcium gradient plays a crucial role in allowing the dynamic changes of calcium to generate a signalling system. This signalling system regulates the epidermis formation and functions [33, 23]. Previous studies have shown that a disruption to the skin barrier or the onset of a disease such as psoriasis causes the calcium gradient to be lost [23, 34]. Figure 2.3 shows an immunostaining of four types of epidermis - normal, non-lesional, lesional and isotype control and the disruption of the calcicum gradient, Transient Receptor Potential Canonical-1 (TRPC-1), between normal, non-lesional and lesional epidermis. The TRPC channel consists of a group of receptor-operator which are calcium-permeable cation channels of the TRP family [35, 36]. Therefore, immunostaining of TRPC channels can show how the calcium gradient looks like in the epidermis both normal and psoriasis.

2.2 Transition to Psoriasis

Psoriasis occurs due to an abnormal immune response that causes T cells to secrete cytokines to drive hyperproliferation in the epidermis. This causes keratinocytes to undergo a higher level of proliferation as compared to normal keratinocytes [18]. Therefore, the population of stem and TA cells is proportionally higher in psoriatic epidermis. This not only causes a thicker epidermis but gives rise to deeper rete ridges and an absent granular layer [37, 38].

There are various cytokines secreted by T cells such as Interleukin (IL) 17, IL-22, Tumour Necrosis Factor α (TNF-α) which induce the proliferative cells to grow faster and divide more quickly causing a significantly shorter turnover time. In response to this, proliferative cells

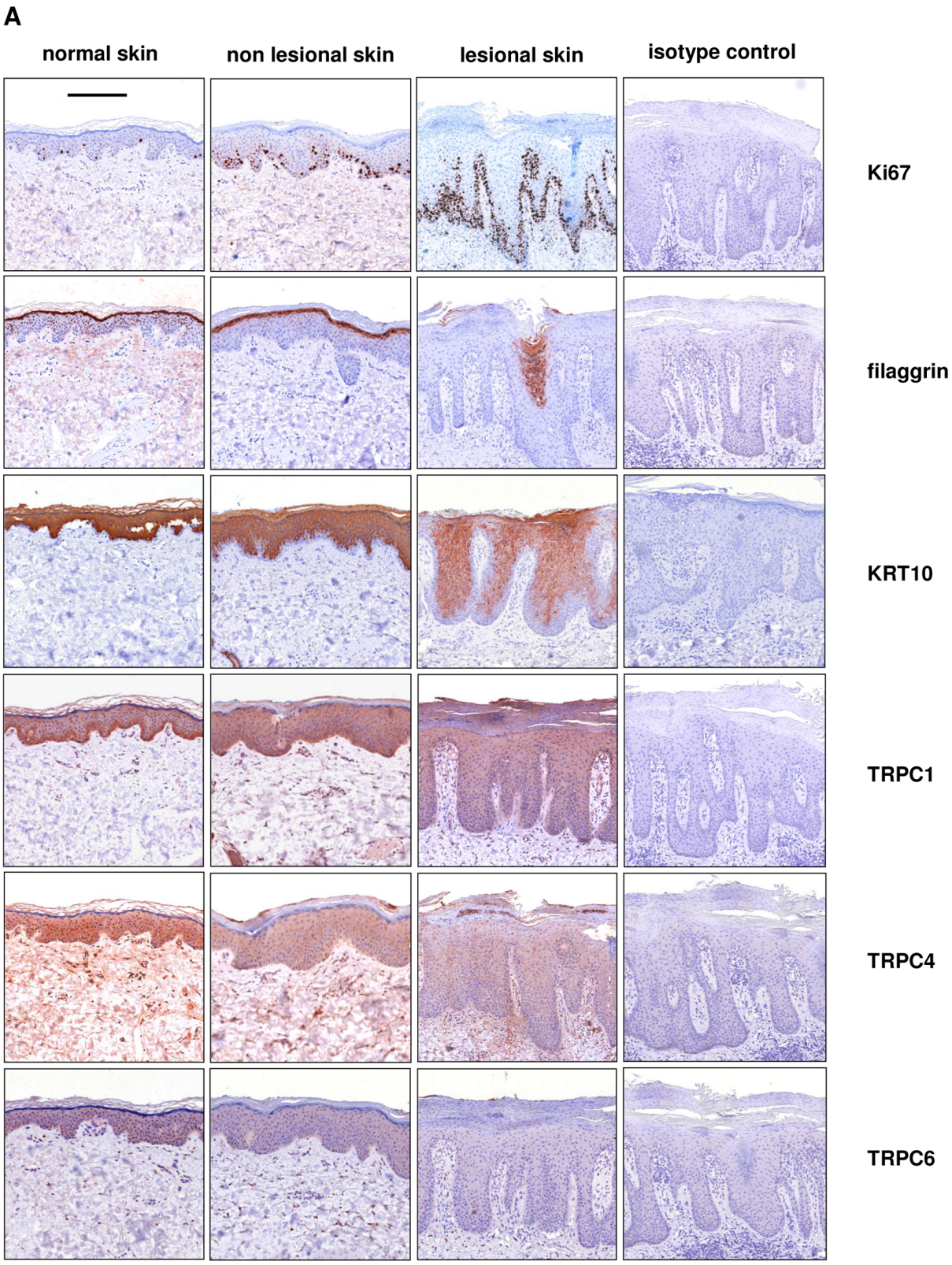

Figure 2.3: Figure adapted from [34]. Transient Receptor Potential Canonical (TRPC) channel immunostaining of psoriatic epidermis. The study by [34] studied on four different skin types to make a comparison on how the TRPC channel is affected during psoriasis onset. In relation to my study, the focus is on TRPC1 non-lesional and lesional skin. This compares and measures the calcicum gradient in the epidermis and shows the calcicum gradient is lost during psoriasis.

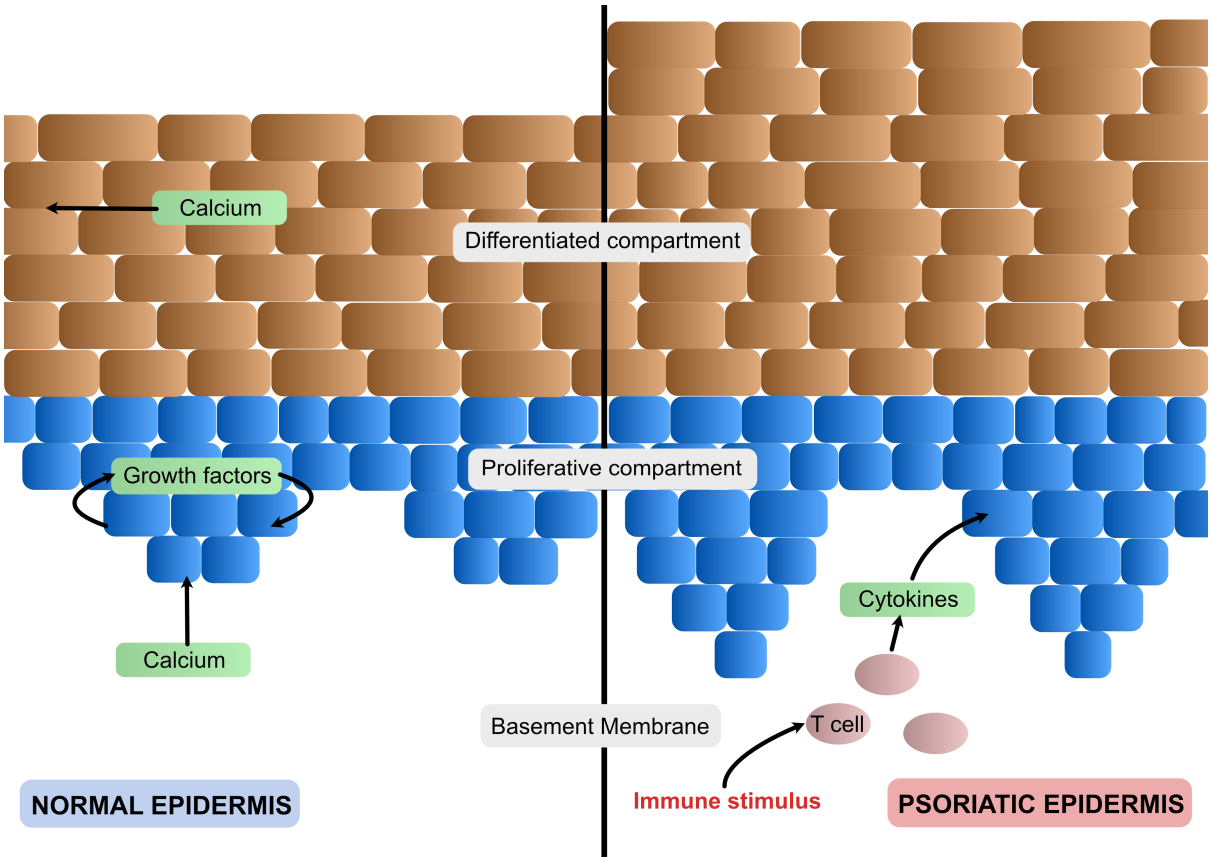

Figure 2.4: Schematic of normal (left) and psoriatic (right) epidermis. The epidermis is made up of two main compartments - proliferative and differentiated. The proliferative compartment is made up of stem and TA cells while the differentiated compartment is made up of terminally differentiated cells. In the normal epidermis, the rete pegs are more shallow and the overall epidermal height is shorter than in the psoriatic state. The nutrients involved in its development can vary. For example, in this case, calcium from the dermis aids proliferation and endogenous growth factors are produced by the stem and TA cells which also regulate their growth. In the psoriatic epidermis, an immune stimulus triggers T cells to produce cytokines such as IL-22 and TNFα, which are diffused into the epidermis and drive stem and TA cells into hyperproliferation. As a result, more cells are produced causing the rete pegs to deepen and the overall epidermis height to increase.

increase their production of growth factors, which in turn results in a positive feedback loop that maintains the psoriatic state (Figure 2.4).

The main differences between normal and psoriatic epidermis are as follows:

- The cell cycle and turnover time from normal to psoriatic epidermis is 3-5 times faster [39, 40, 41].
- The number of proliferating cells can increase by six times although this does not affect the cell cycle time [42].
- Thicker epidermis and deeper rete ridges with an absence of the SG layer [37, 38].
- Disruption of the calcium gradient in psoriasis. Due to the absence of SG layer, the highest concentration of calcium is no longer in the SG layer but scattered throughout the epidermis [43].

2.3 Narrow-band UVB treatment

There are various treatment options for psorasis ranging from topical to systemic to UV radiation therapies. UV radiation therapies range from different UV wavelength used such as UVA (320-400nm), UVB (290-320nm) and UVC (200-290nm). The common UV spectrum used is either UVA or UVB. UVA is able to penetrate deeper into the skin but is not enough to cause clearance alone and is usually used with psoralen (PUVA), a substance commonly used for UVA treatments. However, as UVA uses a longer wavelength and penetrates deeper into the skin, it may affect the dermis and increases the risk of burning and skin cancer, which are disadvantages of this treatment option. UVB uses a shorter wavelength spectrum and does not penetrate as deep into the skin structure and can be used safely [8, 44, 45].

In this project, clearance using NB-UVB therapy is explored. A previous clinical study by our partners has shown that the main mechanism of action for clearance was keratinocyte apoptosis [18]. The study showed that seven 3 MEDs was required for psoriasis to clear using NB-UVB. The treatment was given 3 times a week (i.e. every 56 hours) and the data was then fed into their computational model which showed how psoriasis at its maximum state will lead to remission of the disease after treatment.

However, in any type of therapeutic treatment given to a patient, the therapy outcome may result because of more than one action apart from the apoptosis of keratinocytes. Therefore,

the following can be considered as mechanisms of action and how they relate to apoptosis with respect to the clearance of psoriasis:

- Reduced proliferation of keratinocyte due to a blocking of external cytokine such as IL-23 [8].
- Growth arrest of keratinocytes via cytokines [8].

The question as to what proportions these mechanisms are effective, remains unclear and requires thorough testing in the model to ensure that the results are similar to clinical findings in terms of how long it takes for clearance to occur and how many keratinocytes remain in the epidermis.

2.4 Computational Models

Current computational models found in literature mainly focus on the development of psoriasis based on experimental studies or literature [12, 46, 47, 48, 49, 50] or finding the key mechanisms of psoriasis clearance by certain treatments such as UVB phototherapy [18]. There has not been any study to fully develop a model that aids medical practitioners in determining the effects of the treatment before the end of any treatment course.

2.4.1 Current computational models of epidermis and psoriasis formation

The use of agent-based modelling techniques in skin research has mostly been on normal epidermal development and homeostasis, keratinocyte formation or other diseases or conditions such as wound healing [48], [51, 52, 53, 54, 55, 49]. These are crucial in developing and fully understanding how normal epidermal layers are formed and maintain homeostasis before modelling a disease or condition.

The epidermal structure is marked with a unique wave-like shape at the bottom, right above the basement membrane. Figures 2.3 shows this wave-like shape of the epidermis from the immunostaining of the skin *in vivo* and is especially prominent in lesional (psoriatic) skin. In order to mimic this structural behaviour of the epidermis, an early study by [56, 40] developed an epidermal model based on geometry. The geometric model made use of cylinders to model dermal papillaes which causes this wave-like shape. Each cylinder is of the same size and shape and are arranged hexagonally. During the transition from normal to psoriasis, the cylinders increase in height by three to four times and the model has also been used to investigate psoriasis

with and without a granular layer [40]. Model outputs were validated against literature based on the turnover times obtained by the model.

A multi-scale model of how epidermal layers form was developed by [54] using an agent-based modelling framework and a lattice-free cell-center method to produce both 2D and 3D simulations on epidermal homeostasis. The study looked into how Ovol transcription factors, which regulates cell conversion from DNA to RNA, are important in epidermal proliferation and differentiation. Upregulating or downregulating certain Ovol transcriptions controlled the cell population density and cell population ratio. Epidermal layer stratification was obtained by experimenting with different cell division types and cell adhesion. The difference between symmetric and asymmetric division was tested and found that asymmetric division was essential in ensuring that a well defined basal-suprabasal layer was obtained. In addition, their submodel for selective cell adhesion between different cell types was critical in ensuring that the formation of the different epidermal layers.

In relation to psoriasis, an agent-based model was developed to represent the dynamic development of psoriasis and its therapeutic interventions by NB-UVB phototherapy treatment in 2D using a modelling software, Netlogo [18]. The study previously identified that the key mechanism of action in psoriasis clearance via NB-UVB phototherapy is apoptosis of keratinocytes. Phototherapy was modelled based on this mechanism, apoptosis, with a high dose of NB-UVB of 3 MED based on an *in vivo* study the authors had done. The model was able to obtain remission over a total of seven treatments and extended to individual variation in response to treatment based on the regulating susceptibility of psoriatic epidermis to apoptosis.

A hybrid model using stochastic/ deterministic and agent-based modelling approach was developed for epidermal homeostasis and psoriasis pathogenesis [50]. The model consists of two types - 1. A stochastic/ deterministic kinetics model, which tracked the temporal evolution of keratinocytes at several differentiation stages. For example, how a stem cell grows and divides to produce a TA cell and how a TA cell eventually terminally differentiates. 2. An agent-based migration model, which describes the motion of individual cells generating a stratified structure of the epidermis. The kinetics model can be used as a standalone model to obtain cell population density or used in combination with the agent-based model to produce a visualisation output of how stratification occurs. The deterministic simulation produces trajectories of cell density distribution over all the cell types while the stochastic simulation generates the probability of cellular events occurring using Gillespie's algorithm, which produces statistically correct

trajectories for stochastic systems [57]. The time series events generated are then fed into the agent-based cell migration model to simulate and visualise the spatio-temporal organisation of keratinocytes. Clearance was based on how UVB phototherapy affects the apoptosis rate of keratinocytes to revert them back to normalcy.

2.4.2 Agent-based Modelling Software & Tools

One of the most commonly used modelling technique in systems biology is the use of ordinary differential equations (ODEs) in biochemical reaction networks or gene regulatory networks [58]. While ODEs have been long used in modelling biological systems [59], agent-based models (ABMs) has gained some popularity with more software platforms being developed for this purpose such as NUFEB [60], BioDynaMo [61] and CompuCell3D [62].

The agent-based modelling software chosen to develop the 3D epidermal model uses a combination of the Large-scale Atomic/Molecular Massively Parallel Simulator (LAMMPS) framework and Newcastle University Frontiers in Engineering Biology (NUFEB). LAMMPS is a well developed software which has been used as a tool for material modelling down to the molecular level with various physical interactions already modelled [63] such as Hooke's law [64], a law to calculate spring force, which can be used to solve overlapping cell issues during cell division, for example. NUFEB, on the other hand, is a software that has been built on top of LAMMPS which focuses on the modelling of mircobes in waste water treatment [60], for example, and has several biological and chemical processes already implemented to use or modify such as cell division and chemical diffusion. In addition to both software being well developed, NUFEB is developed within Newcastle University which makes it easy to source for help when implementing my own package.

2.5 Predicting treatment outcomes using machine Learning

Predictive computational models of psoriasis are relatively new despite an increase in clinical studies to better understand the disease and clearance. The majority of the studies explored biological treatments instead of UVB phototherapy and were purely based on patient data such as their PASI scores or images of their condition [65, 66, 67, 68, 69]. The studies looked to identify outcomes such as the biological treatment length, effectiveness of treatment and to discontinue treatment [67, 68]. The machine learning techniques used from these papers

varies from using Generalised Linear Model, Logistic Regression, Deep Learning, Decision Tree, Random Forest, to Gradient Boosted Trees, which are mainly used for classifying and their performance compared to identify which algorithm is best to use.

In relation to psoriasis and NB-UVB treatments, a study in predicting patient response to UVB phototherapy treatments used data mining techniques such as Random Forest, Artificial Neural Network (ANN), Decision Tree, K Nearest Neighbour classifier (k-NN), and Support Vector Machines (kSVM) [1]. The differences between the various algorithms are summarised in Table 2.1. The authors carried out had done four experiments to find out which classifier model had the best fit and used a data set of 9083 patients. First was to evaluate the predictive performance of the classifiers used with the default settings without any hyper-parameterisation. Secondly, to evaluate the predictive performance with hyper-parameterisation. Thirdly, evaluation of the predictive performance of stacked classifiers of size three made of base classifiers with the default settings. Last was a combination of stacked classifiers and hyper-parameterisation. The study found that the best performance was obtained by random forest, kSVM and ANN combination of stacked classifiers in experiment 4. while the worst was ANN in experiment 1.

The predictive models mentioned are useful in identifying certain outcomes such as the potential treatment length and effectiveness of treatment given a patient with a set of features. Although it is great in aiding clinicians when prescribing psoriasis treatments, it has its limitations as well. In most papers relating to personalising treatment, the type of machine learning used was supervised learning [73, 74]. This meant that there is available training data for the algorithm to learn how to classify patients, for example. However, data may not be fully available or useful in some cases such as predicting how patients will react to a particular treatment before finishing the treatment course. It also lacks the ability to explore different types of treatments further. For example, how certain immune cytokines trigger psoriasis and how we can target the specific cytokines for treatment.

Computational models offer a solution to this and can be used alongside real patient data to classify patients' response to treatment. An ODE computational model [19] explored the onset, flare and NB-UVB phototherapy clearance in psoriasis. The model incorporated the three main types of keratinocytes (stem, TA and differentiated cells), dendritic cells and T cells. Dendritic and T cell species are involved in regulating the immune cytokines (IL-23, IL-17 and TNF-α) involved in triggering psoriasis. The model also presents two steady states - non-lesional (healthy) and lesional (psoriatic) skin and enables the switching between states

Algorithm	Description
Random Forest	Random forest algorithm is an ensemble algorithm, unlike a decision tree, this uses multiple decisions trees to train. It takes in three main hyperparameters - node size, number of trees and number of features sampled. It can be used for both classification or regression problems [70, 71].
Artificial Neural Network (ANN)	Inspired by neuron learning in the brain. A neuron receives weighted inputs from other neurons through dendrites and processes them until a threshold is reaches and an output is delivered via the axon. ANN consists of different layers - an input, hidden and output layer. The input layer passes information to one or more hidden layers where the data is processed through a system of different weighted connections. Once processed in the hidden layer, which is connected to the output layer, the output node gives a prediction or classification of that particular input [72, 73].
Decision Tree	A basic classification and regression method that is able to generate results similar to a structure of a tree where a tree node represents a test on an attribute and a branch represents the output. Each leaf node presents the class and the topmost node is the root node. [73, 74]
K Nearest Neighbour classifier (k-NN)	A classification and regression method which uses the proximity to make predictions about the grouping of each data point. It assumes that similar points can be found near each other [75, 76].
Support Vector Machines (kSVM)	This type of algorithm is usually applied to two-class classification and represents a data-driven approach which does not require any assumption about the data distribution. It is used to identify a separation boundary called hyperplane for classfication purposes [73, 74].

Table 2.1: Summary of machine learning algorithms used in predicting NB-UVB phototherapy treatment in psoriasis by [1]. These are the five algorithms used in identifying the performance of NB-UVB phototherapy treatments in psoriasis patients.

when NB-UVB phototherapy is applied by introducing apoptosis as the mechanism of action for clearance. The ODE model outputs were converted to PASI trajectories to identify and emulate real patients. The PASI trajectories, along with 96 real patient data, were fed into a machine learning algorithm using a latent class method [77] to cluster and predict classes of patients who may or may not enter remission. The optimal number of classes identified was three and was able to determine by week 3, if the patient will enter remission if they continued their NB-UVB phototherapy treatment.

2.6 Conclusion

The epidermis consists of various cell types which make up the four main layers of the epidermis [22]. In this study, the focus is on keratinocytes and the three main types, stem, TA and differentiated cells. Among the three cell types, stem and TA cells have the ability to proliferate and produce a daughter of a different type [20, 25]. Eventually, a TA cell terminally differentiates to a differentiated cell and migrates upwards in the epidermis and eventually sheds off [25, 31].

Psoriasis occurs as a result of an abnormal immune response causing T cells to secrete cytokines causing hyperproliferation to occur and the epidermis to increase in thickness [18, 40]. The treatment options for psoriasis are dependent on the severity of the disease and in most moderate to severe cases, NB-UVB and systemtic treatments are given [8, 18].

Clinical studies on psoriasis and its treatment options can be time consuming and costly. Computational modelling provides an attractive solution into better understanding the disease and how it can be treated prior to clinical trials. This can eliminate and create new hypothesis to test in clinical trials. Previous computational models looked at disease formation based on a general trigger to induce psoriasis and lacked cell-cell interactions [12, 46, 47, 48, 49, 50].

This study looks to better understand the development of psoriasis and to develop a 3D model which introduces the complexity of various cell-cell interactions and chemical signalling such as how immune cytokines. The research starts off with reproducing the results from a 2D model developed by our partners [18] and exploring the different mechanisms of action for clearance via NB-UVB. This provides a better understanding of how psoriasis occurs and crucial parameters required to validate the model which are described in detail in Chapter 3. This also includes identifying and implementing new features to replicate as closely as possible how the epidermis behaves in reality which will be further discussed in Chapter 4.

Chapter 3

2D Computational Model

3.1 Introduction

The starting point to understanding how to model psoriasis was a 2D model developed by our partners [18] using Netlogo (version 4.1), an agent-based modelling environment which can simulate the behaviour of cells and their environment in 2D [78]. The model (Figure 3.1a) is a simplification of how the epidermis and psoriasis develops and modelled just the 3 main types of keratinocytes (stem, TA and differentiated cells) as "turtles" or agents. Immune cells and other cell types were not modelled for the simplicity of the model and psoriasis was triggered based on a artificial diffusion of unspecific immune cytokines. The original model implemented apoptosis was the main mechanism of action for Narrowband-Ultraviolet B (NB-UVB) phototherapy based on known literature and clinical studies (Figure 3.1b). However, other studies have found that apoptosis may not be the only mechanism of action in NB-UVB treatments and it may also cause cell cycle arrest, where the cell stops cycling due to the treatment exposure. This difference in mechanism of action was explored in this 2D model and compared against the original results where apoptosis was the mechanism of action for NB-UVB clearance.

Figure 3.1b describes the cell types and the interactions modelled. NB-UVB doses are given in units of Minimal Erythema Dose (MED) defined as the minimum amount of UV exposure to cause minimal sunburn or redness to the treated area [12]. The usual dose given to a patient is around 0.75 to 1 MED. In an *in vivo* study by our partners [21], it was found that seven 3 MEDs, 3-times weekly (i.e., 56 hours apart), was able to cause remission. The 2D model implements this high dose of NB-UVB to replicate the clinical results and revert the model back to normalcy (i.e. non-lesional skin). However, giving 3 MED to patients is not ideal in

reality as a guideline on how patients may react to treatment as it may cause burning to the skin instead. Therefore, the current model is not a good representation as to how a patient reacts and requires some modification to emulate how a patient may react. The model has been modified and extended to simulate a lower NB-UVB dose of 1 MED and to match the actual frequency of treatment that patients will receive instead of using an average of 56 hours. The model results are then validated with patient data obtained by our partners by using a clustering algorithm [19] to identify how the model outputs closely relate to patient data and how it is able predict remission of psoriasis by emulating different classes of patients response to NB-UVB therapy.

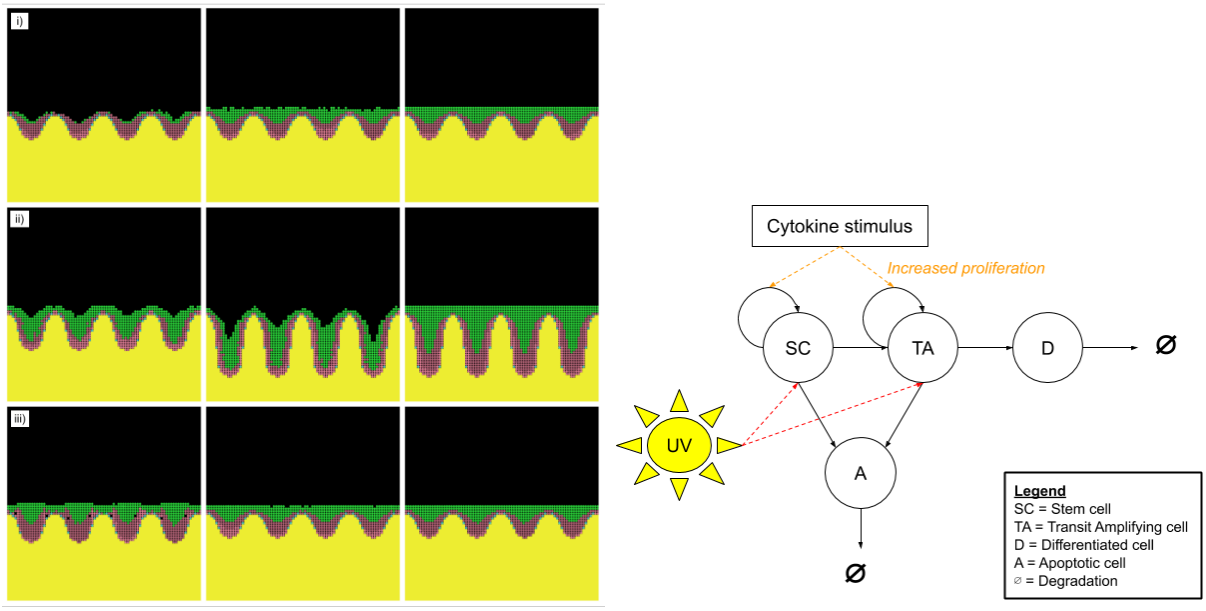

(a) (b)

Figure 3.1: (a) Snapshot of a Netlogo simulation. Stem cells (in blue) are placed at the bottom of the rete pegs, TA cells (in pink) and differentiated cells (in green). The basement membrane (in yellow) changes from its transition from the normal epidermis to psoriatic state. i) Simulates how the normal epidermis forms. ii) An activation in cytokine stimulus causes a transition to psoriatic epidermis. iii) NB-UVB treatment is given and the epidermis reverts back to normalcy. (b) Interactions between the different cell types in the model where SC, TA, D, A and ∅ represents stem cell, transit amplifying cell, differentiated cell, apoptotic cell and degradation respectively. The activated cytokine stimulus causes an increase in SC and TA cell division (i.e. hyperproliferation) developing into psoriasis. NB-UVB treatment affects these by killing these cells.

3.1.1 2D Model

Netlogo was written in Java and is able to run from a graphical user interface. The concept used in Netlogo introduces a "world" that appears as a grid to create a modelling space [78], in

this case, a 2D cross-section of the epidermis. Within each grid, consists patches with x- and y-axes where turtles act as agents (i.e. a cell) which can be manipulated to move and change its type based on a set of rules or criteria. Each turtle is unique and has its own identity number which can be used to track individual progress of turtle manipulation. In this case, it allows the user to track individual cells to trace how it grows and divide and eventually terminally differentiate. All commands are directed by the user using the user interface as seen in Figure 3.2 which shows the original user interface of the model with various parameters able to change such as stem and TA cell cycle time. This allows the user to test various combinations of cell cycle time for stem and TA cells and what percentage of stem cells are cycling. The number of treatments and irradiation frequency can also be controlled by the user via the scroll bar in the graphical interface. For example, if the user wanted to test a different percentage of cycling stem cells, they could move the scroll bar "percent-stem" located on the left.

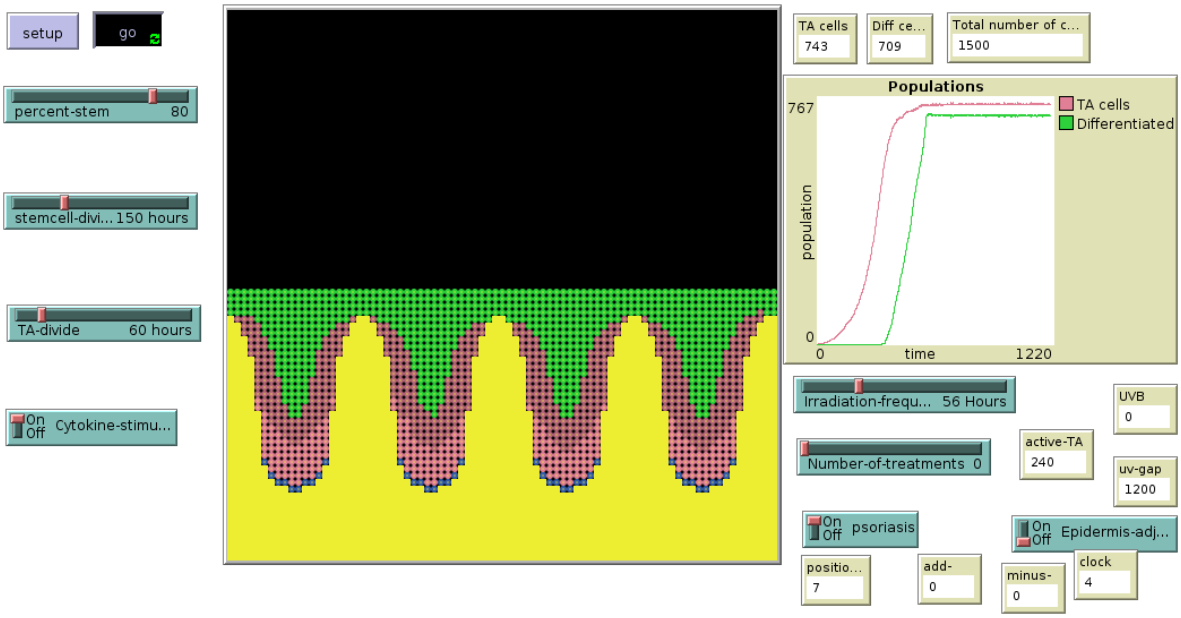

Figure 3.2: A screenshot of the original user interface for the NetLogo code previously developed [18]. The user is able to simulate various scenarios by changing the sliders and buttons. For example, modifying the cell cycle time for stem (stemcell-divide) or TA (TA-divide) cells in hours. Users are also able to control the irradiation frequency (irradiation-frequency) in hours and total number of treatments to give (Number-of-treatments).

The model follows a series of procedures. To setup and start the simulation, the user has to click on the "setup" button, which initialises the basement membrane and stem cells positions, and once the parameters have been set by moving the scrolls, the user will then click on the "go" button and the simulation will start. The user can choose to change various parameters

to identify which parameter mimics how the epidermis and psoriasis form in reality and how it affects other factors such as the turnover time. For example, what is the ideal cell cycle length of stem cells in the model? What happens if we increase or reduce the cell cycle time? The known cell cycle length in literature is found to be between 100 to 200 hours [29, 79]. It was found that increasing the cell cycle time from 100 to 175 hours in stem cells caused an overall increase in turnover time by 16 days, while reducing the cell cycle time to 60 hours caused the model to mild psoriasis [18]. The parameters used in the model of the normal epidermis are summarised in Table 3.1

Parameter	**Value used in model**	**Evidence**
Percentage of stem cells cycling (percent-stem)	80	[18]
Stem cell cycling time (stemcell-divide)	150 hours	[29, 79]
TA cell cycling time (TA-divide)	60 hours	[80]
Frequency of UVB treatment (irradiation-frequency)	56 hours	[18]
The total number of UVB treatment given (Number-of-treatments)	7	[18, 21]
To start the simulation in the psoriatic state (psoriasis)	On/ Off switch	-
Initialising a cytokine stimulus, triggering hyperproliferation of stem and TA cells to develop psoriasis (Cytokine-stimulus)	On/ Off switch	-

Table 3.1: Parameters in the model's user interface which can be controlled by the user. Users can modify these values and the parameter values used in the model to model the normal epidermis are mentioned. The last two parameters has no evidence as they are on/ off switch to start the model simulation and to introduce psoriasis, respectively.

The information on the right-hand side of the interface as seen in Figure 3.2 displays the following:

- The current number of TA cells in the domain (TA cells).
- The current number of differentiated cells in the domain (Diff cells).
- Total number of cells (Total number of cells) of which the maximum number of cells in the domain was 1500.
- Number of NB-UVB treatments given, labelled UVB (UVB).
- Position of the basement membrane (position), where position 1 is the normal epidermis and 7 being the thickest psoriatic state (position).

Some assumptions have been made in the model to simply the processes and development of the epidermis and psoriasis and are listed as follows:

- The stratum corneum layer is not modelled as it consists of dead cells and cannot undergo apoptosis. As this model does not attempt to deal with NB-UVB penetration, this layer has been omitted [18].
- In the normal epidermis, stem cells only divide asymmetrically as the focus of this model is not on the development of the normal epidermis which starts off with just stem cells [18, 79].
- TA cells divide 4 times in the normal epidermis and 5 times in psoriasis before migrating and terminally differentiating as described in previous literature [18, 25, 20].
- An unspecified gradient diffuses from the basement membrane to aid cell proliferation and differentiation [56, 81].
- Stem cells always remain at the same position and do not move [18, 79].
- The changes to the basement membrane are based on the number of TA cells dividing. If there are too many TA cells dividing, the basement membrane will elongate to accommodate the cells. If there are fewer TA cells dividing, the model automatically switches to a basement membrane with a shorter rete peg.
- The difference in the total cell density in psoriatic state is assumed to be twice the normal density [31, 41, 82].

3.1.2 Predicting simulation outcomes using a clustering algorithm

Patients taking part in a clinical study by our partners underwent NB-UVB treatment 3-times weekly and had their data collected consisting of PASI trajectories and other data such as gender, age, and ethnicity collected over a period of 10 weeks. With the data collected, we are able to use machine learning techniques to better understand how the NB-UVB treatment affects each patient and if remission occurs during the course of their treatment, enabling us to cluster and make predictions on how a patient is doing. The clustering algorithm developed by a colleague was in R [19] to cluster the patient data and make predictions on whether a patient will clear by a certain week. This enables clinicians to decide if the patient should continue

or change treatment frequency and/or type such as moving onto biological treatments instead. The model uses a latent class classifier package called lcmm. The lcmm package allows us to make estimations of extended mixed models such as latent class mixed models using a maximum likelihood estimation method [77].

The original model featured NB-UVB treatments based on the number of hours apart from each treatment. For example, a 3-time weekly treatment would be 56 hours apart. However, in reality, clinics are not open over the weekends therefore, this model does not depict how treatment is given in reality. The model has been modified to depict how NB-UVB treatment is given only on weekdays (i.e. follows a day schedule as compared to hours). A 3-time weekly treatment will, therefore, be given on Monday, Wednesday and Friday, excluding weekends. A comparison will then be made to simulate the effects of a more personalised treatment where weekends are taken into account to determine if a patient will benefit from this and perhaps, change the way clinics operate. Two other treatment frequencies were tested in this model: 5-times weekly and a mixture of 3-times and 5-times weekly. In addition, the mechanism of action for NB-UVB treatment was also explored where growth arrest alone was modelled and a mixture of growth arrest and apoptosis was modelled. Once simulation data was collected for the above scenarios, it was fed into the clustering algorithm to compare the results against patient data.

3.2 Methods

3.2.1 2D Modelling

The original model was first tested to ensure that the results obtained were similar to the published results. As the runtime for the code to reach a steady state for the normal epidermis and psoriasis could take almost a day, I have adapted the code to automatically switch from the normal state to psoriasis and start the NB-UVB treatment based on the set treatment frequency and total number of treatments. This way, every simulation result is consistent, especially when analysing the effects of various NB-UVB doses and frequencies. Figure 3.3 shows a snapshot of the code modified in the "to go" function, where the model starts running. Once the original model was reproduced, modifications were made to test for the following:

- Comparison for clearance between the two mechanisms of action apoptosis and cell cycle arrest as a main mechanism of action. This is to test if cell cycle arrest could potentially

play a bigger role in clearance and cause remission the same way as apoptosis.

- The time between each treatment where instead of using an average of 56 hours between each treatment to represent 3-times weekly using the days in a week to exclude weekends.
- Modify and compare the different frequencies of NB-UVB doses given (i.e. 3-times vs 5-times weekly).
- Validate model results against real patient data using the clustering algorithm.

Apoptosis vs Cell cycle arrest

Inducing cell cycle arrest as the main mechanism of action of clearance was based on inactivating stem cells and stopping proliferation from occurring in both stem and TA cells. In doing so, it should stop hyperproliferation in stem and TA cells and in turn, it slows down growth and division allowing the system to move out of a psoriatic steady state and move towards remission. The modification to NB-UVB phototherapy treatment from apoptosis to cell cycle arrest was implemented in the "to uv" function using the command "set arrest? true" as seen in Figure 3.4. As described earlier, the original model parameters were used to test this. Hence, the NB-UVB dose emulated was 3MED and was compared against apoptosis, the original mechanism of action for clearance.

Modification of irradiation frequency from hours to days in a week

As treatment doses are not given over the weekends, the time between each dose is slightly different and should not be averaged out based on the number of doses given per week to mimic how it is actually treated in clinic. Therefore, the treatment time was modified to automatically change after three doses are given per week under the assumption that treatment always starts on a Monday. This is to reduce complexity of the model in calculating the next dosing. This results in the treatment given 48 hours apart between the first and second (i.e. Monday and Wednesday) and second and third (i.e. Wednesday and Friday) doses and 72 hours for the next dose (i.e. the following Monday) to be administered per week. It was predicted that there may be a slight difference in clearance when taking into account the additional time taken from the last dose of the week (i.e. Friday) to the next dose (i.e. the following Monday).

```
  ;;if there is treatments added and if it hits the same number of treatments per week
  ;; then it takes into account the weekends and changes accordingly
if (treatments-per-week = 5)
[
   ifelse (treatments = (treatments-per-week + tx-count))
   [
     set irradiation-frequency 48
     set tx-count (tx-count + treatments-per-week)
   ]
   [ set irradiation-frequency 24 ]
]
if (treatments-per-week = 3)
[
ifelse (treatments = (treatments-per-week + tx-count))
   [
     set irradiation-frequency 72
     set tx-count (tx-count + treatments-per-week)
   ]
   [ set irradiation-frequency 48 ]
]
 ]

...

if ((ticks = 1200) and (ticks mod 2 = 0))
 [
   ;;movie-start "psoriais_1.mov"
   movie-grab-interface
 ]
 if ticks = 1200
 [
   set cytokine-stimulus true
   set percent-stem 80
   set epidermis-adjust true
 ]
 if ticks = 2300 [
   set cytokine-stimulus false
   set Number-of-treatments 24
   set treatments-per-week 3
   set irradiation-frequency 48
]
if ticks = 2804 [
set treatments-per-week 5
set irradiation-frequency 24
]
```

Figure 3.3: Screenshot example of the model's "to go" function. In this example, the first half shows the implementation of UVB treatment frequencies. In this case, a mixed frequency UVB treatment. The second half of the code shows the implementation to automate the model based on the number of ticks (i.e. timesteps in hours). At ticks = 1200, psoriasis development begins. At ticks = 2300, UVB treatment begins after the model reaches a steady state in psoriasis. The example starts off with 3-times weekly UVB treatment for 3 weeks, then switches to 5-times weekly. The total number of treatments are kept at 24.

```
to uv
;; irradiate the epidermis
  set UV-gap 0
  set cycle-count 0
  set treatments treatments + 1
  ;;ta cells - they divide so they can go into cell arrest
   ask turtles with [(color = pink) or (color = 134) ]
          [
          let t random 99
          if t < 20
          [
          ;;die
          set arrest? true
          ]
          ]
  ;;stem cells - they divide so they can go into cell arrest
  ask turtles with [color = blue]
          [
          let s random 99
          if s < 13
          [
          set color grey
          set grey-clock 0
          set arrest? true
          ]
          ]
  ;;differentiated cells - they don't divide so no cell arrest
          ask turtles with [color = 65]
          [
          let d random 99
          if d < 8
          [
          die
          ]
          ]
end
```

Figure 3.4: Snapshot example of the model's "to uv" function. In this example, only cell cycle arrest has been implemented as the mechanism of action for NB-UVB phototherapy treatments. This is done by using the command "set arrest? true" (highlighted in yellow).

Modification of NB-UVB dose

The next modification was made to reduce the dose of NB-UVB given each time in the model. Apoptosis was modelled based on a random kill rate for each cell type found in a clinical study [18]. The original 3MED dose resulted in a random kill rate of 13%, 20% and 8% for stem, TA and differentiated cells respectively (Figure 3.5). Reducing the dose to 0.75 MED and 1 MED resulted in a random kill rate of 2%, 2% and 1% and 2%, 3% and 1% respectively. The calculations for modifying the MED concentration were based on [18] where the mean number of apoptotic cells per 1000 epidermal cells were as follows:

0.75 MED = 1.3, 1 MED = 2.1, 2 MED = 9.1, 3 MED = 14.3

As the dose has been reduced, this will require the number of treatments to also increase and in clinical practice, patients usually have a total of approximately 24-25 doses given. Table 3.2 summarises the number of apoptotic cells for each cell type based on the MED and the number of treatments required.

MED	**Apoptotic cells** *(%)*	**Number of treatments**
0.75	SC = 2, TA = 2, D = 1	24
1	SC = 2, TA = 3, D = 1	24
2	SC = 8, TA = 13, D = 5	7

Table 3.2: Summary of MED concentration tested and the percentage of cells undergoing apoptosis. The number of treatments for 0.7 5MED and 1 MED are based on the treatment frequencies given by our partners while the number of treatments for 2MED is estimated to be around 7.

3- vs 5-times vs Mixed frequency NB-UVB irradiation

In addition to modifying the treatment frequency and NB-UVB dose, additional tests were done to test for 5-times weekly and a mixture of frequencies where 3-times weekly was given for the first 3 weeks and 5-times weekly thereafter. In the case of 5-time weekly, NB-UVB phototherapy treatment was given every 24 hours for 5 times a week and a break of 72 hours for the next dose, simulating the weekend. The mixed frequencies were modelled the same way for 3-times weekly for the first three weeks and switches to 5-times weekly until the end of treatment. The user interface has also been modified to accommodate some of these changes as seen in Figure 3.6.

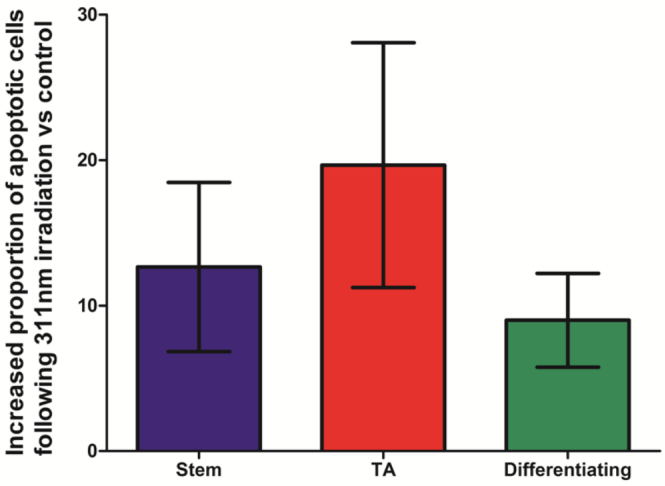

Figure 3.5: Figure adapted from [21]. Proportion of apoptotic cells when undergoing 3MED NB-UVB irradiation. Each cell type has a similar susceptibility to apoptosis following NB-UVB irradiation ex vivo. The increase in the actual number of apoptotic cells by each cell type was compared following a 3MED single dose (311nm) and sham-irradiated controls (n=3). Mean and standard error of the mean are shown. No significant difference between the three cell types were found (p=0.51).

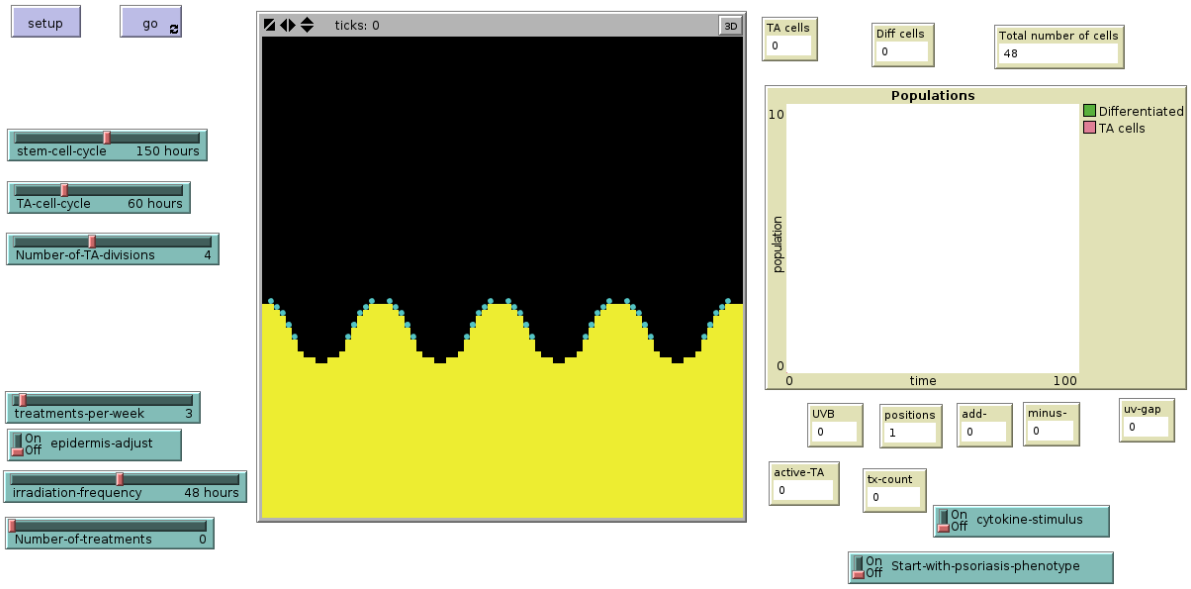

Figure 3.6: A screenshot of the new user interface for the NetLogo model. The user interface now displays the number of treatments given (tx-count) and has been set to automatically run the various scenarios and treatment frequencies. Therefore, the user will not need to manually change the slider and wait for correct timing.

Modelling different treatment recovery & Adding randomness

Nine scenarios were developed based on the rate of cycling stem cells based on the number of TA cells cycling at a given time to control sudden drop in cell population (see Figure 3.7) in the original code after a few courses of NB-UVB phototherapy treatment (see Figure 3.8). This sudden, rapid drop is not realistic as it goes below the normal epidermal cell count which would represent a side effect of the treatment such as burning. Hence, to eliminate this behaviour, nine different scenarios were created to control the rate of stem cells cycling to ensure a more gradual clearance and to mimic real patient data. Table 3.3 describes the changes made to cycling stem cells based on the number of TA cells cycling.

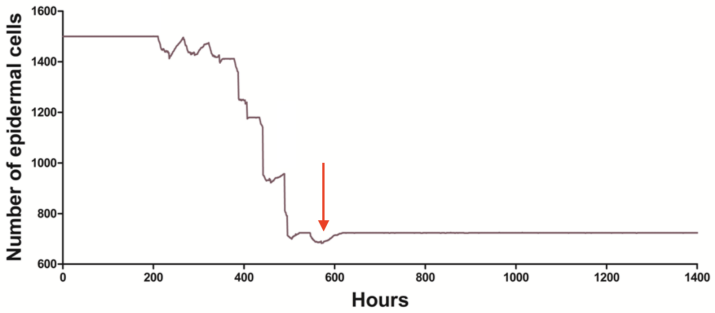

Figure 3.7: Figure adapted from [21]. Plot of the total number of cells during remission after 7 3MED doses of NB-UVB. The red arrow points at the point where normalcy is reached, however, the number of cells drops below normal which could potentially be a sign of burning of the skin before it makes a full recovery.

```
if (count turtles with [color = pink] >= 200)
        [ set percent-stem 65 ]
if (count turtles with [color = pink] < 200) and (count turtles with [color = pink] >= 150)
        [ set percent-stem 55 ]
if (count turtles with [color = pink] < 150) and (count turtles with [color = pink] >= 100)
        [ set percent-stem 45 ]
if (count turtles with [color = pink] < 100) and (count turtles with [color = pink] >= 75)
        [ set percent-stem 35 ]
if (count turtles with [color = pink] < 75)
        [ set percent-stem 20 ]
```

Figure 3.8: Screenshot of the 2D model code where the percentage of cycling stem cells are modified based on the number of TA cells proliferating at a given time implemented in the function "to uv". Note that the pink turtles mentioned in the code represents the TA cells that are actively cycling.

In addition to these 9 scenarios, 20 random seeds were chosen to run in each scenario. These 20 random seeds each represent a simulated "patient", producing a total of 180 simulation

Scenario	**Number of TA cells cycling**	**Stem cells cycling** *(%)*
1	≤200	70
	≤150, <200	60
	≤100, <150	50
	≤75, <100	40
	<75	20
2	≤200	65
	≤150, <200	55
	≤100, <150	45
	≤75, <100	35
	<75	20
3	≤200	65
	≤150, < 200	60
	≤100, < 150	50
	≤75, <100	40
	<75	20
4	≤200	70
	≤150, < 200	65
	≤100, < 150	55
	≤75, < 100	40
	< 75	20
5	≤200	60
	≤150, <200	50
	≤100, <150	40
	≤75, <100	30
	<75	20
6	≤200	55
	≤150, <200	40
	≤100, <150	30
	≤75, <100	25
	<75	20
7	≤200	50
	≤150, <200	40
	≤100, <150	30
	≤75, <100	25
	<75	20
8	≤700	75
	≤600, <650	72
	≤500, <550	68
	≤400, <450	65
	≤300, <350	62
	≤200, <250	45
	<100	20
9	≤730	75
	≤500, <600	70
	≤400, <500	68
	≤330, <400	62
	≤200, <250	45
	<100	20

Table 3.3: The nine scenarios with the different rate of cycling stem cells based on the number of TA cells cycling at a given time. 8 and 9 attempts to define more rules to reduce the dip (Figure 3.7) that occurs during remission.

trajectories which can be added to the real patient data for clustering. The random seeds were generated using a random seed generator between the numbers 0 to 99999. Table 3.4 summarises the random seeds used for the 20 simulated "patients".

Case	Random Seed	Case	Random Seed
1	11111	11	46156
2	12306	12	52366
3	12357	13	63958
4	12651	14	64564
5	17254	15	72162
6	23564	16	76953
7	25621	17	83695
8	33333	18	84564
9	36154	19	91226
10	45631	20	95555

Table 3.4: Summary of the 20 random seeds used for each scenario in the 2D Netlogo model. Each random seed was randomly generated using a random seed generator.

3.2.2 Clustering algorithm

The data used to train the clustering algorithm used was based on the data collected by our partners and consisted of 96 real patients [19]. The type of data collected were PASI trajectories for up to 10 weeks, age, gender, skin type, and BMI, for example.

The results obtained from the model simulations differed from the input data used in the algorithm. As mentioned earlier, the input data used was based on PASI trajectories while the simulation output was the total cell densities. A conversion was done based on the assumption made in the model where the maximum psoriatic state would have a total cell density of 1500 which would be the maximum PASI score.

3.3 Results

3.3.1 Apoptosis vs Cell cycle arrest

The original model parameters were used to test the differences and validate the results against previously published results [18]. In the previous study, it was shown that if cell cycle arrest was the main mechanism of action for NB-UVB clearance, it had a lag time of approximately 14 days from the start of treatment (Figure 3.9). This resulted in visible clearance seen only

after the entire treatment course has been completed, something that does not occur in reality.

Replication of this scenario in the new model with a lower MED showed a lag time of approximately 12-13 days after the first dose was given. This is similar to the results obtained in the case of 3 MED NB-UVB treatments. In Figure 3.10, the red line represents the main mechanism of action for clearance is just cell cycle arrest, while the blue line represents just apoptosis as the mechanism of action for clearance. Therefore, it is unlikely that cell cycle arrest is the main mechanism of action for clearance to occur.

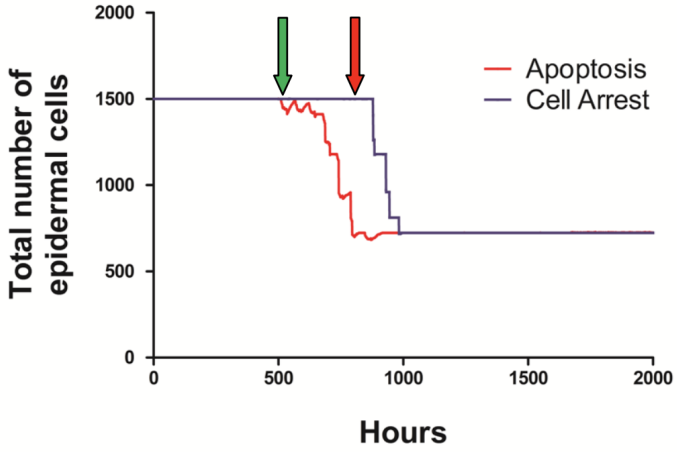

Figure 3.9: Figure adapted from [21]. Comparison between apoptosis and cell cycle arrest as main mechanism of action clearance following a course of 3 MED NB-UVB phototherapy. In this model, 13% of stem and 20% of TA cells undergo either apoptosis (in red) or cell cycle arrest (in blue). The first irradiation was given at T = 500 hours (green arrow) and last at T = 836 hours (red arrow). If cell cycle arrest was the main mechanism of action for clearance, no change in epidermal thickness will be visible until the completion of treatment. This results in a lag time of approximately 14 days post treatment for clearance to occur which is unlikely to occur in reality. Hence, it is unlikely that cell cycle arrest is the main mechanism of action for NB-UVB clearance.

3.3.2 Modelling different treatment frequencies

The treatment frequencies that were modelled were 3-, 5-times weekly and a mixed frequency of 3-times weekly for the first three weeks and 5-times weekly thereafter. For each treatment regime, simulations were ran under the nine scenarios with the averages of each scenarios plotted (Figure 3.11).

A comparison was made between the different treatment frequencies based on the start of visible clearance (i.e. cell numbers start to drop) for each scenario. The results showed no significant difference between the treatment frequencies for each scenario (p-value = 0.561007,

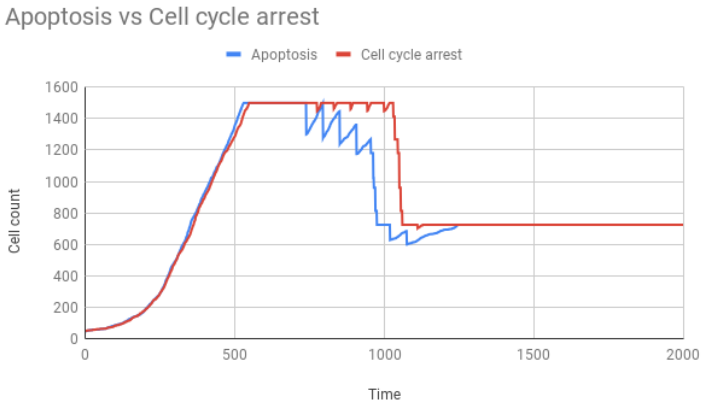

Figure 3.10: Comparison between cell cycle arrest and apoptosis. In apoptosis, clearance begins after the first dose of NB-UVB was given (i.e. no visible lag phase). In cell cycle arrest, on the other hand, a lag time of approximately 12-13 days was seen for clearance to start after the first dose of NB-UVB given. The lag time was calculated based on the time taken for a reduction total cell count from the first drop seen in apoptosis.

one-way ANOVA test) (Figure 3.11d). This shows that there is no significant difference when taking weekends into account (i.e. 72 hours between the last treatment of the week on Friday to the next treatment on the following Monday) and that assuming an average of 56 hours for 3-times weekly produces results that are reliable.

3.3.3 Model simulation clusters using 1 MED doses

The simulation data were fed into the machine learning clustering algorithm developed in [19] to identify latent classes. The original clustering algorithm explored several trends such as identifying patients who would obtain remission and those who would not. It was shown that based on the PASI scores, after three weeks of UVB treatment, the model was able to predict which classes of patients would obtain remission with an accuracy of 87%. Clearance was defined as obtaining a PASI score of 90 (i.e. PASI 90), which meant that the skin would revert back as closely to normal skin. Based on this, the algorithm showed that three to four classes were optimal in determining the types of patients. Figure 3.12 shows the results obtained when clustering the 96 patient data into three classes and a comparison on the PASI scores at the end of the treatment course.

The number of classes chosen was three and simulation data set chosen to compare between patients' were 3-, 5- times and mixed frequency. The reason why three classes were chosen was based on the original analysis [19]. This allowed some consistency for comparison when clustering the simulation data and real patient data. Although the patient data was based on

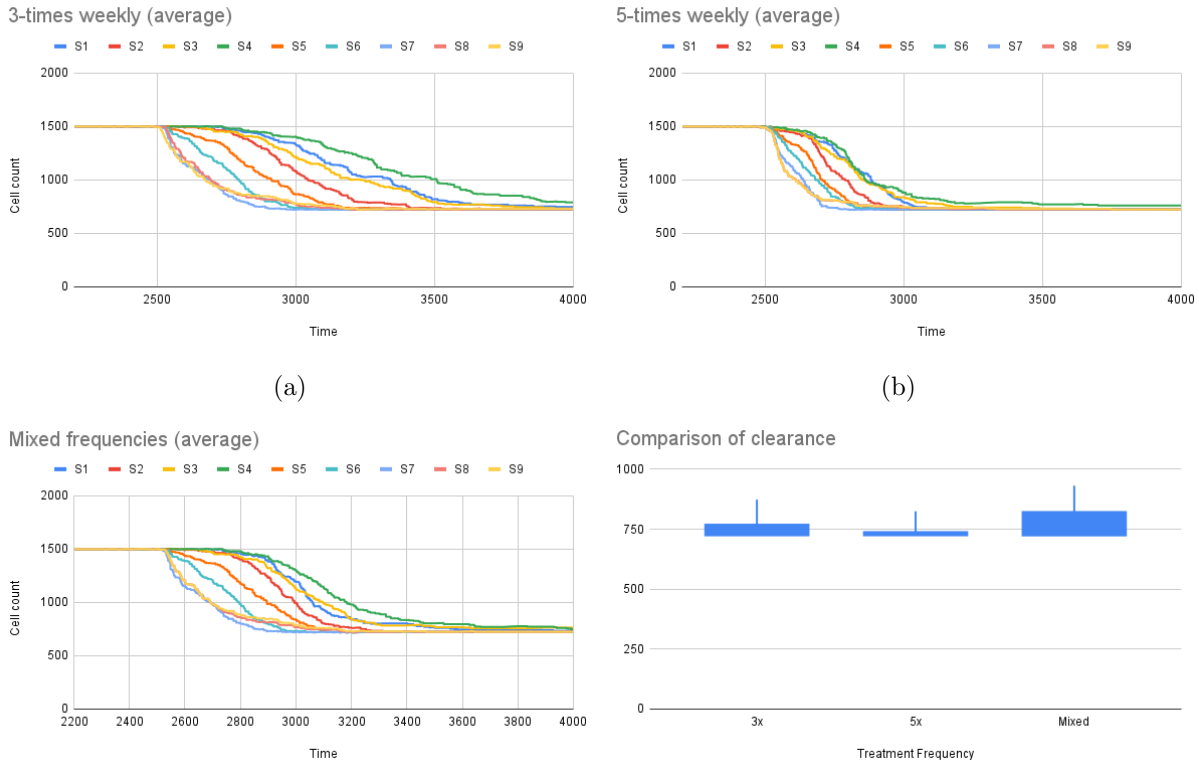

(a) (b)

(c) (d)

Figure 3.11: The average results for the three different NB-UVB treatment frequencies modelled in 9 different scenarios and its average results plotted. (a) 3-times weekly NB-UVB treatment; (b) 5-times weekly UVB treatment. (c) Mixed frequency NB-UVB treatment, where the model is given 3-times weekly NB-UVB treatment and 5-times weekly thereafter; (d) Box-plot comparing the results from 3-, 5-times and mixed frequency treatment. One way ANOVA test showed no signficant differences (p-value = 0.561007) between the treatment types.

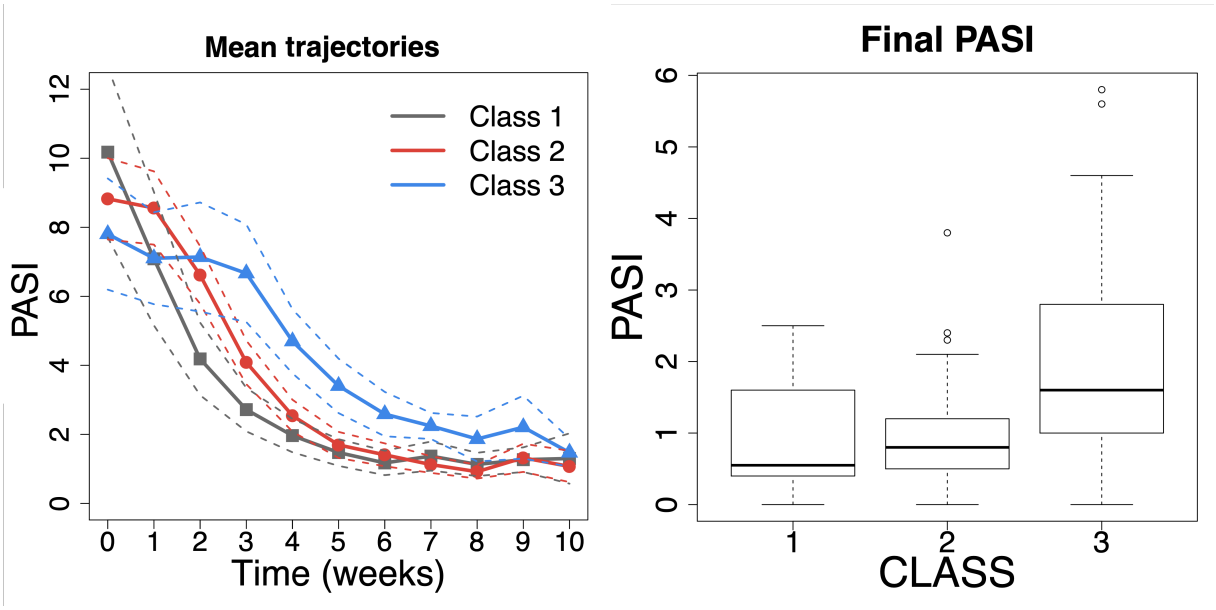

(a) (b)

Figure 3.12: (a) Mean trajectories of patient data for three classes. Solid lines represent the mean trajectories and the dotted lines represent the lower and upper bounds. (b) Comparison based on the end PASI data with patient data.

3-times weekly treatment, the additional clustering with 5-times weekly and mixed frequencies was done to check for differences in clearance between patients and simulation data (Figure 3.13).

The mixed frequency plot (Figure 3.13e) follows a similar trend to the real patient data (Figure 3.12a) where class 3, patients who do not obtain remission (i.e. PASI 90), shows visible clearance at the later time, in week 4, rather than classes 1 or 2 where visible clearance can be seen in weeks 1 or 2 following the start of NB-UVB treatment.

3.4 Discussion

The simulation results comparing the two mechanisms of action show how quickly clearance occurs (Figure 3.10). The lag time found in cell cycle arrest is 12-13 days which is similar to what was reported previously by [18]. However, if cell cycle arrest was the mechanism of clearance following NB-UVB phototherapy treatment, the model shows a delay before visible clearance is seen which is only after the completion of the treatment. In the clinical data obtained previously, further clearance of psoriasis was not observed after the completion of NB-UVB phototherapy treatment. Therefore, it is unlikely that cell cycle arrest is the only cause of clearance for psoriasis after NB-UVB phototherapy treatment but rather apoptosis of

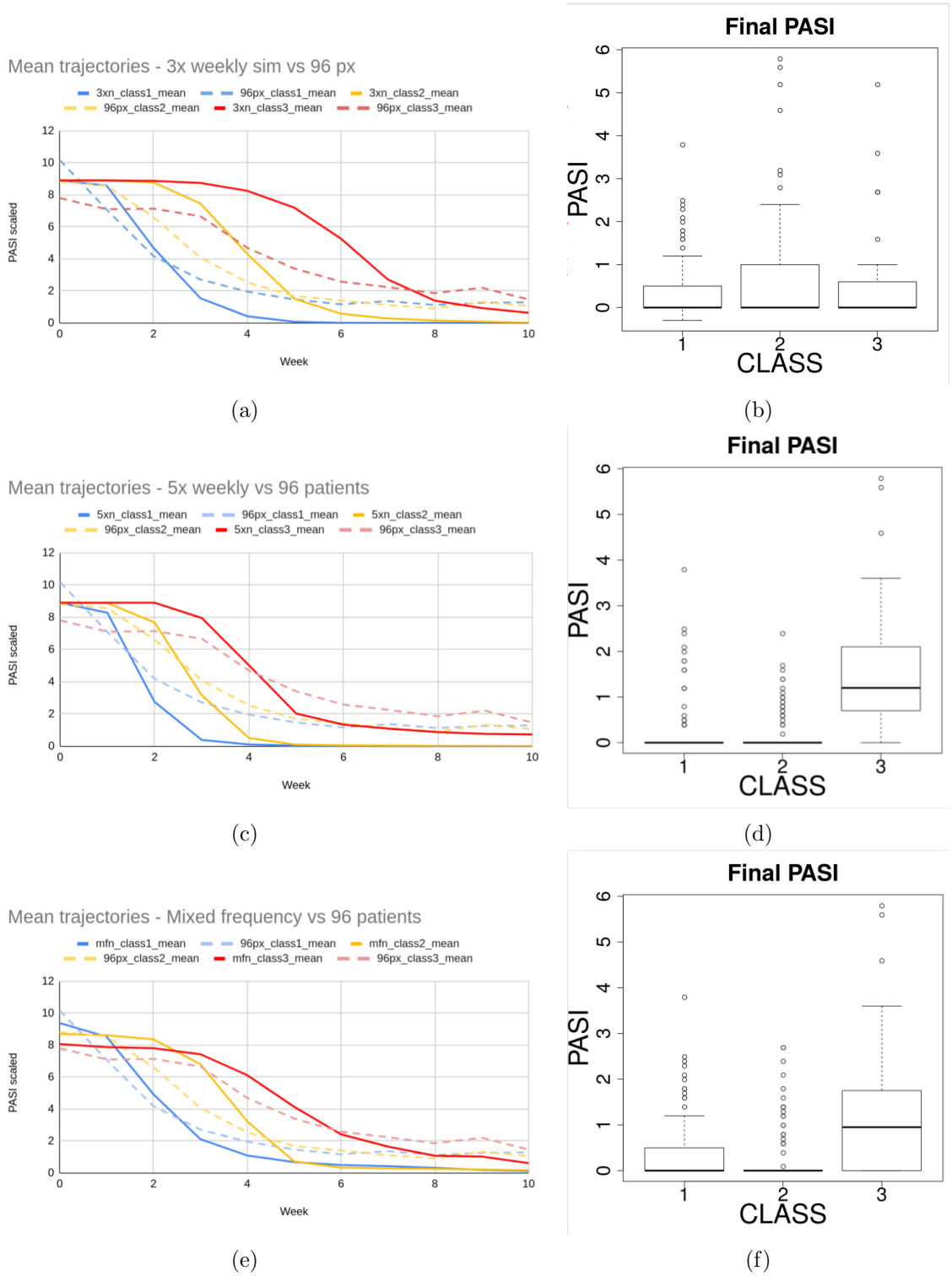

Figure 3.13: (a) Mean trajectories of 3-times weekly simulation (solid lines) vs real patient data (dotted lines). 3-times weekly comparison between real patient data in the same clusters. (b, d, f) Comparison based on the end PASI data with both the simulation and patient data. (c) Mean trajectories of 5-times weekly simulation (solid lines) vs real patient data (dotted lines). Clearance for class 1 and 2 starts around the same time, however, there is a difference in end PASI between the simulation output and patient data. (e) Mean trajectories of mixed frequencies simulation (solid lines) vs real patient data (dotted lines). Clearance times in this case looks much closer to the patient data as compared to 3-times weekly.

keratinocytes [18, 83, 84].

Since it is unlikely that NB-UVB phototherapy only causes apoptosis but cell cycle arrest [85, 86] as well, it will be interesting to look into how the two mechanisms of action interplay and cause clearance of psoriatic plaques in depth. This includes identifying the proportion of apoptosis and cell cycle arrest in computational models which can aid *in vivo* experiments in the future.

The modified treatment doses in the model were compared with varying treatment frequencies, 3-, 5-times weekly and a mixed frequency regime where the first three weeks follow a 3-time weekly treatment and 5-times weekly thereafter. The results showed no significant differences between the three treatment frequencies and therefore suggest that there may not be any benefit in changing the frequency of treatment from 3-times weekly to 5-times weekly or even starting with 5-times weekly [12]. However, as this model is just a simplification of the disease, further studies are required to justify this finding.

Replication of real patient data with the 2D model was obtained by controlling the number of proliferating stem cell to simulate nine different scenarios with 20 random seeds to simulate patients (see Figure 3.8) and Table 3.3. A total of 180 outputs were obtained. In addition to the 96 real patient data, a total of 276 PASI trajectory scores were available to cluster. Although the clustering algorithm was able to cluster which simulations could represent a possible treatment outcome, there is significant difference in the rate of clearance. As seen in Figure 3.13a, the solid lines which represent the simulation data clears at a slightly faster rate as compared to real patients (dotted lines). This is partly due to the way the model has been programmed, where there are fixed positions for the basement membrane based on the number of actively dividing TA cells. However, the trends from the model and real patient data are similar. The accuracy in clustering model patients into class 3 (i.e. poor responders), were 96.9%, 99.7% and 98.8% in 3-, 5-times weekly and mixed frequencies, respectively. Hence, although there are some limitations to using this model for measuring and personsalising psoriasis clearance to emulate real patients, it is able to predict poor responders with an accuracy of over 96%, depending on the treatment frequencies given.

3.4.1 Limitations

The current 2D model of psoriasis provides an insight of how psoriasis develops based on an unspecified trigger and clearance is controlled by the number of TA cells cycling. The model

has been replicated and validated based on the cell cycle and turnover time known in literature [29, 80, 25] before proceeding to experiment on how different mechanism of action affects NB-UVB clearance and the treatment frequency. However, there are limitations to using Netlogo to model complex biological systems. Some of the limitations of this model is that it is in 2D which is not a good representation of how the skin structure is like as it is not a uniform flat surface and there is no specific gradient used in the model to promote proliferation of stem and TA cells. In reality, there are many different signalling chemicals and immune cytokines involved in normal and psoriatic epidermis. Some of the parameters have also been fixed in this 2D model such as the maximum cell population density of 1500 cells and stem cell do not move from their starting position. The model also takes a significant amount of time to run that can be as long as 24 hours for a single simulation. As seen in the clustering results, the simulations clear faster than in the patient data and this may be due to the fixed positions set in the model.

Therefore, development of a newer model is required to add these complexities of how the epidermis behaves and how psoriasis develops when triggered by immune cytokines. Netlogo allows for modelling simple biological models, however, it lacks the ability to produce emergent behaviours of large models since it requires too much time to run a single simulation. Hence, development of a newer model and in 3D to solve some of these challenges.

Chapter 4

3D Model and Normal Epidermal Formation

4.1 Introduction

The previous chapter, Chapter 3, used a 2D model to obtain insights of how psoriasis develops and how NB-UVB treatments can cause remission of psoriasis. However, there are several limitations to the model that does not represent the spatial aspects of the skin and its cellular structure in reality. For example, in the 2D model, some of the model parameters are fixed and do not change (i.e. lacks randomness) such as how the stem cells initialised are always in that fixed position and do not migrate or move. The total number of cells in the epidermis is also fixed and therefore, the model always produces the same results. The 2D model also lacked the capability to introduce different chemicals to induce psoriasis. In addition, the time to complete a single simulation run could take almost 24 hours. Therefore, instead of modifying or working from the 2D model, it was best to develop an entirely new framework to model the epidermis and psoriasis which can reproduce similar results to that of the 2D model and from literature. The new 3D model also aims to solve some of the limitations mentioned in Chapter 3.

This chapter introduces the methods used to develop the normal epidermis structure from 2D to 3D. Similar to how the 2D model has been developed in Chapter 3, the 3D model development starts off with the development of the normal epidermis before transitioning to psoriasis. The model takes into account several factors and concepts from the 2D model and literature which will be described in this chapter. The model outputs are then qualitatively and quantitatively validated against literature before transitioning to psoriasis.

The normal epidermis formation is based on its interaction with two types of chemicals, endogenous growth factors (GF) and calcium as seen in Figure 2.4. It as been known in literature that calcium from the dermis diffuses in an upward gradient that aids proliferation in stem and TA cells. Upon terminally differentiating, differentiated cells will migrate upwards into the upper layers of the epidermis and before desquamating (i.e. shedding), cells change their morphology from spherical to flat shape and secrete their contents such as calcium in the stratum granulosum (SG) layer. This results in a high concentration of calcium towards the upper layers and in this model, calcium is used to control proliferating to maintain a steady state [24, 32].

The following assumptions have been made:

- Cells are of a spherical shape [18]. Differentiated cells morphology remain a sphere instead of flattening towards the upper layers of the epidermis for simplicity.
- A continuous flow of calcium is secreted from the bottom of the domain, emulating the dermis [33, 23].
- The growth factor involved in proliferation is only from stem and TA cells [19]. Growth factors that originate from the dermis are not considered in this case.
- All types of differentiating cells are labelled as "differentiated cells" for simplicity [18].

The 3D model was developed using the Newcastle University Frontiers in Engineering Biology (NUFEB) software which runs under the Large-scale Atomic/Molecular Massively Parallel Simulator (LAMMPS) framework. LAMMPS is an open-source software that makes use of Message Passing Interface (MPI). It was developed as a tool for material modelling down to the molecular level, allowing the modeller to model particles in different states as liquid, solid or gas [63]. NUFEB was developed as an extension to LAMMPS which allows the simulation of microbial communities in 3D [60]. It uses an individual based modelling technique, where microbes are represented as discrete units and the changes of their behaviours over time due to a number of processes that occurs such as cell division[60, 87].

NUFEB has the capability of modelling microbes as mentioned, however, epidermal cells behave slightly differently and require different nutrients to grow and proliferate. A new package, USER-PSORIASIS, was added to my version of the repository to model the additional functions required for the development of the epidermis and its transition to psoriasis. For example, cellular behaviours and their interactions with endogenous GF and calcium described in Chapter

1 (Figure 2.4) in the epidermis. The additional functions added were approximately 5000 lines of code.

The following behaviours have been added to the NUFEB framework based on behaviours from Chapter 3 and known literature:

1. Cellular growth for each cell type [60, 19].
2. Cellular division for proliferative cells, stem and TA cells [18, 50].
3. Maximum division counter for TA cells as they are known to divide 3-5 times before terminally differentiating [18].
4. Wave-like structure to depict the irregular surface of the basement membrane [18, 38, 50].
5. Diffusion of chemicals and cytokines for cellular growth [19].
6. Mechanical interactions between cells to solve overlapping and adhesion between the various cell types to aid stratification of the epidermis [60].
7. Potential for mechanical changes to basement membrane during the transition from normal to psoriatic state [18].

Figure 4.1 summarises how the normal epidermis will be simulated based on the type of cell it is. To begin, extracellular calcium is diffused into the system which signals to the proliferative cells to grow. As the model starts off with just stem cells, stem cells would grow and eventually divide to either a stem or TA daughter cell. When TA cells are produced, they would divide a fixed number of times as described earlier (i.e. maximum TA division count). If it is not reached, the TA cell would remain a TA cell until it is ready to terminally differentiate. Once terminally differentiated, the differentiated cell will migrate upwards as the epidermis grows and eventually reach the stage of cell desquamation and end of the cell's lifespan.

4.2 Methods

The model was split into three main sub-processes - biological, physical and chemical processes. The biological processes focus on how the different cell types grow and divide, while the physical processes focus on the spatial aspects such as rete peg formation, mechanical relaxation and spatial regulation for cell division on the wave-like basement membrane. Finally, the chemical

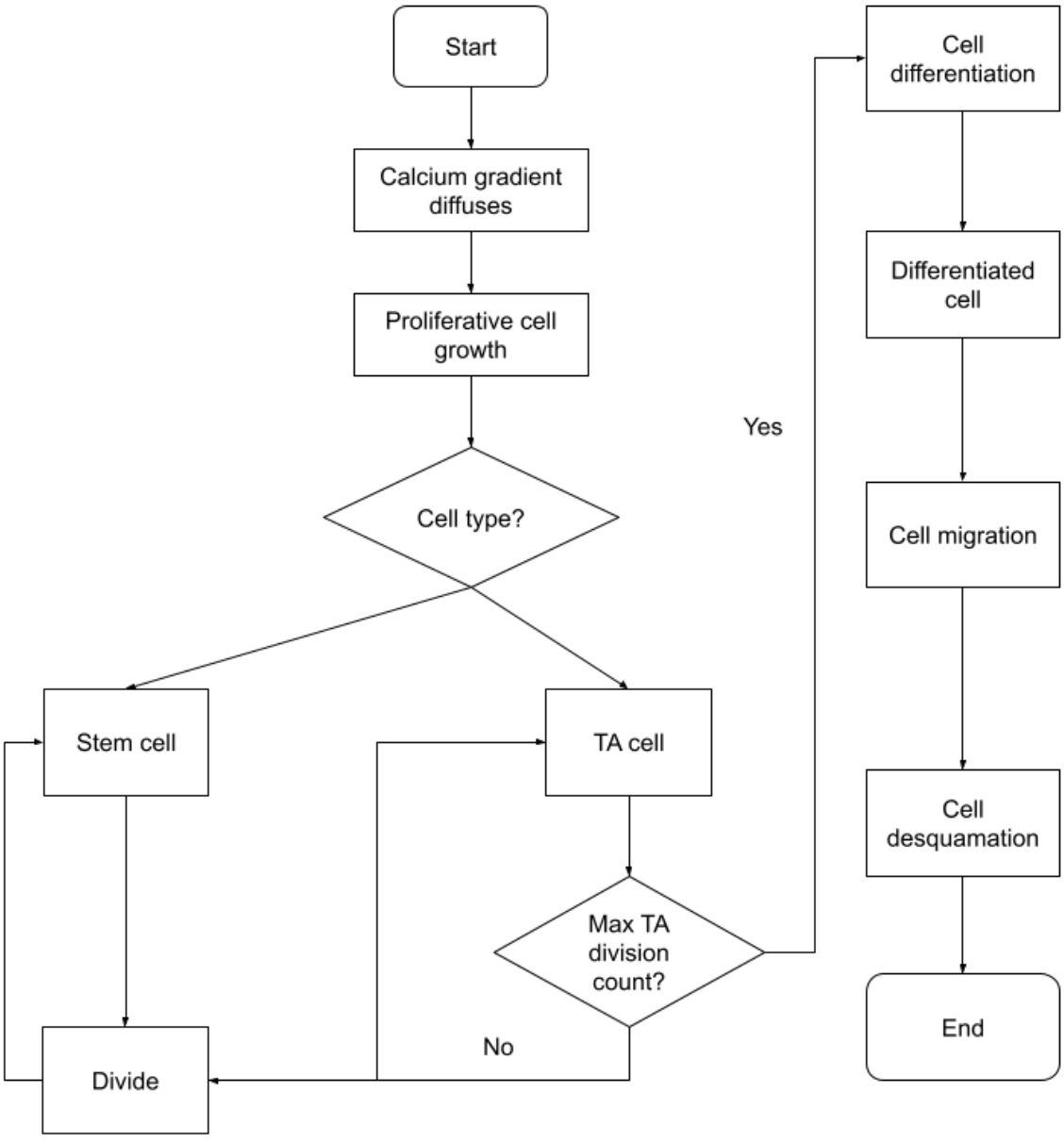

Figure 4.1: Flow chart summarising how the normal epidermis is simulated based on the what cell type it is. It describes how stem cells grow and divide and transitions to a TA cell and eventually terminally differentiating. Once it has terminally differentiated, it will migrate upwards and end its lifespan after it has been desquamated.

processes focus on how the chemicals, growth factors and calcium are regulated in the model. Figure 4.2 summarises the processes that occur during the simulation. It starts off with the initialisation of the model where the stem cells are initialised based on the user input and runs ith time. Diffusion of chemicals starts and proliferative cell growth occurs and once a threshold is reached, cell division starts and eventually cell differentiation occurs. In as the chemical and biological processes occur, physical processes are introduced to ensure that during cell division and differentiation, overlapping of cells do not occur and leads to the stratification of layers in the epidermis.

4.2.1 Biological Processes

The biological processes consists of cell growth and division which are based on the chemicals and cytokines involved and consist of two states, normal and psoriatic. The growth model for both is based on various chemicals and cytokines that have been found in literature and in clinical studies [18, 19, 88]. Cell division of stem cells and TA cells are based on having two interconvertible modes as mentioned in [2] where proliferative cells change their division type based on an expanding or balanced state. Figure 4.5 describes the epidermal cell pathway and the types of division the cell undergoes (self-proliferation, asymmetric and symmetric). The difference between the expanding and balanced state is in the probability rate when a stem or TA cell produces a daughter cell of a different type. This will be further explained in this section.

Epidermal Cell Growth

Cell growth in the normal epidermis is determined by the concentration of growth factors produced by the proliferative cells, and calcium. As each cell grows, its mass increases by consuming the chemicals in its environment. The growth process is described by the following equation already implemented in the NUFEB framework [60]:

$$\frac{dm_i}{dt} = \mu_i m_i, \tag{4.1}$$

where μ_i is the specified growth rate and m_i is the biomass of the ith cell. The growth rate μ_i is determined by

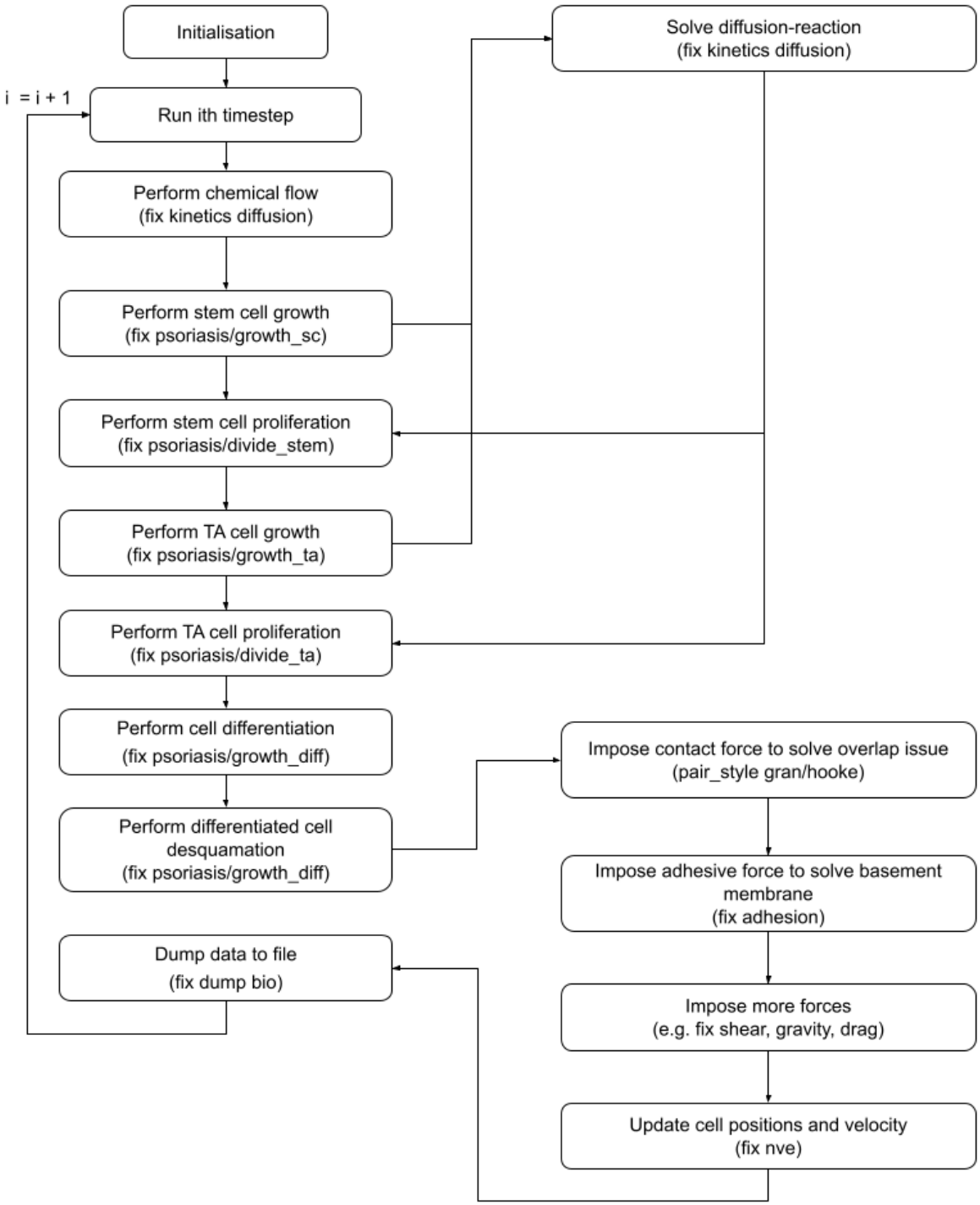

Figure 4.2: Flow diagram describing the processes of the simulation. Simulation starts off by initialising the number of stem cells input and run ith number of timesteps. The various biological, chemical and physical processes occurs to model cell proliferation and differentiation to develop the epidermis.

- Monod-based kinetics where cell growth is driven by the chemicals, growth factor and calcium, in the voxel of the diffusion gradient where the cell resides.

- Haldane inhibition model based on the calcium concentration in each voxel governs the cell growth and structural development. When the calcium concentration is high as a result of differentiated cells migrating and secreting calcium before desquamating, proliferating cells will "sense" this high concentration to slow down their growth, which in turn, maintains a steady state.

Equation 4.2 describes the growth model used, which is based on a Monod style equation and Halden's inhibition [89, 90].

$$\begin{aligned} \frac{dSC}{dt} &= (\mu_{max} \frac{S_{gf}}{Ks_{gf} + S_{gf}} \frac{Ks_{ca}}{S_{ca} + Ks_{ca}}) SC \\ \frac{dTA}{dt} &= (\mu_{max} \frac{S_{gf}}{Ks_{gf} + S_{gf}} \frac{Ks_{ca}}{S_{ca} + Ks_{ca}}) TA \end{aligned} \tag{4.2}$$

where μ_{max} is the maximum growth rate specified, S_{gf}, S_{ca} are the current concentration of growth factor and calcium within the voxel respectively, and Ks_{gf}, Ks_{ca} are the half-velocity constants for growth factor and calcium. SC and TA are the number of cells in the system.

Cell division and desquamation

Cell division occurs as a result of cell biomass growth and desquamation occurs to emulate the shedding of differentiated cells at the top of the epidermis. Division occurs if the diameter of a cell reaches the specified threshold value and the cell splits into two daughter cells. The mass of one daughter cell is a randomly assigned value between 40-60% of the parent's total mass and the other daughter cell receives the rest. In addition, one daughter cell will take the position of the parent's while the other daughter is placed randomly in either a horizontal or vertical direction from the parent cell depending on its type. Stem cells are known to be only found along the basement membrane and so, if the daughter cell is a stem cell, it will be placed adjacent to its parent while a TA cell can be placed in either direction [91, 26].

Figure 4.5 described the epidermal cell pathway and the three different types of division, self-proliferation, asymmetric and symmetric, that can occur with different probabilities. Calcium is used to control the division probabilities in the system. The cell division probabilities are determined by the state the model is in. In the expanding stage, where the simulation starts

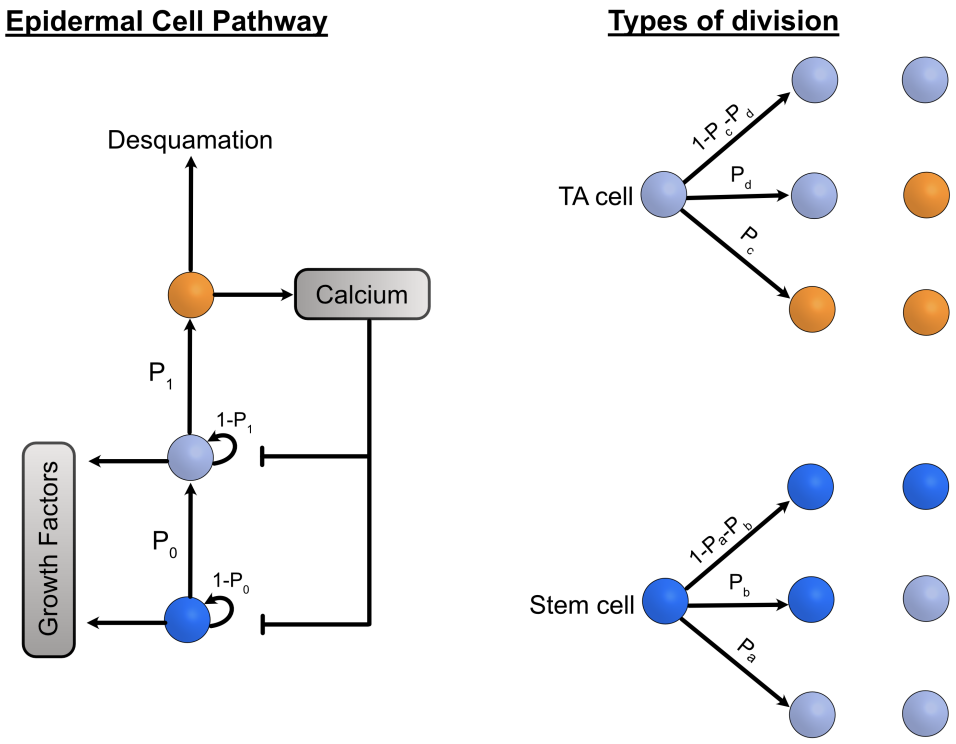

Figure 4.3: (Left) Description of the epidermal cell pathway from a stem cell (in dark blue). Stem and TA cells growth and divide to either one of the three division methods mentioned in Figure 2.2 where their probabilities to have a daughter cell of a different type (i.e. TA or differentiated cell, respectively) is $P0$ and $P1$ while having a daughter of the same type is 1 - $P0$. Stem and TA cells produce growth factors that drive their growth and proliferation and differentiated cells secrete calcium which inhibits stem and TA cells growth in order to maintain a steady state. (Right) Stem and TA cell division can be divided further to the three different ways and are based on the probabilities Pa, Pb for stem cells and Pc, Pd for TA cells. The probabilities derived for stem cell were based on an estimate during a parameter scan with TA cell division probabilities based on a previous paper [2], which traced epidermal cell proliferation lineage. As the paper traced the lineage of proliferative cells differentiation, it is assumed that the rates are for TA cells in the model.

with just stem cells, self proliferation occurs at the faster rate and once the model reaches a steady state, the model switches to a balanced stage to maintain the cell density at a steady state. Equation 4.3 describes the division equations used for stem (Pa and Pb) and TA (Pc and Pd) cells.

$$\begin{aligned} Pa &= Pa_e + Pa_b \frac{S_{ca}}{Ks_{ca} + S_{ca}} \\ Pb &= Pb_e + Pb_b \frac{S_{ca}}{Ks_{ca} + S_{ca}} \\ Pc &= Pc_e + Pc_b \frac{S_{ca}}{Ks_{ca} + S_{ca}} \\ Pd &= Pd_e + Pd_b \frac{S_{ca}}{Ks_{ca} + S_{ca}} \end{aligned} \tag{4.3}$$

where Pa and Pc represent symmetric division and Pb and Pd represent asymmetric division while the remainder is self proliferation. The first variable (i.e. Pa_e, Pb_e, Pc_e, Pd_e) in the equation is the probability used during the expanding state to get the model to a steady state and switches to a balanced state with a different set of probabilities (i.e. Pa_b, Pb_b, Pc_b, Pd_b) governed by a Hill function based on the calcium concentration in the system.

TA cells are known to divide a finite number of times (4-5 times) before terminally differentiating [18, 20, 25]. An additional rule has been added to TA division, where the maximum number of times a TA cell can divide is 4, based on a previous model developed [18].

Endogenous Growth Factors and Calcium production

The Monod-based kinetics allows stem and TA cells to produce growth factors and differentiated cells to secrete calcium into the environment. The concept of growth factors production by stem and TA cells is based on an ODE model developed on [19] while calcium is stored in the proliferative cells as they grow, divide and terminally differentiate and gets secreted when a differentiated cell reaches the SG layer.

4.2.2 Physical Processes

The model consists of various physical processes to solve issues related to overlapping cells during growth and division, development of the rete pegs and the transition from normal to psoriatic state where there is morphological change to the shape and height of the rete pegs. In addition, different cell types have different cortical and adhesive forces [92, 93].

Formation of rete pegs and Stem cell initialisation

The structure of the basement membrane is known to be of a wave-like structure instead of a flat surface. To emulate this morphology, the formation of the rete pegs is assumed to be of a sine wave structure and made out of spherical agents holding the structure. The LAMMPS command "create_atoms" allows us to specify the x-,y-, and z-axis for atoms to be created based on region blocks and the wave was created using the following command as seen in Figure 4.4.

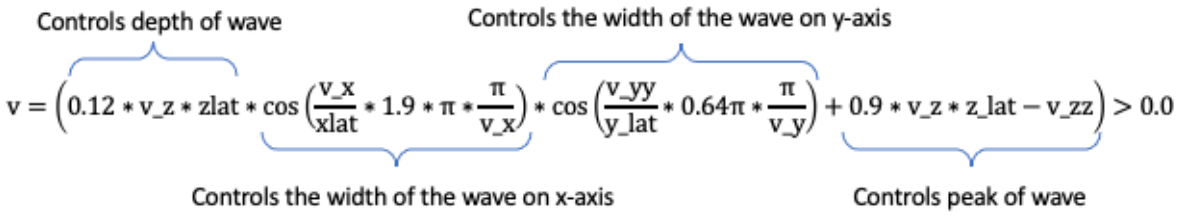

Figure 4.4: Description of the LAMMPS command used for wave-like basement membrane.

Figure 4.4 describes how the wave-like basement membrane is developed, where the variable v stores the formula to create the waves. The first part of the command, $0.12 * v\_z * zlat$, affects the depth of the wave while $cos(v\_xx/xlat * 1.9 * \pi * \pi/v\_x)$ affects the width of the wave on the x-axis. The second part, $cos(v\_yy/ylat * 0.64 * \pi * \pi/v\_y)$, controls width of the wave on the y-axis. Lastly, $0.9 * v\_z * zlat - v\_zz$, affects the top peaks of the waves. Having a larger value (i.e. more than 0.9), results in a flatter top.

As the basement membrane surface was no longer flat, stem cell initialisation had to be modified and a new fix was implemented to ensure that the stem cells were able to initialise on top of the basement membrane rather than having some cells initialised in the top peaks. A "fix" is a type of operation command in LAMMPS that can have multiple functions such as applying constraints to atoms, creating boundaries and so on and so forth. The fix is written in C++ and is part of the software's source code. This makes it cleaner and easier for the user to specify parameters in the input script rather than in the source code itself. The new fix I have implemented, fix_pso_atoms, consists of two additional functions added to the original source code to add atoms. The first function was to gather all the free locations on top of the basement membrane and the second function adds the stem cells specified on the free locations available.

The pseudocode is shown in Algorithms 1 and 2:

Algorithm 1: Get list of free locations for stem cell to initialise

Result: List of x-, y-, and z-coordinates of free location

```
// Array to hold the free locations available
free_location[];
// Array to store x-, y-, and z-coordinates of the available space
coord[3];
for i = 0; i < n; i++ do
    // If the top is empty (i.e.  z-axis), then add x-, y- and
       z-coordinates
    if z[i] == 0 then
        coord[1] = x[i];
        coord[2] = y[i];
        coord[3] = z[i];
        add.free_location[coord];
    end
end
```

The algorithm first looks to identify the free locations on top (i.e. z-height) of the basement membrane cells. If the top of the particular basement membrane cell, $z[i]$, is free, its coordinates, *coord*, are added to the list of free locations ($free\_location[]$). The function then returns a list of all the free locations that are available for a stem cell to be placed on top.

Algorithm 2: Initialising stem cell

Result: Add stem cell, where n is the total number of basement membrane cells, z[i] is the z-height of the current basement membrane.

```
// Shuffle the list of free locations to create randomness
free_location[].shuffle;
// Create a list based on the number of stem cells to initialise
stem_location[] = (free_location[0], free_location[0] + nstem);
// Loop through all the available stem cell location list
for j = 0; j < stem_location; j++ do
    // If the location is available, create a stem cell based on its
       diameter and place it on the z-axis (i.e. on top of the basement
       membrane)
    if stem_location[j] is available then
        z[j] = z[j] + diameter;
        add.stem[stem_location[j]];
    end
end
```

Once the list of free locations is obtained, the list is shuffled and a new list is created of the same size of the number of stem cells (nstem) to initialise ensuring that stem cells are randomly placed along the basement membrane surface. It then loops through the new list and places a stem cell right on top of the current basement membrane cell in the list.

Mechanical relaxation

During cell division, two cells are formed and may overlap each other and form two nicely separated and distinct cells. Hence, mechanical relaxation is required to update the cell's position to prevent this. Mechanical relaxation is done by using a discrete element method and the Newtonian equations of motion which can be found as part of the LAMMPS framework as a command. The following equation describes how the movement of cell is modelled [60]:

$$m_i \frac{d\overrightarrow{v_i}}{dt} = F_{c,i} + F_{a,i} + ... \tag{4.4}$$

where m_i is the mass and $\overrightarrow{v_i}$ is the velocity. As a cell divides, two types of forces act on each cell which are based on the contact and adhesive force.

The contact force $F_{c,i}$ is a pairwise force exerted on cells to resolve the overlapping issues and to ensure that cells do not enter the basement membrane. This is based on Hooke's law as follows [94]:

$$F_{c,i} = \sum_{j=1}^{N_i} (K_n \delta n_{i,j} - m_{i,j} \gamma_n v_{i,j}) \tag{4.5}$$

where N_i is the total number of neighbouring particles of i, K_n is the elastic constant for normal contact, $\delta n_{i,j}$ are the overlapping distance between the center of particle, i, and neighbouring particle, j, $m_{i,j}$ is the effective mass of particles i and j, γ_n is the viscoelastic damping constant for normal contact, and $v_{i,j}$ is the relative velocity of the two particles.

The adhesive force between basal cells, stem and TA cells, $F_{a,i}$ is the pairwise interaction modelled based on van der Waals force as follows [95] :

$$F_{a,i} = \sum_{j=1}^{N_i} \frac{H_a r_{i,j}}{12 h_{min,i,j}^2} n_{i,j} \tag{4.6}$$

where H_a is the Hamaker coefficient, $r_{i,j}$ is the effective outer-radius of particles i and j, and $h_{min,i,j}$ is the minimum separation distance of the two particles, and $n_{i,j}$ is the unit vector from particle i to j.

Table 4.1 summarises the mechanical interactions based on what type of cell it is interacting with.

Cell Type	**Repulsive force**	**Adhesive force**
Same cell type	+	++
SC-TA	+	+
TA-D	+	+
SC-D	++++	+
SC-BM	+	+++++
TA-BM	++	+++
D-BM	+++++	+

Table 4.1: Summary of forces between each cell type and between the basement membrane in the model where the strongest force is 5+ and the weakest force with just 1+. It has been noted in previous literature [96, 51] that stem cells have the strongest bond to the basement membrane. As it proliferates and differentiates, the attraction between the cell and the basement membrane weakens, allowing layer stratification to occur. The parameters for the model physical forces are input into a script where it makes use of the LAMMPS framework. The repulsive force is modelled based on Hooke's law [94] while adhesion is modelled based on van der Waals force [95].

Spatial regulation for cell division

Stem and TA cells are known to have different division directions such as horizontal or vertical. As stem cells reside only on top of the basement membrane, the division direction for daughter cells that are self cells will be horizontal from the parent cell's position, while the daughter TA cell would be placed vertically (Figure 4.5a). In TA cells, the division direction will mainly be vertical to ensure that differentiated cells are on top. However, this concept requires additional spatial regulation as the surface of the basement membrane is not flat but a wave. Figure 4.5b shows how division would occur on the wave surface according to the horizontal and vertical rules. The stem cell on top first self proliferates and produces two stem daughter cells. However, in the next division, one of the stem cells divides asymmetrically and produces a daughter TA cell which takes the parent's position while the daughter stem cell divides on top, thereby allowing stem cells to leave the SB layer.

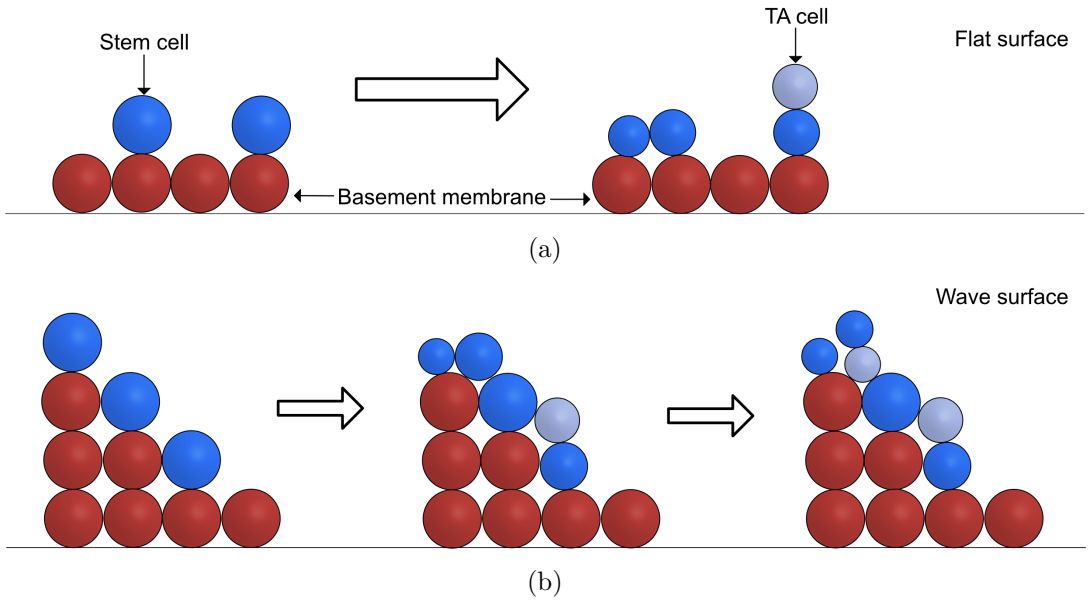

Figure 4.5: (a) Division direction for stem cells. If the stem cell undergoes self proliferation, it will divide horizontally while in asymmetric division, the TA daughter cell will be placed on top (i.e. vertically). This is straightforward if the basement membrane was a flat surface. (b) In the wave surface, a stem cell divides asymmetrically, a TA cell could be positioned on top of the basement membrane. However, there will be an issue if another stem cell around it divides to produce a daughter stem cell. The daughter stem cell, will end up positioned on top of the TA cell instead.

A solution to this is to include a check for stem and TA cells to be aware of their location, whether it is on top of the basement membrane or away from it. Figure 4.6 describes how different proliferative cell will divide.

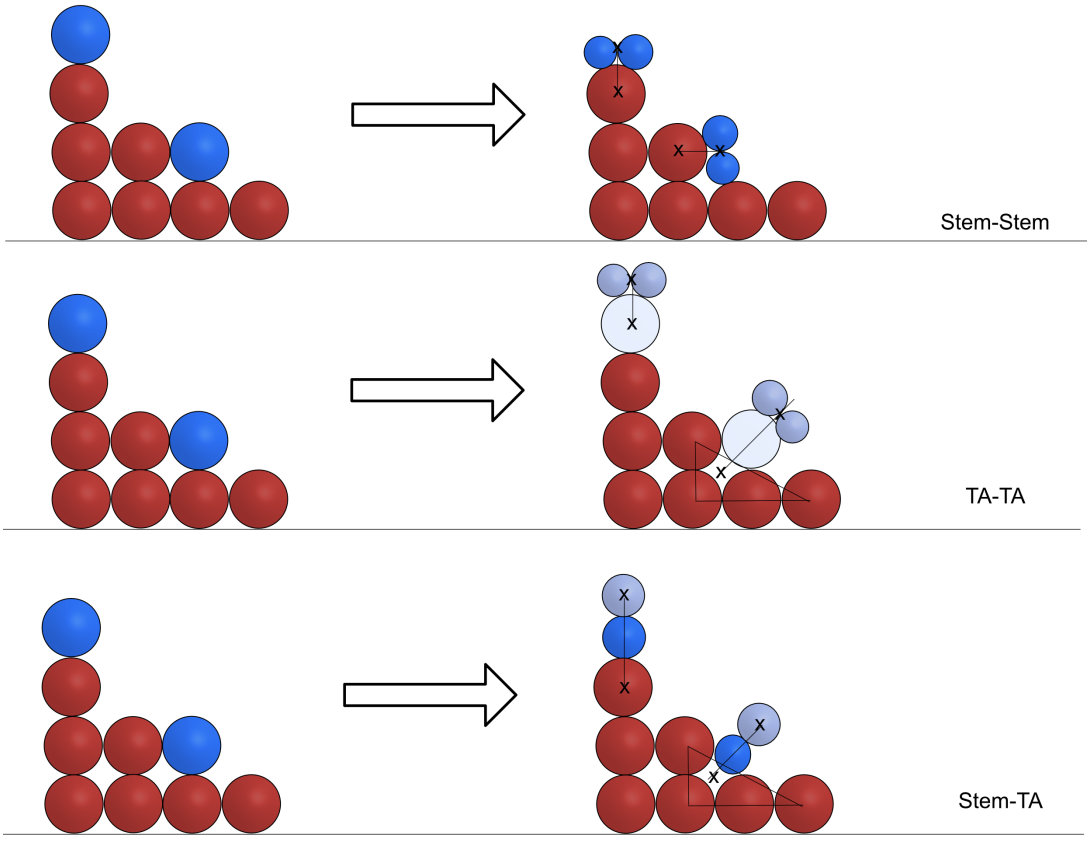

Figure 4.6: Schematic of spatial regulation implemented for stem cells. Self proliferation has been assumed to divide horizontally and TA daughter cells are assumed to be positioned vertically [97, 25, 98]. The concept of spatial regulation is based on these as follows: (Top) Stem cell self proliferation daughter cells are positioned side-by-side in the middle of the cell it is on top of. (Middle) Symmetric division behaves in a similar fashion when the division occurs on the top of the rete peg. If the cell was at the bottom of the rete peg, its position is calculated from the middle of the surrounding cells. (Bottom) Asymmetric division occurs in a similar fashion as symmetric, however, the daughter TA cell will always be on top of the daughter stem cell based on the assumption that TA cell will divide vertically.

4.2.3 Chemical processes

Immune cytokine and calcium transport is described by using the diffusion-advection-reaction equation. In this section, we will briefly discuss the main concepts behind the chemical processes involved such as singalling chemical and immune cytokine consumption and mass balance.

Chemical consumption

The rate of chemical consumption is based on the function available in NUFEB where chemical consumption of growth factors and calcium are based on their concentration within each voxel where the cell resides. The reaction rates are based on the Monod-based kinetics implemented in NUFEB [60] for microbial growth with a slight difference where the rate of growth is based on chemicals for epidermal growth and can be defined as follows:

$$R_i = \mu_i(\frac{1}{Y_i}(R1 + R2))X \tag{4.7}$$

where Y_i is the yield coefficient, $R1$ is the growth during the normal epidermal state and $R2$ is the growth during psoriasis and X is the biomass density.

Chemical mass balance

Chemical distribution within the simulation domain is calculated by solving a diffusion-advection-reaction equation (transport equation) implemented in NUFEB [60] for the signalling chemicals as follows:

$$\frac{\partial S}{\partial t} + \overrightarrow{\mathrm{U}}.\nabla S = \nabla.(D_e \nabla S) + R \tag{4.8}$$

where the chemical update, R, is calculated in the growth model, S is the chemical involved. In this case, it is either calcium, growth factors or immune cytokines.

The equation above is discretised on a Marker-And-Cell (MAC) uniform grid where the scalar S, is defined at the centre of voxel and velocity components U for x-, y- and z-axes are defined at the centre of the 6 faces of the voxel. The time derivative and spatial derivative are discretised by the Forward Euler and Central Finite Differences respectively.

4.3 Results

4.3.1 Rete Peg Formation and Stem Cell initialisation

The rete peg formation was based on the sine wave formation specified in Section 4.2.2. A new fix command was implemented based on Algorithms 1 and 2 to ensure that stem cells were only initialised on top of the basement membrane. The new fix command stores a list of the available locations on top of the basement membrane and randomly adds the stem cells on top of it by shuffling the free locations list and having a new list with the available locations the same size as the number of stem cells initialised. Figure 4.7 shows the basement membrane (in orange) and stem cells (in dark blue) at the start of the simulation. The rete pegs in the normal epidermis will remain in place as cell population increases as seen in Figure 4.9a.

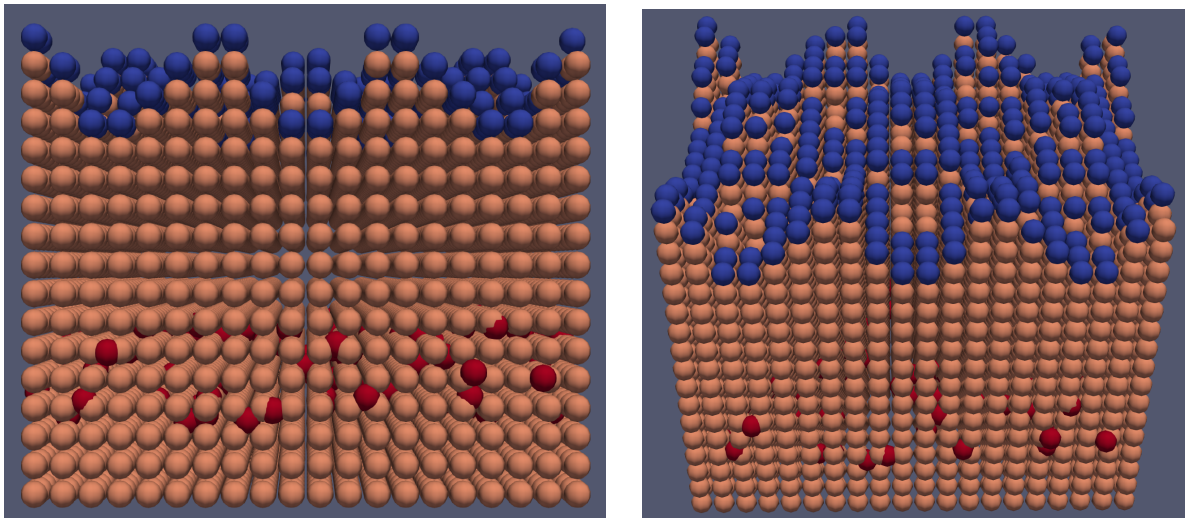

(a) (b)

Figure 4.7: Screenshot of the wave formation use in the model. The basement membrane (in orange) is formed by creating atoms using the LAMMPS command "*create_atoms* and the structure is fixed to ensure that no movement occurs during epidermal growth. Stem cells (in dark blue) are initialised on top of the basement membrane based on the free locations available with small amounts of T cells (in red) initialised in the basement membrane.

4.3.2 Number of stem cells to initialise

The number of stem cells initialised in the system has been tested from a range of 100 to 317 cells at intervals of +10 cells initially and further refined to +5 cells step. The maximum number of stem cells that can be initialised to cover the entire surface of the basement membrane is 317. If more than 317 stem cells are initialised, they are "removed" from the system as there is insufficient space for them to be placed on top of the basement membrane. The results showed

that for the ideal cell densities to populate the epidermis, the number of stem cells required for initialisation is found to be between 260 to 317 cells. If less than 260 stem cells are initialised, the model fails to reach the ideal cell densities and proportions reported in previous studies where the estimates cell population ratio was 4.7%, 26.4% and 40-66% for stem, TA and differentiated cells respectively [80, 18]. Table 4.2 summarises the average results for stem cell initialised from 100 to 300 (in steps of 50).

Stem cells initialised	**Stem cells (%)**	**TA cells (%)**	**Differentiated cells (%)**
100	306 (3.2)	1,500 (15.8)	7,526 (79.4)
150	365 (3.7)	1,678 (16.8)	7,803 (78.1)
200	482 (4.1)	2,369 (20.4)	8,618 (74.2)
250	594 (4.5)	3,033 (22.8)	9,544 (71.6)
300	729 (4.6)	4,053 (25.4)	11,039 (69.1)

Table 4.2: Average cell population where the number of stem cells initialised are from 100 to 300, in steps of 50. The average cell population were calculated based on ten simulation runs. If the number of stem cells initialised was too low, it does not reach the known ideal cell population ratio of approximately 4-, 24-, 65% for stem, TA and differentiated cells, respectively.

In addition, stem cells were randomly initialised on the basement membrane surface and no specific location is set. Previous studies on stem cell location report conflicting results which show stem cells either residing at the bottom or top of the rete pegs. In this work, the location of stem cells was randomly initialised due to two main reasons. Firstly, the model starts off with the basement membrane shaped as a wave structure, which means that the stem cell growth and division did not form this irregular shape as compared to embryonic studies which looked at how the epidermis was formed from the beginning of time. Secondly, as mentioned earlier, this model does not study how the epidermis forms from an embryo. Therefore, the number of stem cells has to start at a larger number to obtain a well and ideally proportioned epidermis with all three types of cells as stem cell growth is slower than TA cells. It has also been noted in the model output that although the stem cells are initialized at random throughout the basement membrane, the steady state model shows that majority of the stem cells resides at the bottom of the rete pegs. This behaviour observed could explain previously published studies [99, 100, 101] where they have found stem cells mostly residing in the bulge of hair follicles. Previous studies [99, 100, 101] suggested that the bulge in hair follicles represents a major repository of keratinocyte stem cells as it does not only give rise to the hair follicle but the epidermal structure. Hence, the model's output can be supported by this observation in previous studies on why stem cells mostly reside at the bottom of the rete ridges rather than

the top as hair follicles would be found beneath the epidermis.

4.3.3 Cell division probabilities

Chapter 1 and 3 describe the rate of actively dividing stem and TA cells and how it differs slightly when stem cells divide at a slower pace as compared to TA cells. In our model, we adapt this concept based on [2] where they have labelled and measured the types of division that occur. They have also identified how proliferative keratinocytes have two convertible proliferative states - balanced and expanding states. During the development of epidermis, the skin enters an expanding state where proliferation occurs at a higher rate and eventually enters a steady state and converts to the balanced state. Both states have different probabilities for each type of division. Here, we adapt this concept and base the division probabilities found in this study for TA cells. The reason for doing so is due to the fact that in the study [2], there is no differentiation between the types of proliferative cells (i.e. stem and TA cell types). The cell is either a proliferative or differentiated cell. The proliferative cell eventually terminally differentiates, a similar behaviour to TA cells, after a set number of divisions. Therefore, the parameter is not a good representative of how stem cells divide. In addition, other clinical studies have shown that only about 5% of stem cells are actively cycling at any time. Hence, parameter estimation is required for stem cell division probabilities, $P0$, Pa and Pb (see Figure 4.5 and Equation 4.3), where $P0$ in balanced state is assumed to be 0.5 as there will be an equal rate of stem and TA cell produced.

Based on the above assumption where $P0$ is 0.5 in the balanced state, the values for $P0$ in expanding state tested are from 0.1 to 0.4, in 0.05 steps. The value for Pa and Pb are based on previous studies on proliferative cell division probabilities, where self and symmetric proliferation are equal and are approximately 10% with asymmetric division at 80% [20, 98, 97]. Parameter estimation for Pb was done in steps of 0.1, while Pa was 0.05 in both the expanding and balanced state (see Table 4.3).

The results can be seen in Figure 4.10, where the parameters found to maintain a steady state and obtain the ideal cell population ratio that was within the normal range are $Pa_e = 0.05$, $Pa_b = 0.05$, $Pb_e = 0.1$, and $Pb_b = 0.7$.

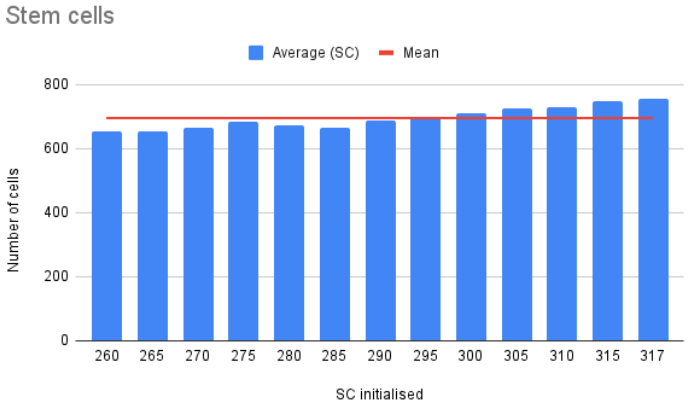

(a)

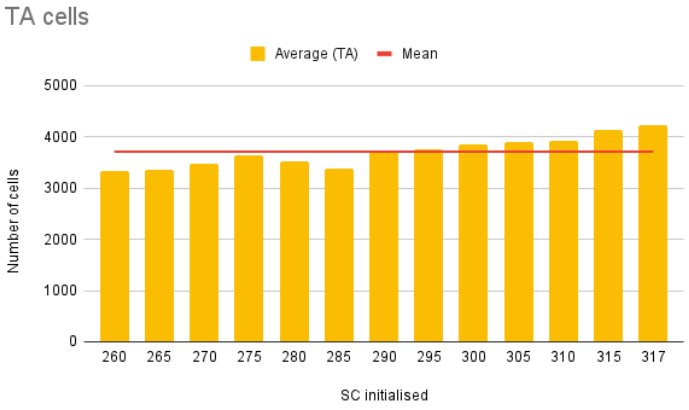

(b)

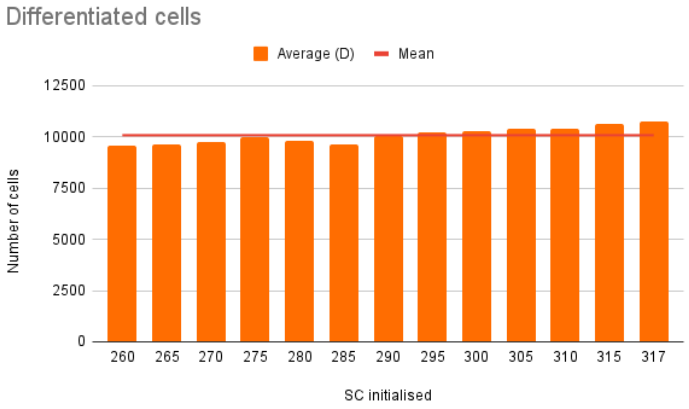

(c)

Figure 4.8: Average cell population based on the number of stem cells initialised where the best range was found to be between 260 to 317 stem cells initialised. (a) Stem cell population in steady state. (b) TA cell population in steady state. (c) Differentiated cell population in steady state. The average out of all simulations are represented by the horizontal line in the plots, where the average numbers are 695, 3,709, and 10,080 for stem, TA and differentiated cells respectively. The results obtained were measured based on an average run of 10 simulations for each test case. Table 4.4 summarises the parameters used. Legend: Average (SC, TA, D) refers to the average number of cells out of 10 simulation runs. Mean refers to the average number of cells based on the number of stem cells initialised.

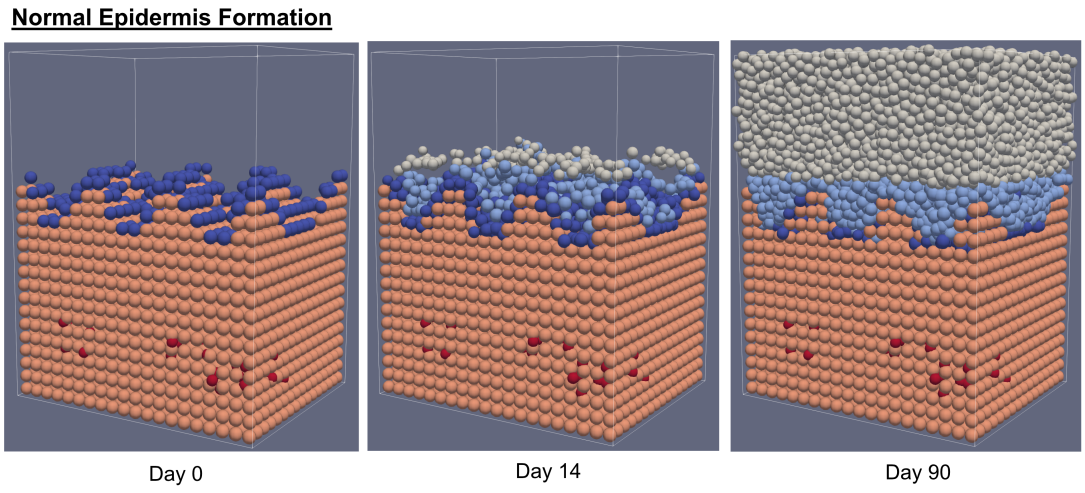

(a)

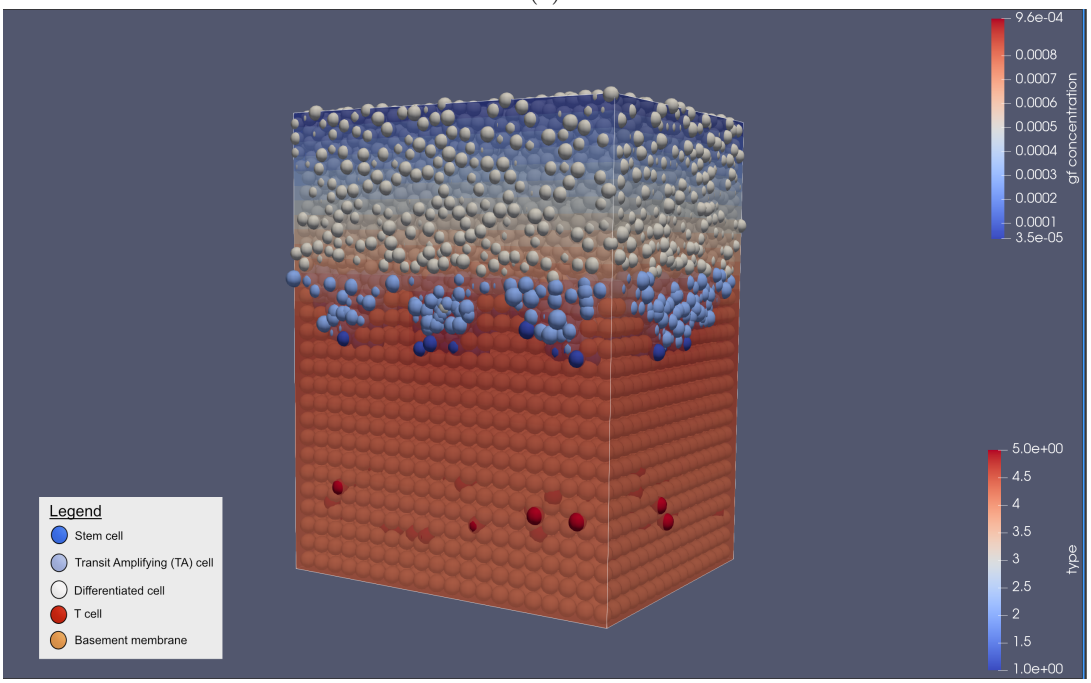

(b)

Figure 4.9: Visualisation output from the model. (a) Snapshot of the model at three different time points (Day 0, 6 and 30). (b) Snapshot of diffusion gradient in the model. In this case, growth factor, with the highest concentration being around the stratum basale layer where stem and most TA cells reside. Cells represented: stem cells (in dark blue), TA cells (in light blue), differentiated cells (in white), T cells (in red) and basement membrane (in orange). The heat map on the top represents the concentration of growth factors while the heat map on the bottom represents the colors used for each cell types. For example, stem cells are represented in dark blue.

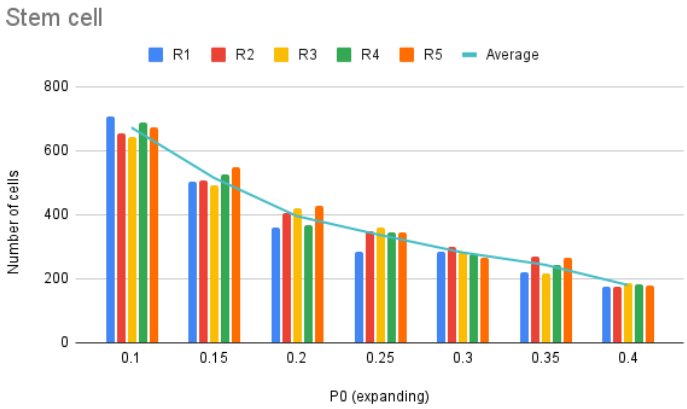

(a)

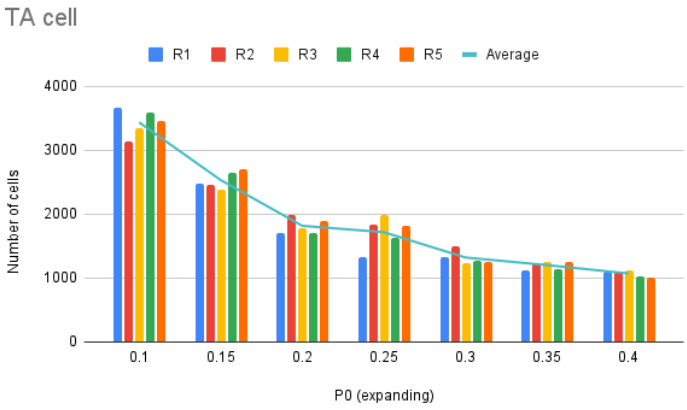

(b)

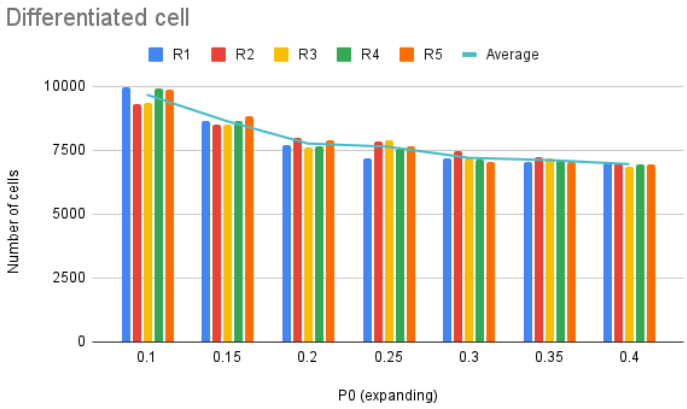

(c)

Figure 4.10: Average cell population based on the parameter estimation for $P0$. The best range was found to be 0.1, which produced the highest number of cell population. (a) Stem cell population in steady state. (b) TA cell population in steady state. (c) Differentiated cell population in steady state. The average out of each test case is represented by the horizontal line in the plots each cell type. The results obtained were measured based on an average run of 5 simulations (R1-R5) for each test case. Table 4.4 summarises the parameters used.

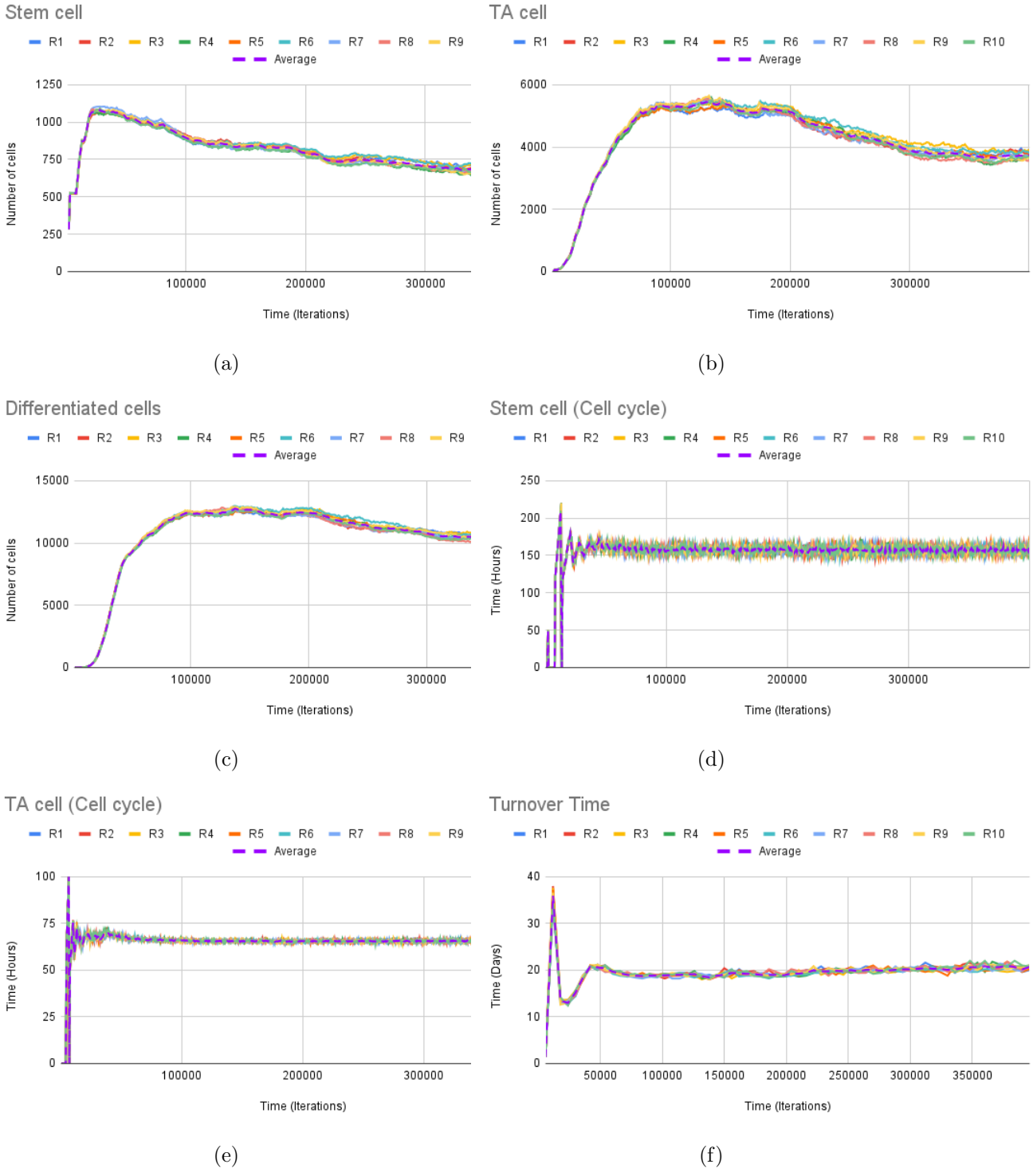

Figure 4.11: Cell numbers plot of stem cells (a), TA cells (b) and differentiated cells (c). The average ratio of stem, TA and differentiated cells are 4.49% (693), 24.3% (3,751) and 67.98% (10, 494), respectively. (d-e) Cell cycle for stem (d) and TA cells (e). The average cell cycle times predicted are 157.2 and 65.5 hours, respectively. (f) Total turnover times for both proliferative and differentiated compartment. The average turnover time in the model is 20.5 days in the steady state. The simulations were ran 10 times under different random seed (R1-10) with the average plotted in purple dotted line. Each simulation ran under the same initial conditions such as the extracellular calcium diffused, growth rates, and diffusion rates. Table 4.4 summarises the parameters used.

Pa_e	Pa_b	Pb_e	Pb_b	$P0_e$
0.05	0.05	0.1	0.7	0.1
0.05	0.05	0.2	0.6	0.15
0.05	0.05	0.3	0.5	0.2
0.05	0.05	0.4	0.4	0.25
0.05	0.05	0.5	0.3	0.3
0.05	0.05	0.6	0.2	0.35
0.05	0.05	0.7	0.1	0.4

Table 4.3: Values tested for parameter estimation of stem cell division probabilities $P0$, Pa and Pb in both expanding and balanced state, where $P0$ in balanced state is assumed to be 0.5 once the model reaches a steady state.

4.3.4 Cell population density

The cell population density reported in previous studies was of $73{,}952 \pm 19{,}426$ $cells/mm^2$ (SD) [80] with each cell population ratio estimated at 4.7%, 26.4% and 40-66% of them being stem, TA and differentiated cells respectively with keratinocytes comprising of 96% of all epidermal cells [18]. As the model only takes keratinocytes into account, the model has a cell population ratio of 4.49% stem cells, 24.3% TA cells and 67.98% differentiated cells, which translates to the cell population ratio of keratinocytes being 4.3%, 23.33% and 65.2%.

4.3.5 Cell cycle and Turnover times

The reported cell cycle times in clinical studies were found to be between 100-200 hours [29, 18] and 50-65 [80, 18] hours in stem and TA cells respectively. The measured cell cycle time range in the model was between 152.9 to 162.0 hours for stem cells and 65.0 to 66.0 hours for TA cells with an average of 157.2 and 65 hours, respectively.

The turnover time is calculated based on [56, 40] and [30] where the total epidermal turnover time is the sum of the proliferative and differentiated compartment. Each compartment's turnover time is based on Equation 4.9. Hence, giving us Equation 4.10.

$$\frac{\text{Total number of cells in compartment}}{\text{Newly entering cells in compartment}} \tag{4.9}$$

$$\frac{SC + TA}{selfsc + asymsc + 2symsc + selfta} + \frac{D}{asymta + 2symta} \tag{4.10}$$

where the first term is for the proliferative compartment, stem and TA cells, and the second term is for the differentiated compartment, differentiated cells. Variables $self_x$, $asym_x$ and $2sym_x$

represent the three types of division modelled, self-proliferation, asymmetric and symmetric division while x represents the cell undergoing division, which could either be a stem (SC) or TA (TA) cell. It is also important to note that symmetric division produces two daughter cells of a different type from the mother cell, hence, producing two cells for that compartment. For example, $2sym_{sc}$ will produce two TA cells from a stem cell, in the proliferative compartment.

In this work, the stratum corneum is not modelled and therefore, the model only takes into account the proliferative and differentiated compartments. Therefore, the model predicts the total turnover times to be between 19.6 and 21.3 days with an average of 20.5 days, slightly lower than the measured 23-25 days in [31].

4.3.6 Parameters

Normal epidermis				
Parameter description	**Parameter**	**Value**	**Units**	**Reference**
Stem cells initialised	SC_{init}	290	Cells	Assumed
SC maximum growth rate	SC μ_{max}	1.28e-06	s^{-1}	Modified from [18]
TA maximum growth rate	TA μ_{max}	3.21e-06	s^{-1}	Modified from [18]
Ks value for growth factor	Ks_{gf}	2.5e-7	kgm^3	Assumed
Ks value for calcium	Ks_{ca}	2.5e-3	kgm^3	Assumed
SC symmetric division in expanding stage	Pa_e	0.05	-	Assumed
SC symmetric division in balanced stage	Pa_b	0.05	-	Assumed
SC asymmetric division in expanding stage	Pb_e	0.1	-	Assumed
SC asymmetric division in balanced stage	Pb_b	0.7	-	Assumed
TA symmetric division in expanding stage	Pc_e	0.02	-	[2]
TA symmetric division in balanced stage	Pc_b	0.32	-	[2]
TA asymmetric division in expanding stage	Pd_e	0.1	-	[2]
TA asymmetric division in balanced stage	Pd_b	0.18	-	[2]
Maximum TA division	max_{TA}	4	-	[18]
Diffusion coefficient	Ks	1.0e-9	m^2s^{-1}	[102]
Extracellular Calcium initialised	eCa^{2+}	1.0e-7	kgm^3	[54]

Table 4.4: Model parameters and initial conditions for the normal epidermis formation.

The parameters used in the normal epidermis formation can be found in Table 4.4. The assumed parameters are described as follows:

- The number of stem cells initialised and division probabilities for stem cells were based on the parameter scans as described earlier in this chapter. The parameters were chosen based on known results such as the cell population ratio, cell cycle and turnover times.
- The maximum growth rate, μ_{max}, for stem and TA cell was based on the conversion

from the cell cycle times known in literature [18, 29] and 2D model in Chapter 3. The conversion was done using the following equation from [103]:

$$\mu_{max} = \frac{\ln 2}{t_d} \tag{4.11}$$

where t_d is the doubling time.

- The stem cell division probabilities were calculated based on a parameter scan described earlier in this chapter. The parameters were chosen based on the known results such as the cell cycle and turnover times while being able to produce the ideal cell population ratio.

- The maximum number of times TA cell can divide has been set to 4, similar to the 2D model implementation in Chapter 3.

4.4 Conclusion

The development of a 3D normal epidermal model aimed to address some of the disadvantages and limitations of the 2D model as described in Chapter 3. A limitation as mentioned was how the 2D model was that the number of cells in both normal and psoriatic state was always fixed and reached the maximum of 724 and 1500. Another main disadvantage which led to the development of a new framework is the time taken to run a simulation where it could take up to 24 hours.

The new 3D model framework is built using LAMMPS and NUFEB where implementation of physical and some biological processes has already been built in. The new model takes into account the physical, chemical and biological processes known in literature and the spatial aspects of cellular behaviours. The model also takes into account how the basement membrane is not a flat surface but rather an irregular, wave-like surface as seen in Figure 4.5b. An additional feature for the spatial regulation of stem cell division has been implemented to model the horizontal division that occurs for stem cells as seen in Figure 4.6.

Previous studies [18, 19] have shown that the cell population ratio of keratinocytes are approximately 4-,24-, and 65-% for stem, TA and differentiated cells, respectively. When identifying the number of stem cells required to be initialised, this proportion was used as a gauge. It was found that the number of stem cells required to be initialised had to be more than 260

for this proportion to be reached. This could be due to the fact that the model does not start from an embryonic state but rather from an adult epidermis and requires a much higher amount of stem cells to be initialised.

The model has been able to predict an average cell cycle time of 157.2 and 65.5 hours for stem and TA cells, respectively, in line with clinical data [29, 80, 18]. The turnover times are within the lower bounds known in literature with an average of 20.5 days in the steady state. This could be due to the way the model has been presented where the compartments we are mainly concerned are the proliferative and differentiated compartment and does not represent all layers in the epidermis such as the stratum corneum.

Chapter 5

Psoriatic Epidermal Formation

5.1 Introduction

The previous Chapter 4, describes how the normal 3D epidermis model was implemented and developed in NUFEB and how it solves some of the challenges faced by the 2D model. The 3D model took into account some of the additional aspects of how the skin develops in reality. This includes having a wave-like structure to depict the basement membrane and having specific nutrients for the proliferative cells, stem and TA, to grow and divide. This chapter follows the next step of the model where the normal epidermis transitions to psoriasis.

In the model, psoriasis occurs with the introduction of an abnormal immune response in the epidermis. This causes the T cells, located in the basement membrane and dermis, to activate when an immune response is triggered. The T cells secrete immune cytokines into the epidermis, altering the proliferative state of keratinocytes, stem and TA cells, to hyperproliferate (i.e. to divide at an abnormally higher rate). T cells can be categorised into different types and each type produces a particular type of immune cytokine which reacts to different triggers. For example, in the case of psoriasis, some of the known cytokines produced are IL-17, IL-22 [104], and TNF-α [19, 105].

The immune cytokine chosen is a general label based on a previous mathematical study, where IL-22 and TNFα were modelled as they have been known to influence hyperproliferation in epidermal stem and TA cells [19]. In that study, the amount of both immune cytokines, IL-22 and TNF-α, were almost identical in concentration. Therefore, the immune cytokine stimulus have been simplified to just a single stimulus in this model. Figure 2.4 in Chapter 1, describes the schematics of how psoriasis develops when an immune stimulus is introduced from

the basement membrane and regulated by T cells to produce cytokines. These cytokines cause stem and TA cells to hyperproliferate causing psoriasis.

In addition, hyperproliferation not only causes an increase in cell density in the epidermis but a change in its structure, as well [104]. Figure 5.1 shows the immunofluorescence of proliferative cells in the epidermis in psoriasis. Immunofluorescing CD44 and p63 represent stem cells while K10 represents TA cells and shows the difference between control (i.e. healthy skin) and psoriasis. The number of cells highlighted has not only increased but the structure has changed significantly, producing a thicker epidermis and rete ridges which are thicker with a slightly flatter base as well. This is due to the fact that more cells are produced during this process, the forces between the cells start pushing downwards, resulting in deeper rete ridges and thickening of the skin. The model mimics this behaviour and structure as described earlier in Figure 2.4.

In order to simulate hyperproliferation from the normal epidermis, the immune cytokine stimulus needs to revert the division model, as mentioned in Chapter 4, back to its expanding state.

The following behaviours and assumptions have been added to mimic the way psoriasis develops:

- Increase amount of T cells introduced in the system [19].
- Flexible basement membrane and dermis to increase epidermal height and deeper rete ridges [18, 38, 104].
- Introduction of immune cytokine stimulus to trigger hyperproliferation in stem and TA cells [19, 104, 106].
- Cytokines are introduced once the normal epidermis reaches a steady state by using a separate script and are maintained by the introduction of T cells [18, 19].
- Cell growth rate parameters remain the same as normal epidermis [18, 19, 50].
- Cell division probabilities differ from the normal epidermis [2, 107, 108] due a change in starting state (i.e. normal epidermis formation starts from just stem cells). Chapter 6 describes this in detail.
- To push the model back into an expanding state, the cytokines concentration initialised is

of a higher dose as compared to what is found in literature. This ensures hyperproliferation occurs in the model [18, 19, 106].

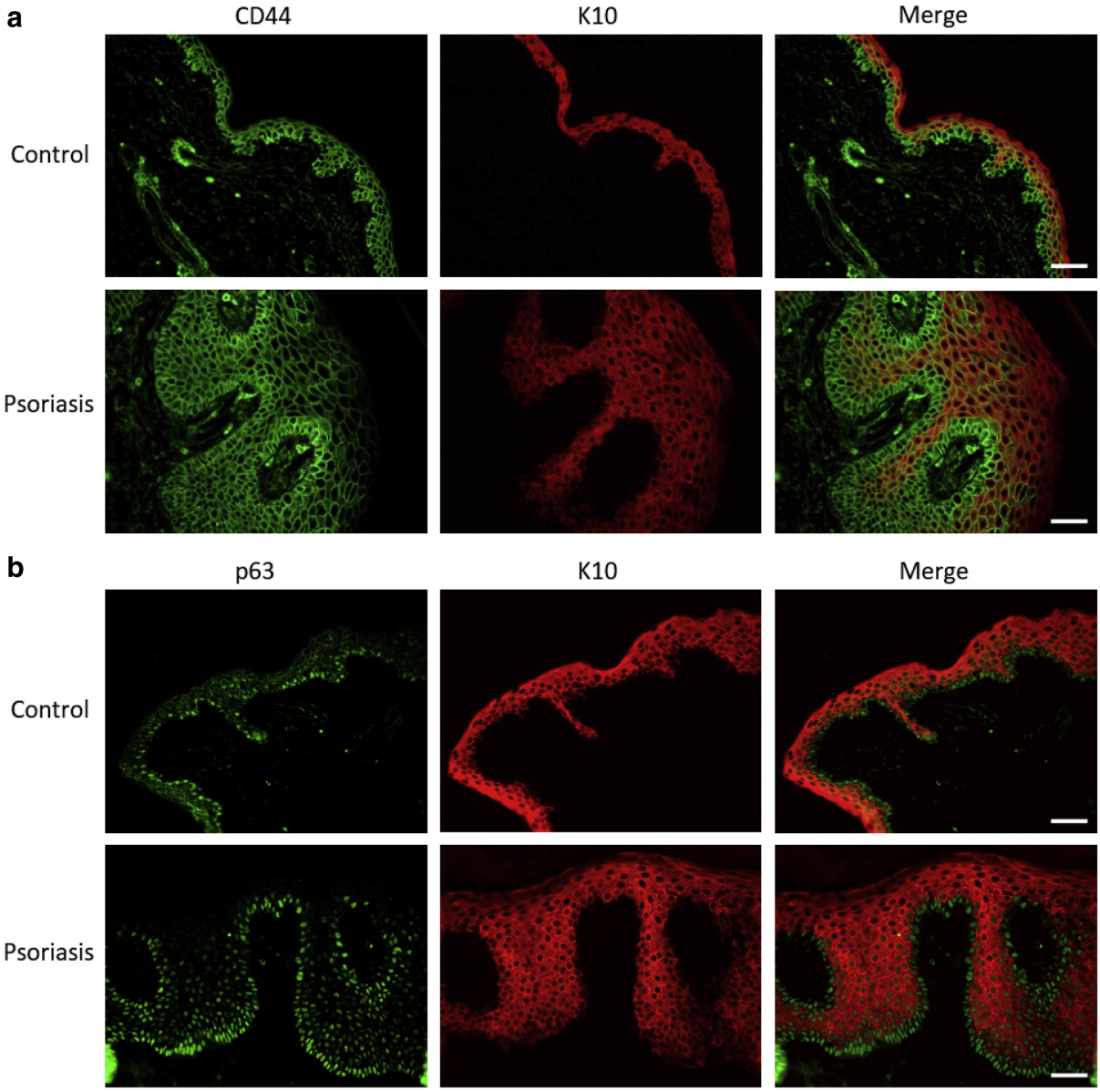

Figure 5.1: Figure adapted from [104]. Double immunofluorescence of psoriatic skin showing the co-localisation of (a) CD44 (in green) and (b) p63 (in green) and K10 (in red) in control and psoriatic skin, where CD44 and p64 represent stem cells and K10 represents cells in the suprabasal layer (i.e. TA and differentiated cells). The column on the right shows the merged stainings. Images represent three experiments.

Similar to how the normal epidermis is developed, Figure 5.2 summarises how the normal epidermis transitions to psoriasis based on the type of cell it is. Unlike in the normal epidermis, there is an additional signalling chemical added to the system, immune cytokine stimulus. The cytokine stimulus is diffused into the system which signals to the proliferative cells to grow, divide and eventually terminally differentiate. Once terminally differentiated, the differenti-

ated cell will migrate upwards as the epidermis grows and eventually reach the stage of cell desquamation and end of the cell's lifespan.

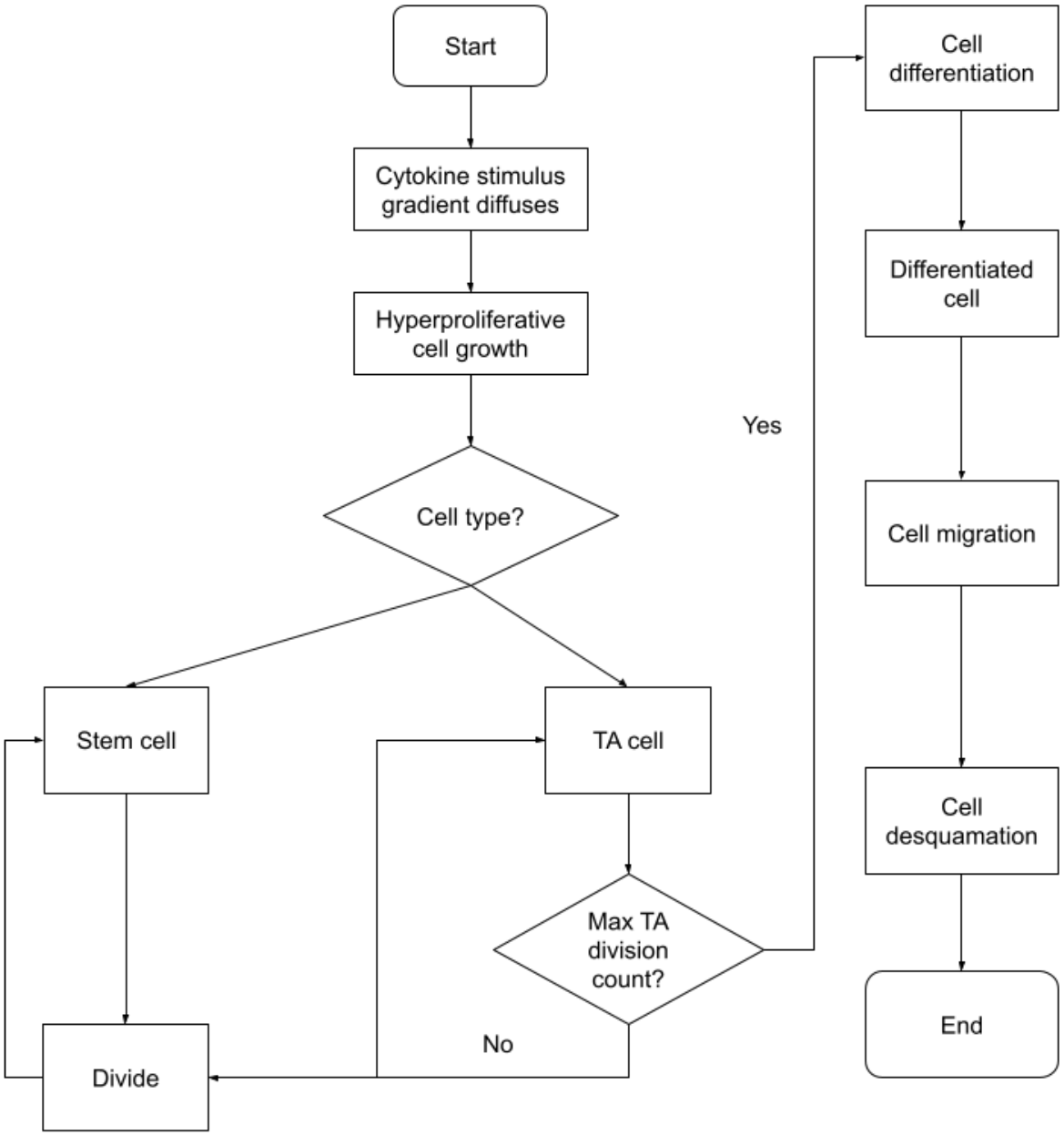

Figure 5.2: Flow chart summarising how the epidermis transitions to psoriasis based on what cell type it is. It describes how proliferative cells hyperproliferate due to the diffusion of immune cytokines and eventually terminally differentiating. Once it has terminally differentiated, it will migrate upwards and end its lifespan after it has been desquamated, similar to the normal epidermis.

5.2 Methods

The simulation flow is similar to the normal epidermis as summarised in Figure 4.2 where the simulation starts and chemical diffusion occurs, cells start to grow and proliferate and eventually terminally differentiating. Physical processes solves some of the issues that can occur during cell division such as overlapping of cells and ensuring layer stratification. The biological and chemical processes are similar to the normal epidermal model with some additions that will be further discussed in this section. The physical processes have been altered to take into account how the rete ridges deepen while hyperproliferation occurs. This is done to ensure that the wave-like shape is maintained as much as possible and to prevent the rete ridges from flattening out.

5.2.1 Biological Processes

Psoriasis is modelled by activating an immune cytokine stimulus such as IL-22 and TNFα into the model, which causes an onset between 7 days to 14 weeks and a time lag between the time the patient gets an immunological response (such as from a streptococcal sore throat) to the appearance of the disease itself [18, 109, 110]. In this model, the immune cytokine stimuli is induced for a total of 7 days following the previously developed ODE model [19].

The growth rate of proliferative keratinocytes and differentiation in the psoriatic state increases by approximately three times in stem and TA in the model, which is similar to previous experimental data. In vivo experiments showed that the number of proliferating keratinocytes increases by 2-3 times to 6-8 times in psoriasis [28, 42]. This results in a 2-5 times increase in cell population [31, 82]. In this model, the increase in cell population, cell cycle and turnover times are predicted to be approximately 3-times than normal and are controlled by an "activator" switch that alters both the growth and division model from Chapter 4 as follows:

$$\begin{aligned}\frac{dSC}{dt} &= (3 * \mu_{max}\frac{S_{gf}}{Ks_{gf}+S_{gf}}\frac{Ks_{ca}}{S_{ca}+Ks_{ca}} + (\frac{S_{stim}}{Ks_{stim}+S_{stim}})^2)SC,\\ \frac{dTA}{dt} &= (3 * \mu_{max}\frac{S_{gf}}{Ks_{gf}+S_{gf}}\frac{Ks_{ca}}{S_{ca}+Ks_{ca}} + (\frac{S_{stim}}{Ks_{stim}+S_{stim}})^2)TA\end{aligned} \tag{5.1}$$

where the addition of cytokines stimulus, $stim$, into the growth equation, Equation 4.2, for stem and TA cell growth.

$$
\begin{aligned}
Pa &= Pa_e + Pa_b\left(\frac{S_{ca}}{Ks_{ca} + S_{ca}} - \frac{S_{stim}}{Ks_{stim} + S_{stim}}\right),\\
Pb &= Pb_e + Pb_b\left(\frac{S_{ca}}{Ks_{ca} + S_{ca}} - \frac{S_{stim}}{Ks_{stim} + S_{stim}}\right),\\
Pc &= Pc_e + Pc_b\left(\frac{S_{ca}}{Ks_{ca} + S_{ca}} - \frac{S_{stim}}{Ks_{stim} + S_{stim}}\right),\\
Pd &= Pd_e + Pd_b\left(\frac{S_{ca}}{Ks_{ca} + S_{ca}} - \frac{S_{stim}}{Ks_{stim} + S_{stim}}\right),
\end{aligned}
\tag{5.2}
$$

The division model from Equation 4.3, on the other hand, immune stimulus, *stim*, causes the model to go back into an expanding state resulting in hyperproliferation (see Figure 2.4).

5.2.2 Physical processes

The transition from normal and psoriatic epidermis results in a change to the epidermal structure causing the structure to be thicker and having deeper rete ridges.

Although there have been studies on identifying how the rete ridges form in the epidermis, the main cause it still unknown. In a study [111] on rete ridges in the oral cavity, the results showed that rete ridges form due to the sucking action in the mouth as a baby. This sucking action along with a higher density of stem cells causes a change in the oral cavity and forms the rete ridges. The depth of rete ridges is determined by the density of stem cells. Hence, the higher the stem cell density, the deeper the rete ridges. A similar mechanism of action can be assumed in the case of the skin, where physical forces come to play, causing rete ridges to form in the epidermis.

The model assumes a similar mechanism where mechanical forces are used to mimick this "sucking" action causing the deepening of rete ridges during psoriasis. To model these changes, the following changes have been made when switching states:

- Unfreeze the basement membrane to allow the deepening of rete ridges.
- Additional forces applied to stem and TA cells to ensure that these cells remains in the lower epidermal layers as the rete ridges start to deepen (Figure 5.3).
- An increase in height of the domain box to simulate a thicker epidermis.

In addition, to ensure that the wave shape is maintained in the model, the basement membrane has been sub-divided into different regions where the peaks and toughs of the waves are

sub-divided into columns. The column regions with the peaks are "frozen" in place to ensure that only the toughs are deepened, hence, producing deeper rete ridges.

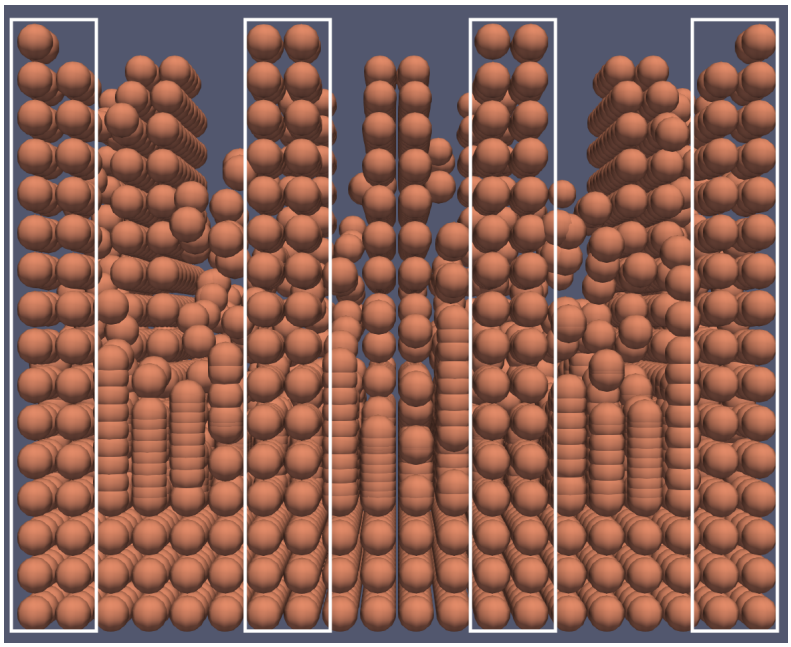

(a)

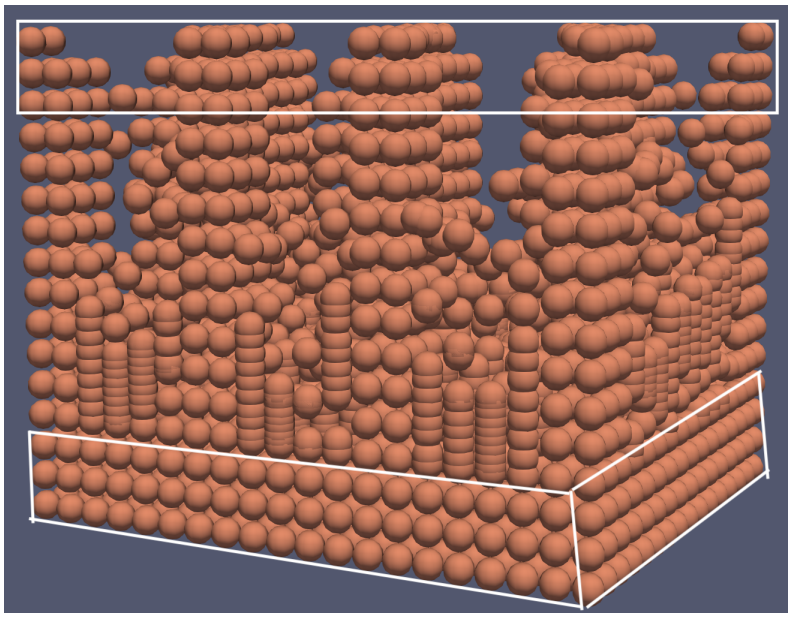

(b)

Figure 5.3: Regions highlighted in the white boxes where basement membrane (in orange) are "frozen" to ensure that wave shape is maintained when transitioning to psoriasis. (a) Peak columns are frozen to ensure that only the toughs of the wave moves. Hence, producing the deepening of rete pegs as more cells are produced in the epidermis. (b) The top and bottom of the rete pegs are "frozen" to ensure the wave shape is maintained. The top of the rete peg also has an additional adhesive force between stem and TA cells during the transitional state. This ensure that stem cells remain on top of the basement membrane and for TA cells to remain in the lower layers of the epidermis.

Alterations to TA cell division

The transition from normal and psoriasis development differs slightly as the model does not start off with a clean slate of just stem cells but rather a domain filled with the various cell types. In addition to the difference in starting state, TA cells may also reside in the stratum basale layer which lies in the rete ridges. Hence, additional rules applied to TA cells are required to ensure that 1. TA cells do not push sideways causing the epidermal structure to lose that wave-like shape during the transition to psoriasis, 2. epidermal layer stratification is maintained. The changes made to the direction of how TA cells divide ensured that they divide vertically [50, 48], or oblique [112] manner as seen in previous models and clinical studies. Figure 5.4 shows a time-lapse immunofluorescence images tracking the direction of proliferative cell division in mice [112]. The study investigated in different parts of hairless mice such as the dorsal, ear, hindpaw and tail skin. It was revealed that most division along the basement membrane in the dorsal and ear epidermis were parallel, whereas in the hindpaw and tail epidermis, cell division occurs in parallel and oblique in direction. Although, the area investigated differs slightly from how the human epidermal structure is, this provides some insights on how TA cell division may differ slightly when the epidermis has been fully developed. In this model, I have adapted this concept and applied it to TA cell division in the development of psoriasis.

5.2.3 Chemical processes

The chemical processes used in psoriasis are similar to how the normal epidermis model has been developed. The processes involved are chemical consumption and mass balance which have been described in Chapter 4.

In addition to the two nutrients, calcium and growth factors, involved in the growth and proliferation of stem and TA cells, a single immune cytokines stimulus is initialised in the model to induce psoriasis. The immune cytokines stimulus initialised is maintained by introducing T cells into the system, where they reside in the basement membrane and the dermis region. The function of T cells has been simplified where they do not grow and migrate out of the basement membrane. The introduction of T cells is there to mainly regulate the amount of stimulus in the system, to activate and maintain psoriasis. The chemical consumption and production are based on the same reaction rates in Equation 4.7.

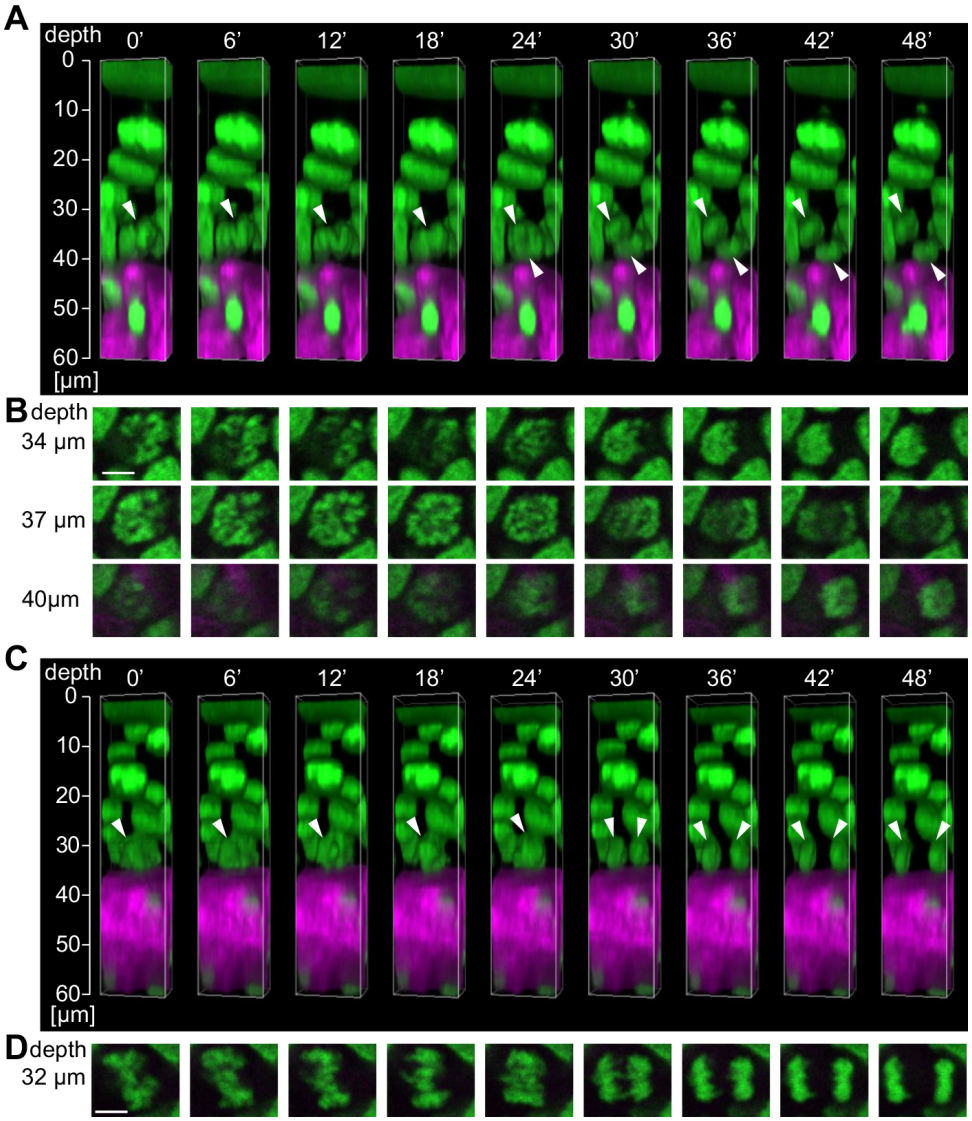

Figure 5.4: Figure adapted from [112]. A four-dimensional imaging of cell division in the hind paw epidermis in a living mouse. The images trace how proliferative cells divide, in particular, which direction - oblique or horizontal. (A) A reconstruction 3D image of oblique division to the basement membrane. Images are take every 6 minutes. (B) Time-lapse x- and y-axis images of mitotic cells in (A) at different depths. (C) Reconstructed 3D images of parallel division along the basement membrane. Images are take every 6 minutes. (D) Time-lapse x- and y-axis images of mitotic cells in (C) at depth of 32μm from the skin surface. White arrows represents the cell dividing. Scale bar = 5μm.

5.2.4 Deepening of rete ridges

The deepening of rete ridges was obtained by allowing movement of cells at the bottom of the waves. This allows the forces during cell division to push downwards, hence, developing the deeper rete ridges. Figure 5.5 shows the visualisation output from the simulation at days 0, 7 and 30, with day 0 the start of the immune cytokine stimulus initialised in the system. The cytokine stimulus was initialised for 7 days and allowed to stabilise and reach a steady state. The height of the rete ridges increased by approximately 3.5-times than in the normal epidermis, similar to literature where the thickness increases 2- to 3-times [50, 80, 113].

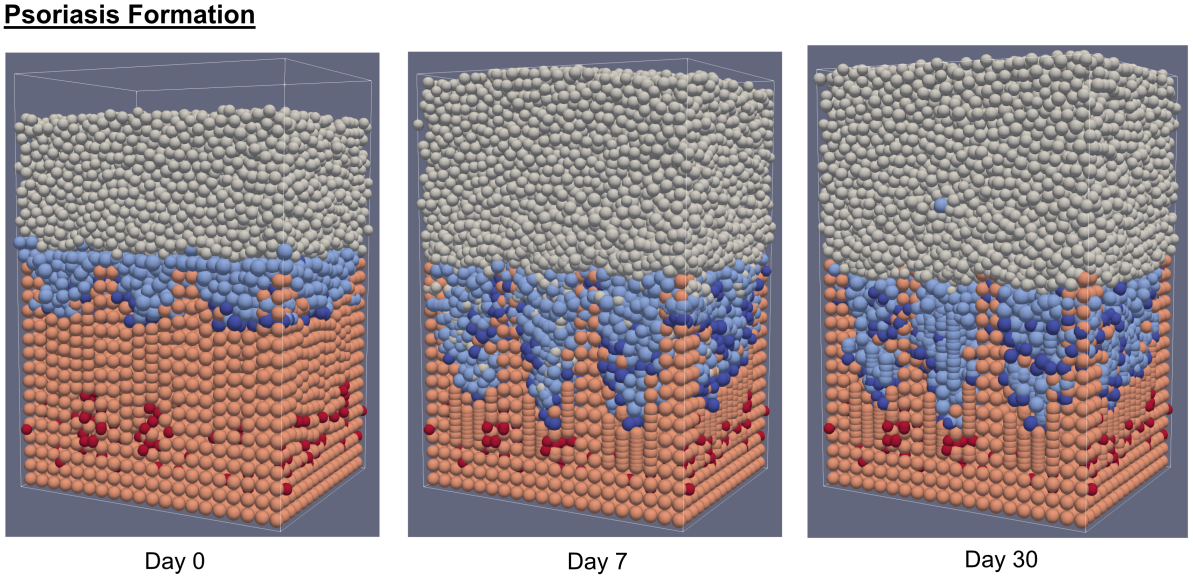

Figure 5.5: Visualisation output from the model. Snapshot of the model at three different time points (Day 0, 7 and 30). Cells represented: stem cells (in dark blue), TA cells (in light blue), differentiated cells (in white), T cells (in red) and basement membrane (in orange).

5.2.5 Cell population density

A previous computational study [19] showed that the cell population ratio remained the same in both normal and psoriasis. In addition, the overall number of epidermal cells is known to increase by up to two to five times as compared to the normal epidermis [31, 41]. The model predicted similar cell populations with the ratio being 4.7% (2,203) , 25.6% (11,976) and 68.6% (32,088) for stem, TA and differentiated cells, respectively. As only keratinocytes are taken into account, this translates to a cell population ratio of 4.5%, 24.6% and 66.0% for stem, TA and differentiated cells. This is similar to the cell population ratio in the normal epidermis with 4.3%, 23.33% and 65.2% being stem, TA and differentiated, respectively. The overall number

of epidermal cells has also increased by approximately three times as seen in Figure 5.6 showing the model outputs and average for 10 simulation runs under different random seeds.

5.2.6 Cell cycle and turnover times

In psoriasis, it is known that the cell cycle and the turnover times are three to five times faster than in normal epidermis [31, 40, 41]. The cell cycle and turnover times were calculated using Equations (4.9) and (4.10) found in Chapter 4. Using the equations, the predicted cell cycle and turnover times in psoriasis are approximately 4-times shorter than in the normal epidermis. The average cell cycle times are 47 and 20 hours for stem and TA cells, respectively, while the total turnover time was 5-times faster at approximately 4 days.

5.2.7 Parameters

Psoriatic epidermis				
Parameter description	**Parameter**	**Value**	**Units**	**Reference**
SC maximum growth rate	SC μ_{max}	1.28e-06	s^{-1}	Modified from [18]
TA maximum growth rate	TA μ_{max}	3.21e-06	s^{-1}	Modified from [18]
Ks value for growth factor	Ks_{gf}	2.5e-7	kgm^3	Assumed
Ks value for calcium	Ks_{ca}	2.5e-3	kgm^3	Assumed
SC symmetric division in expanding stage	Pa_e	0.05	-	Assumed
SC symmetric division in balanced stage	Pa_b	0.05	-	Assumed
SC asymmetric division in expanding stage	Pb_e	0.4	-	Assumed
SC asymmetric division in balanced stage	Pb_b	0.4	-	Assumed
TA symmetric division in expanding stage	Pc_e	0.25	-	Assumed
TA symmetric division in balanced stage	Pc_b	0.1	-	Assumed
TA asymmetric division in expanding stage	Pd_e	0.25	-	Assumed
TA asymmetric division in balanced stage	Pd_b	0.05	-	Assumed
Maximum TA division	max_{TA}	5	-	[18]
Diffusion coefficient	Ks	1.0e-9	m^2s^{-1}	[102]
Immune cytokine stimulus initialised	$Stim$	5.0e-4	kgm^3	Assumed

Table 5.1: Model parameters and conditions in psoriatic epidermis. The growth rates for stem and TA cells remain the same as the normal epidermis while the division probabilities for both stem and TA cells are altered. A new parameter scan was done to obtain the estimated results which will be further described in the next chapter. The maximum number of time a TA cell can divide now increases from 4 to 5 based on [18].

The parameters used in the psoriatic model are described in Table 5.1. The assumed parameters are described as follows:

- The maximum growth rate, μ_{max}, for stem and TA cell are kept the same as in Chapter 4 and were calculated based on Equation 4.11 using the cell cycle times. The maximum

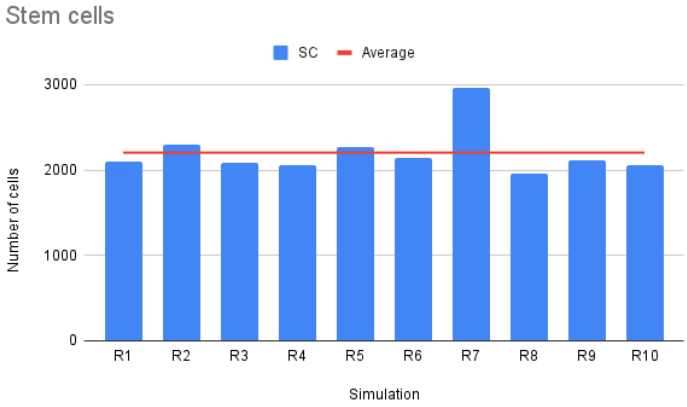

(a)

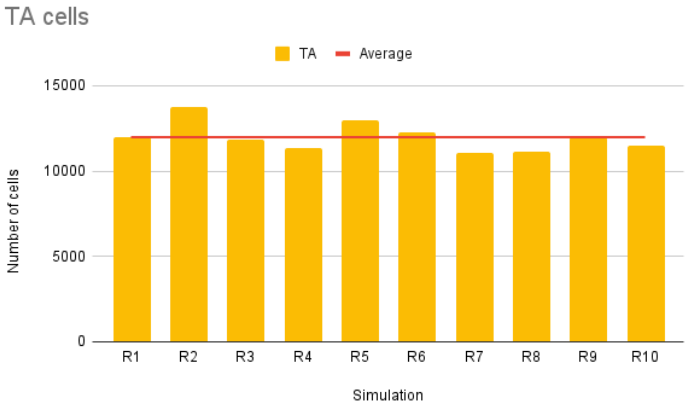

(b)

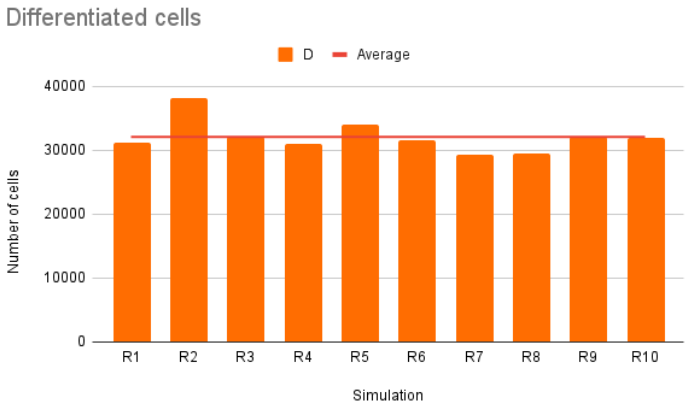

(c)

Figure 5.6: Average cell population numbers in the psoriatic steady state. (a) Stem cell population in steady state. (b) TA cell population in steady state. (c) Differentiated cell population in steady state. The average out of all simulations are represented by the horizontal line in the plots, where the average numbers are 2,203, 11, 976, and 32, 088 for stem, TA and differentiated cells respectively. The overall number of epidermal cells has increased by 3-times as compared to the normal epidermis. The results obtained were measured based on an average run of 10 simulations for each test case. Table 5.1 summarises the parameters used.

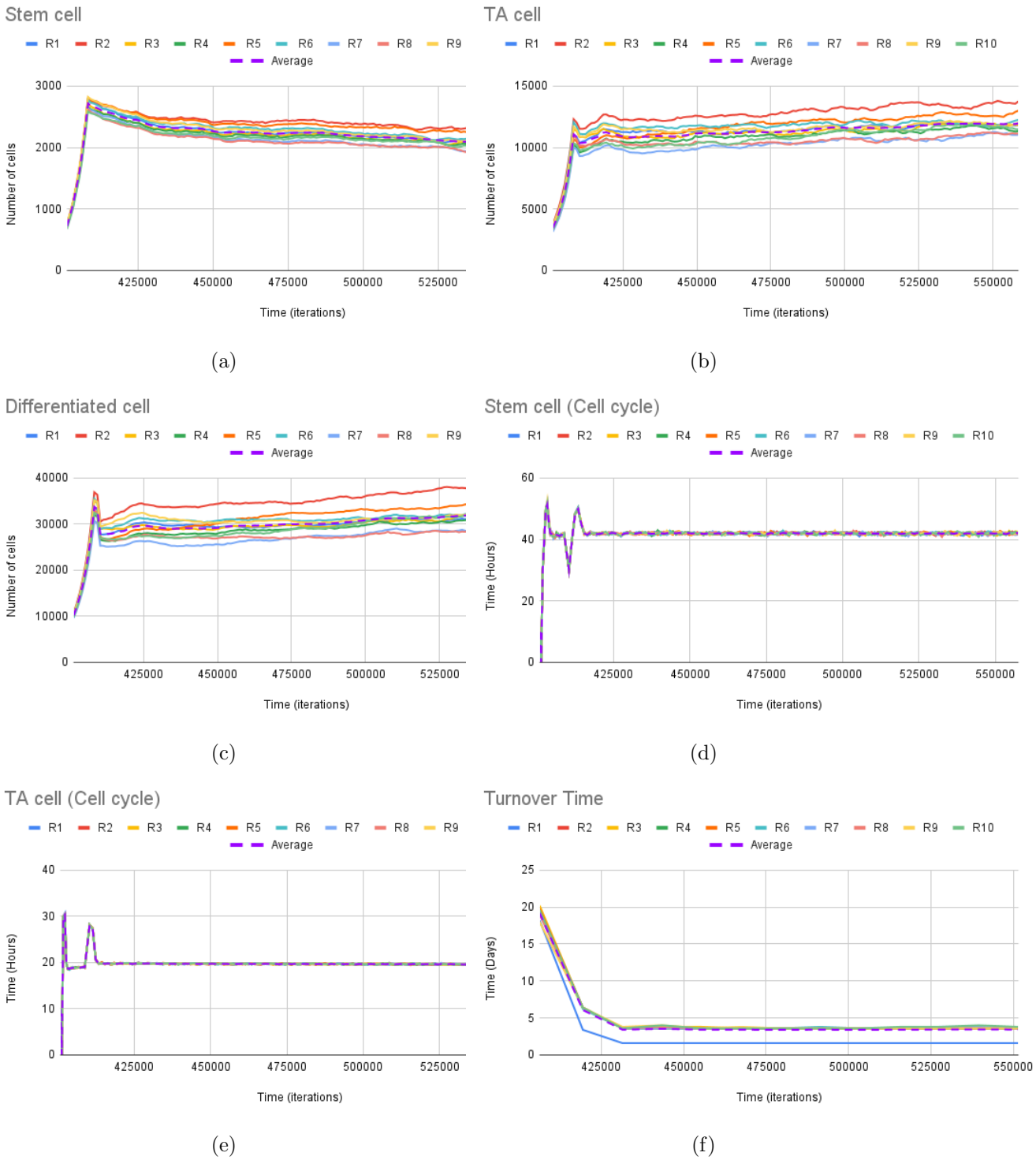

Figure 5.7: (a-c)Cell numbers plot of stem cells (a), TA cells (b) and differentiated cells (c). The average ratio of stem, TA and differentiated cells are 4.7% (2203), 25.6% (11,976) and 68.6% (32,088), respectively. (d-e) Cell cycle for stem (d) and TA cells (e). The average cell cycle times predicted are 42 and 19.7 hours, respectively. (f) Total turnover times for both proliferative and differentiated compartment. The average turnover time in the model is approximately 4 days in the steady state. Overall, the model is able to simulate psoriasis with the cell cycle and turnover times approximately 3.5- and 4-times faster, respectively. The simulations were ran 10 times under different random seed (R1-10) with the average plotted in purple dotted line. Each simulation ran under the same initial conditions such as the immune cytokine stimulus initialised, growth rates, and diffusion rates. Table 5.1 summarises the parameters used.

TA cell division has increased from 4 to 5 in psoriasis, similar to the implementation in Chapter 3.

- The Ks values for both growth factor and calcium were kept the same as in the normal epidermis as hyperproliferation is driven by a change in division.
- It has been noted in previous clinical studies that a change of state such as recovering from a wound or disease, division in the proliferative compartment is altered [114, 107]. A new parameter scan was done for stem and TA cell division to obtain the new division probabilities which will be further described in the next chapter, Chapter 6.

5.3 Conclusion

This chapter described how the epidermis transitions into psoriasis in the model, taking into account the changes in the physical, chemical and biological processes. This includes the spatial features of how the epidermal structure changes with the deepening of rete ridges and increase in epidermal height as seen in Figure 5.3. A single immune cytokine stimulus has also been modelled to trigger hyperproliferation in stem and TA cells, mimicking how the inflammatory process occurs in reality.

The model predicted an average cell cycle time of approximately 3.5- and 4-times faster than normal with average times of 47 and 19.7 hours in stem and TA cells. The average total turnover time was approximately 5 times faster at 4 days in the steady state. Both results are in line with clinical literature [18, 31, 41] where these timings are around three to five times faster than in the normal epidermis. The total turnover time is in the higher range at 5-times faster, however, this could be the way the model has been presented with the lack of the stratum corneum layer.

Overall, the model has been able to mimic how psoriasis develops using a single immune cytokine stimulus with changes to the epidermal structure such as the deepening of the rete ridges and increase in epidermal height. The model outputs were validated against literature and produced similar results. Although the model is a simplified version of the complex skin structure, the model has potential to be further implemented or modified to test different immune cytokines stimuli to trigger psoriasis. The referenced cytokines used were based on a previous ODE model [19], IL-17 and TNF-α. In that study, the concentration of both cytokines were similar, hence, in this model, it was clustered as a single immune cytokine. The model

serves as a baseline model for future developments in understanding psoriasis and its treatments. Future studies can include changing the type or including more than one immune cytokine to identify how different cytokines trigger psoriasis and its severity. In addition, this could also serve as a guide on how various treatments work, not only for NB-UVB treatments but how the different types of biological treatments, which target different immune cells, can cause clearance in psoriasis.

Chapter 6

Altered proliferative cell division in the psoriatic state

6.1 Introduction

Psoriasis is a chronic inflammatory disease characterised by hyperproliferation of stem and TA cells and abnormal differentiation in the epidermis. Hyperproliferating stem and TA cells are activated by several immune cytokines from T cells, for example. In a hyperproliferative state, the epidermis breaks from the steady state and eventually reaches a new steady state with a higher ratio of each cell type as compared to the normal epidermis.

During the process of hyperproliferation, the T cell immune response not only causes an increase in cell proliferation but also alters how these cells divide. It is not understood how this occurs, however, previous studies found that asymmetric division is the main type of division that occurs to ensure that psoriasis is maintained [114]. In one of their experiments, it was found that both symmetric and asymmetric cell division increased in psoriasis based on a significant reduction of keratin-15 (K15), a keratin marker of stem cells, immunostaining in basal cells. In addition, it was noted that approximately 13% of cells expressing K15 were undergoing asymmetric division while approximately 32% of cells expressing K15 underwent symmetric division. Hence, it was hypothesised that an increase in both symmetric and asymmetric division in stem cells may provide a mechanism on how the epidermis maintains its plaques in psoriasis.

Another previous study also described how cell division changes in psoriasis through a systematic review of studies from 1962 to 2009 [107]. The authors had used a general equation to analyse the evolution of differentiated epidermis and determined what were the necessary

conditions for psoriasis to develop. The results showed that an increase in cell division and/or decrease in physiological apoptosis of germinative cells were required to generate psoriasis.

Alterations of epidermal cell division is widely studied in skin wound healing, as well. In wound healing, there are three main stages - inflammation stage, regenerative stage and remodelling stage [108, 2]. The wound healing process starts off with the inflammatory stage where the skin immediately starts forming blood clots and recruit inflammatory cells to start covering the wound. Next, the regenerative stage where new epithelial cells are produced and form the granulation tissue. Lastly, the remodelling of epidermis, dermis and extra-cellular matrix occur. The last stage could take up to months for the skin to fully heal. The three stages can be seen in Figure 6.1[2], where actively proliferating cells and terminally differentiated cells were traced. In this study, the three stages were labelled migrating front, proliferating zone and post-closure (see Figure 6.1) instead, however, they perform the same actions. In addition, the type of division that occurs is mainly asymmetric or symmetric division - similar to how psoriasis develops [108]. Hence, wound healing experiments are one of the closer references that can be used in determining the changes that occur in psoriasis development.

In this chapter, I look into exploring how proliferative cell division probabilities are altered during the development of psoriasis. Some assumptions have been made as the model represents a simplification of how the epidermis develops. This includes how instead of three stages as in wound healing, I have assumed two different stages similar to how the normal epidermis develops in Chapter 4, expanding and balanced stage. The first stage is governed by the immune stimulus activated mimicking this migrating front. Once the disease is developed, it then moves into the next stage where the model reaches stability in psoriasis. The cell division probabilities are obtained by doing a parameter scan on each division type, self-, asymmetric and symmetric division, to see how the model reaches the targeted cell population densities and ratios.

6.2 Methods

The model assumes two stages when transitioning to psoriasis and adopts the same method of division in the normal epidermis - expanding and balanced stage. Specifically, Figure 4.5 in Chapter 3 described the epidermal cell pathway where division to a daughter cell of a different type is determined by the probabilities, P_0 and P_1, where P_0 determines the rate of which stem cells produce TA daughter cells, and P_1 determines the rate of which TA cells produce

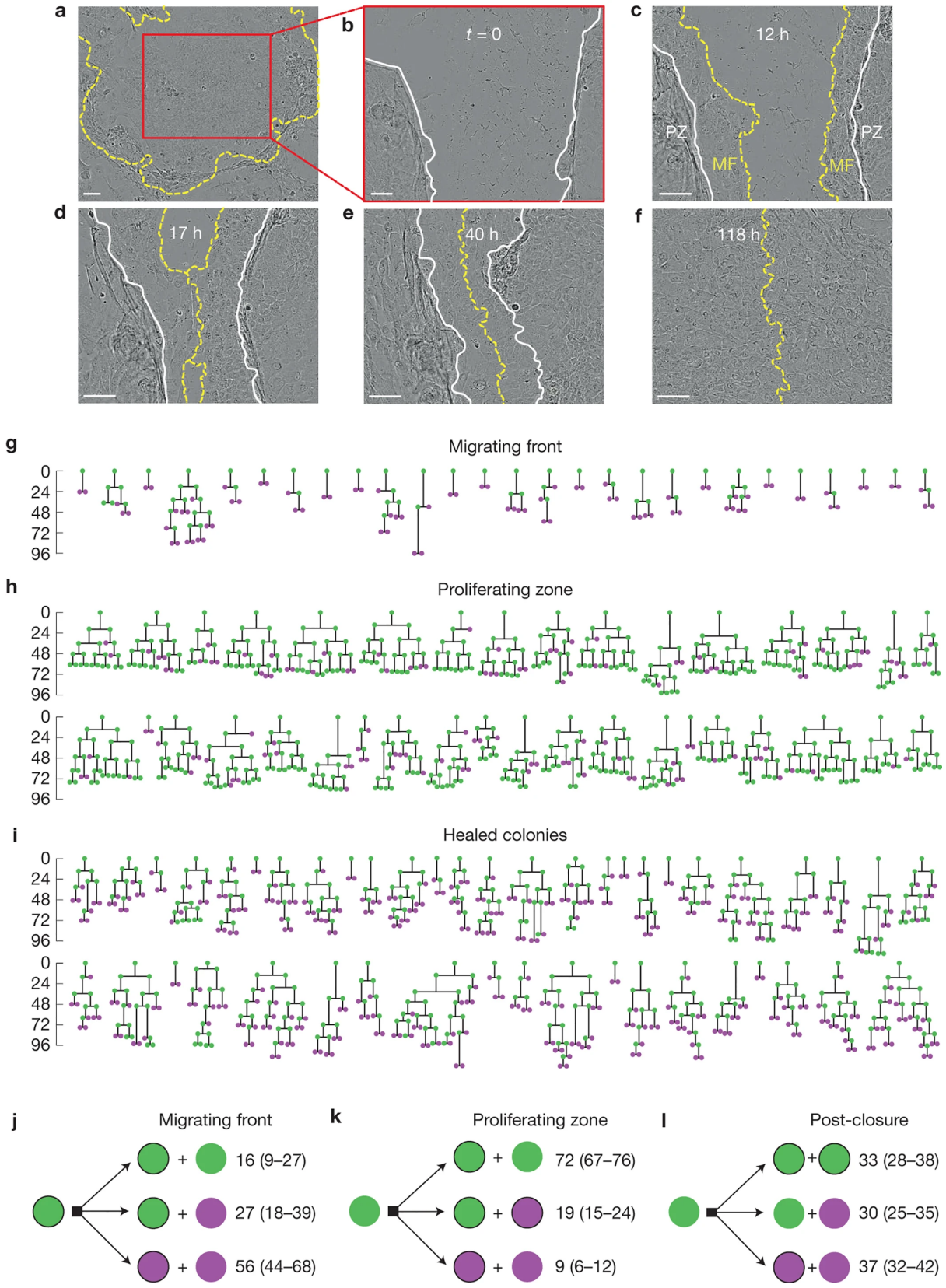

Figure 6.1: Figure adapted from [2]. Three division stages in wound healing example. (a-f) Images from experiments. (g-i) Lineage trees of proliferating cells 9 days after the scratch. (j-l) Summary of cell division on each of the three stages. Green cells and magenta cells represent proliferating cells and differentiating, non-dividing cells, respectively.

differentiated daughter cells. The previous rates in the normal epidermis are $P_0 = 0.1$ and $P_1 = 0.07$ during the expanding state.

However, unlike in the normal epidermis model, there are three more unknowns to identify the changes to TA division probabilities in psoriasis. Hence, two groups of parameter searches were performed. Using the previous study where cell proliferation was tracked [2], the following assumptions have been made based on the normal epidermis division probabilities where:

- Stem cell division is kept at 10-80-10 for self-, asymmetric, and symmetric division, respectively[1] [20, 97, 98].
- TA cell division is kept to a similar balanced ratio of 35-30-35 for self-, asymmetric, and symmetric division, respectively[1] [2].
- P_0 and P_1 values should equal 0.5 in the balanced state (i.e. steady state) while varying in the expanding state [2].

The first group of parameter scan was performed on the stem cell division to obtain values P_a, P_b and P_0 rate in expanding stage that produce the ideal number of stem cells in psoriasis. The P_0 values tested were ranged from 0.1 to 0.4, in steps of 0.05. Once the ideal number of stem cells were obtained, the scan moved to the next group to identify the values for P_c, P_d and P_1 in the expanding stage. The P_1 values tested ranged from 0.075 to 0.425, in steps of 0.025. Tables 6.2 and 6.3 summarise the values tested and average results out of five simulations obtained.

6.3 Results

6.3.1 Normal epidermis division probabilties

The normal epidermis division probabilities were first tested to understand what cell population numbers and ratio can be obtained. The values used for stem cell division are $P_{a_e} = 0.05$, $P_{a_b} = 0.05$, $P_{b_e} = 0.1$ and $P_{b_b} = 0.7$ while TA cell division probabilities are $P_{c_e} = 0.02$, $P_{c_b} = 0.32$, $P_{d_e} = 0.1$ and $P_{d_b} = 0.18$.

[1] In Chapter 4, it was showed that despite having different proportions of self-proliferation, asymmetric and symmetric division, the number of cells do not differ greatly as long as the P_0 and P_1 are identical. Hence, here I assumed that stem cells will retain its 10-80-10 division for self-proliferation, asymmetric and symmetric division respectively. For TA cell, a balanced rate of division 35-30-35 is maintained.

Figure 6.2 shows the results of each cell type over five runs with the average of stem, TA and differentiated cells being 4,355, 161,951, and 37,917, respectively. A high TA cell population is produced using this set of parameters which is much higher than expected as compared to literature. It is known that when psoriasis develops, the cell ratios are maintained with cell population numbers increasing between 3-5 times more than normal epidermis. In this case, the ratio of TA cells are 79.1% instead of approximately 26.7% as in normal epidermis. Thus, this shows that the division probabilities are different between normal and psoriasis and that our computational model can be used to identify estimates of how they differ.

6.3.2 Proliferative cell division probabilities scan

The approximate cell population numbers referenced were based on the results in Figure 4.8 where stem, TA and differentiated cell population had an average of 695, 3,709 and 10,080, respectively. Table 6.1 summarises the average cell population obtained and an approximation of what the expected increase in cell numbers are between three to five times in psoriasis [18, 19].

	Stem cell	**TA cell**	**Differentiated cell**
Normal Epidermis	695	3,709	10,080
Psoriasis (3x)	2,085	11,127	30,240
Psoriasis (4x)	2,780	14,836	40,320
Psoriasis (5x)	3,475	18,545	50,400

Table 6.1: Approximate cell population based on the average cell numbers obtained from Chapter 4 where the cell population is expected to increase by three to five times more than in the normal epidermis.

Based on the assumptions mentioned, model simulations were run for the various P_a, P_b,P_c and P_d parameters. Tables 6.2 and 6.3 show an example of what P_a, P_b, P_c and P_d values were used in the expanding stage and what P_0 and P_1 values were tested. The parameter scan for each set was performed five times using different random seeds and their average used to determine which parameters to be used in the model. The model outputs were then validated against literature of the cell population increment as compared to normal epidermis.

Figures 6.2 and 6.4 describe the model outputs based on the P_0 and P_1 values in the expanding stage. In each test case, the model was run on an average of five runs over five different random seeds that were used in the normal epidermis. The stem cell division probability scan used the 10-80-10 division type which had no duplicates in P_0 values. However, in the case of the TA cell probability scan, the division type used was 35-30-35 which resulted in some

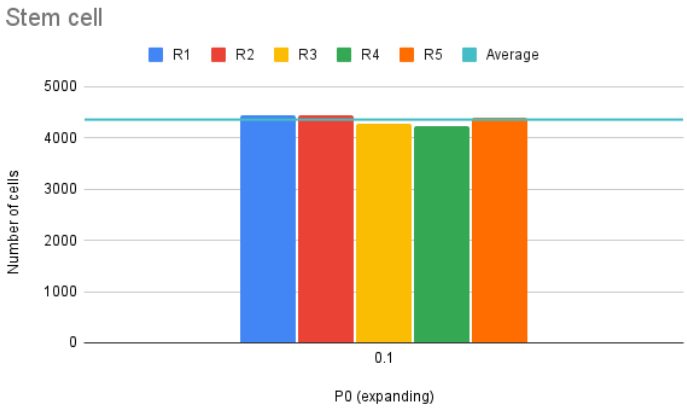

(a)

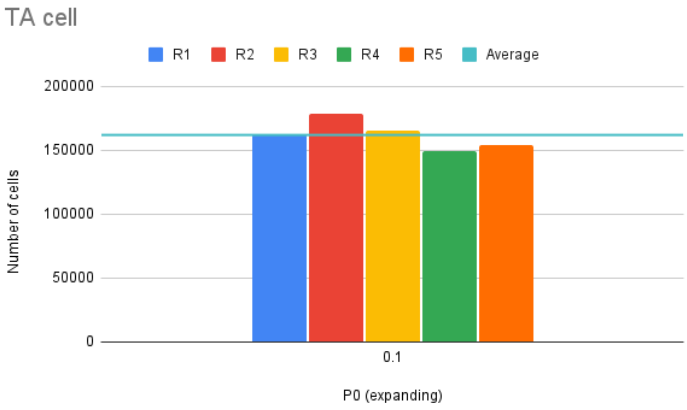

(b)

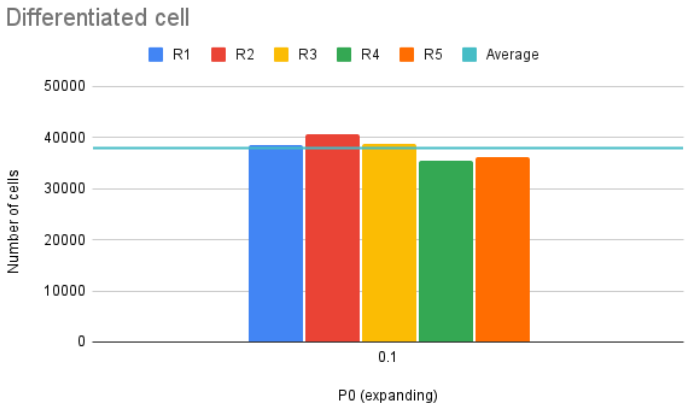

(c)

Figure 6.2: Average number of cells produced when using the normal epidermis division probabilities when transitioning form normal to psoriatic state. (a) Stem cell population with the average of 4,355. (b) TA cell population averaging at 161,951 cells which is over 10 times more than in normal. (c) Differentiated cell population averaging at 37,917 cells. The average out of each test case is represented by the blue shadow in the plots each cell type. The results obtained were measured based on an average run of 5 simulations for each test case.

P_{a_e}	P_{b_e}	P_{0_e}	**Stem cell** *(Avg.)*
0.05	0.1	0.1	5,682
0.05	0.2	0.15	4,750
0.05	0.3	0.2	3,692
0.05	0.4	0.25	3,023
0.05	0.5	0.3	2,080
0.05	0.6	0.35	1,822
0.05	0.7	0.4	1,276

Table 6.2: Stem cell division probability used for parameter scan and the average number of stem cells obtained. The scan was done under the assumption that stem cell division remained in the 10-80-10 ratio for self-, asymmetric and symmetric division, respectively.

P_{c_e}	P_{d_e}	P_{1_e}	**Stem Cell** *(Avg.)*	**TA cell** *(Avg.)*	**Differentiated cell** *(Avg.)*
0.05	0.05	0.075	2,878	176,006	56,629
0.05	0.1	0.1	2,871	206,644	64,916
0.05	0.15	0.125	2,937	173,367	103,067
0.05	0.2	0.15	2,957	125,045	70,123
0.05	0.25	0.175	2,935	104,055	66,270
0.1	0.2	0.2	2,937	80,101	63,148
0.1	0.25	0.225	2,945	60,632	59,231
0.15	0.2	0.25	2,958	45,697	54,700
0.15	0.25	0.275	2,953	33,375	51,013
0.2	0.2	0.3	2,949	26,726	46,956
0.2	0.25	0.325	3,017	20,503	43,226
0.25	0.2	0.35	2,944	15,804	39,670
0.25	0.25	0.375	2,965	11,970	36,412
0.3	0.2	0.4	2,957	9,110	34,131
0.3	0.25	0.425	2,948	6,929	31,222

Table 6.3: TA cell division probability used for parameter scan and the average number of cells obtained. The scan was done under the assumption that stem cell division remained closer to a balanced ratio for self-, asymmetric and symmetric division at 35-30-35, respectively. The P_1 value in the balanced state is 0.5 to ensure that when the model reaches a steady state, it will ideally have equal production of TA and differentiated cells maintained. Note: P_1 values ranging from 0.125 to 0.375 has more than one combination of P_c and P_d. The above table is just a example of some of the values. It is also important to note that similar to the parameter scan of stem call division in Chapter 4, combinations of the same P_1 values produce similar results.

duplicates and therefore the results obtained were averaged out based on the P_1 values. Despite the duplicates, the results between the different P_c and P_d values did not produce results that differed largely. This is similar to the results obtained in Chapter 4 during the stem cell division probability scan. The model predicted for psoriasis to occur within the expected increase in cell numbers of three- to five-times, the expanding cell probabilities are 0.25 to 0.3 and 0.375 for stem and TA cells, respectively. This will produce an average cell numbers of stem, TA and differentiated cells of 2,965, 11,970 and 36,412, approximately 4-times more, during this transition from normal to psoriastic state.

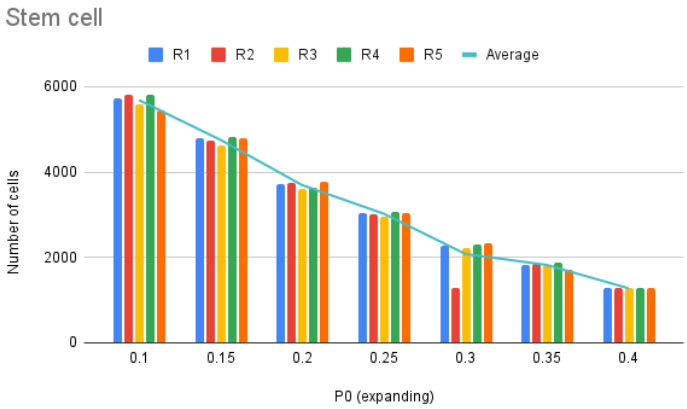

(a)

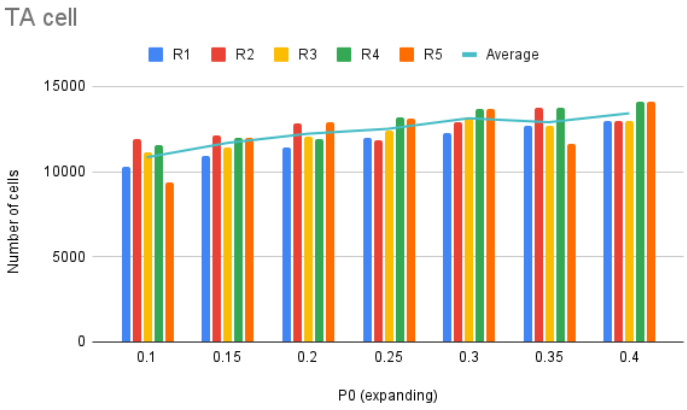

(b)

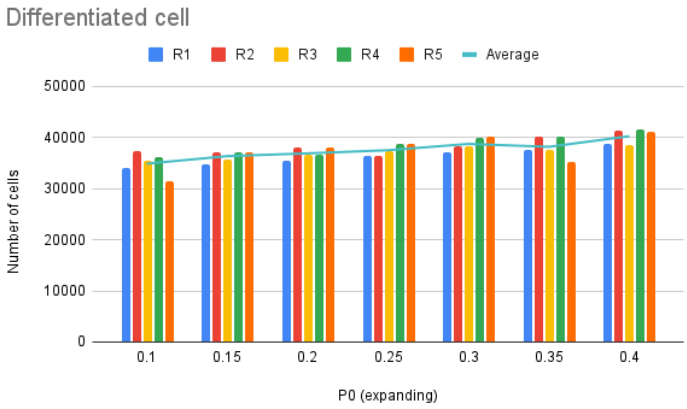

(c)

Figure 6.3: Average cell population based on the parameter estimation for P_0. The best range was found to be between 0.25 and 0.3, which produced an average stem cell population of 3,032 and 2,080. (a) Stem cell population. (b) TA cell population. (c) Differentiated cell population. The average out of each test case is represented by the horizontal line in the plots each cell type. The results obtained were measured based on an average run of 5 simulations for each test case.

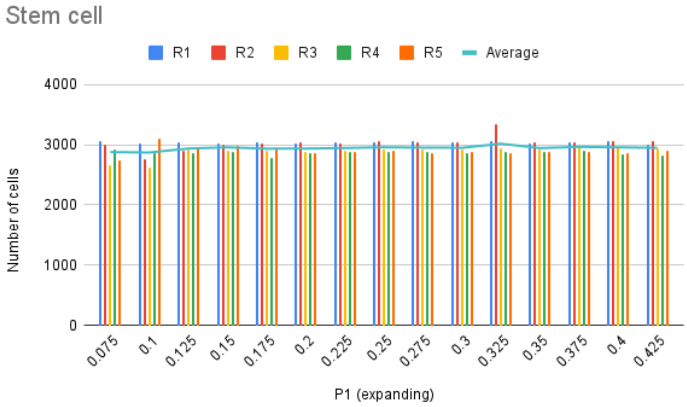

(a)

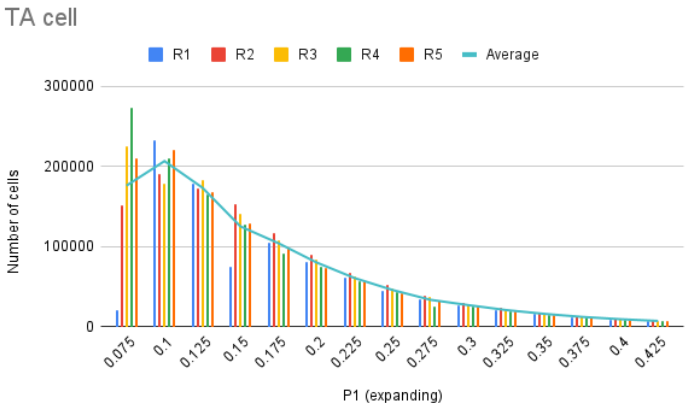

(b)

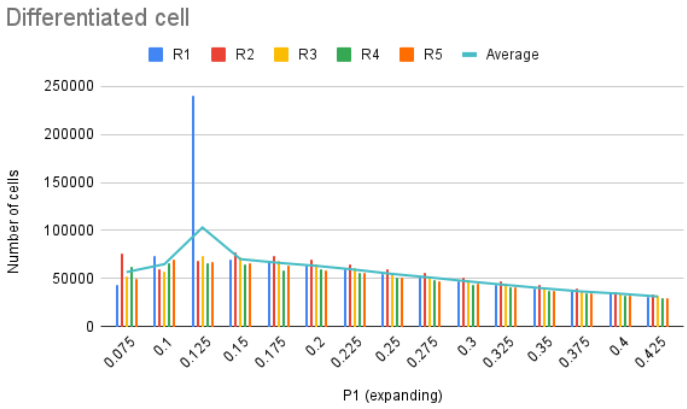

(c)

Figure 6.4: Average cell population based on the parameter estimation for P_1. The best value found was 0.375, which produced an average of 11,970 TA cells. (a) Stem cell population. (b) TA cell population. (c) Differentiated cell population. The average out of each test case is represented by the horizontal line in the plots each cell type. The results obtained were measured based on an average run of 5 simulations for each test case.

6.4 Conclusion

This chapter looked into exploring how computational modelling can provide an insight to the changes in proliferative cell division when psoriasis occurs due to an immune cytokine stimulus. Using the same division probabilities in both normal and disease state, the model predicted an unusually high TA cell population which does not reflect how psoriasis occurs and breaks the balance of the different cell type ratio of 4.7%, 26.4% and 40-66% for stem, TA and differentiated cells, respectively [80]. This supports the hypothesis that in a disease state, hyperproliferation breaks this balance of division state and changes how each cell type responds and alters its division probabilities to reach a new steady state while ensuring that each cell ratio remains.

In this investigation, I have applied a similar concept to how wound healing occurs at different stages with different sets of division probabilities for each stage when the wound is first inflicted and how it will then switch division probabilities to obtain a new steady state [2]. In the model, a new set of division probabilities were obtained by parameter scans for both stem and TA cells. The results obtained showed how the division probabilities differed from the normal epidermal state to psoriasis. In stem cells, the P_0 changed from 0.1 to 0.25 while P_1 changed from 0.07 to 0.375 in the expanding stage. In both cases, the rate of producing at least one daughter cell of a different type has changed significantly and requires a much higher rate of producing a daughter cell that is of a different type (i.e. stem to TA cell and TA to differentiated cell). Similar results can be seen during wound healing where in the proliferating zone, the rate of producing a differentiated daughter cell went up to 0.695 from 0.07 [2], for example. Hence, supporting how a different set of division probabilities are required when modelling any changes that occur to the epidermis such as psoriasis or other inflammatory diseases. This finding could also provide a guide of how psoriasis occurs and how we can trace the lineage of proliferative cells *in vivo*.

Chapter 7

Conclusions

7.1 Summary

Psoriasis is a chronic inflammatory skin disease which affects the patient's quality of life and currently has no cure. There are various treatment options available for patients such as topical corticosteroids to systemic therapies to phototherapies such as NB-UVB [4, 7]. However, with each type of therapy, a generalised form is given to all patients under a largely predefined dosing regime. This may not be ideal for every single patient and may cause them distress if the therapy has little effects after a period of treatment. One way of helping patients is to provide personalised treatment and to use computational models to do so. Computational models provide not only scientists but medical practitioners a better understanding of the disease formation, with the aim of providing specific treatment options. A previously developed 2D model of psoriasis and NB-UVB clearance looked into solving some of these issues when understanding NB-UVB phototherapy treatments. However, the model has some limitations such as the lack of cell-cell interactions, spatial considerations, and high NB-UVB dose given for each treatment. These do not depict how the epidermis develops and behaves and the treatment dose given in reality. This thesis focused on solving some of these limitations with the aim to develop a 3D computational model of immune cytokine interaction and epidermal homeostasis in psoriasis.

7.2 Evaluation of Research Aims

In this thesis, agent-based computational models were developed to explore how psoriasis develops. The 2D model in Chapter 3 described how computational models can be used to understand NB-UVB phototherapy treatments in psoriasis and how different simulations can represent individual patients. The 3D model developed aimed to eliminate some of the limitations the 2D model had such as the lack of spatial considerations, cell-cell interactions and the use of nutrients to aid cellular growth and proliferation. Here, I summarise the key contributions done in this research.

Chapter 3 explored how a previously developed 2D computational model of psoriasis [18] could be used to provide a better understanding on NB-UVB treatments in clinical setting. The model was originally developed for NB-UVB treatment dose of 3 MED, which are much higher than what is given in the clinics about 1 MED. Hence, the dose was reduced to 1 MED in the model and the frequency of treatment increased to what is given clinically. The next investigation was looking into the different mechanisms of action that occurs in NB-UVB phototherapy treatments, cell cycle arrest and apoptosis, including comparing how a combination of the two mechanisms differs from just using one mechanism. In addition, to mimic how patients get their treatments in reality, different frequencies were tested to take into account the weekends where the clinics are closed. The model was able to show how using just cell cycle arrest was insufficient in causing clearance and that apoptosis is the main mechanism of action for clearance. However, both mechanisms can be used together to mimic how clearance occurs in reality. Simulations ran over different random seeds to simulate individual "patients". The results obtained were fed into a clustering algorithm to identify and validate model outputs against real patient data. The results showed how the model outputs were able to simulate real patients and how they can be clustered into different groups to identify and observe treatment progress. This shows how computational models may be useful in simulating different types of patients and predict their treatment outcomes. The model can be used to aid clinicians in determining treatment plans for individual patients such as to continue with NB-UVB phototherapy or to switch to other types of treatments like biologics.

Chapter 4 presents a 3D model of how the normal epidermis develops and aims to solve some of the limitations of the 2D model mentioned in Chapter 3. The 3D model was developed in NUFEB and LAMMPS and took into account the cell dynamics and cell-cell interactions.

The model consists of three main processes, physical, biological and chemical, and features a wave-like basement membrane depicting how the epidermis is in reality. Physical processes solved issues such as overlapping of cells during division and to obtain layer stratification by modelling repulsive and cohesive forces. The biological processes modelled cellular growth and division based on two nutrients, extracellular calcium and endogenous growth factors. Lastly, the chemical process involves the diffusion of these nutrients and production of growth factors by stem and TA cells in the system. The model outputs, cell population ratio, cell cycle and turnover times, were validated against literature.

Chapter 5, explored how psoriasis develops based on a single immune cytokine stimulus. Psoriasis is marked by hyperproliferation and thickening of the epidermis. This thickening not only occurs at the top of the epidermis but affects the rete ridges at the bottom as well with a deepening and flat-like shape as seen in Figure 5.1. The psoriasis 3D model consists of the same processes as the normal epidermis with additional rules applied to trigger psoriasis. The biological processes were modified to include the single immune cytokine stimulus to both growth and division. In the division model, the immune cytokine stimulus pushes the model back into a proliferative state to cause hyperproliferation in psoriasis. Lastly, the chemical process includes the new nutrient, the immune cytokine stimulus, initialised and diffused from the basement membrane. The model was able to predict cell cycle and turnover times within the known range of 3-4 times shorter, while the cell population ratio maintained with the cell numbers increasing by approximately 3 times.

Psoriasis is not only known to cause changes to the biological and physical structure of the skin: it can alter the proliferative state of stem and TA cells [114, 107]. Chapter 6, explored how proliferation rates are altered during psoriasis. If the division probabilities in the model were kept the same as in the normal epidermis, psoriasis did not occur and results in a very high TA cell population. Hence, an investigation was carried out on the alterations to proliferation in psoriasis. Two sets of parameter scans were performed - one on stem cell and the other on TA cell, under the assumption that the target cell numbers are based on getting the model to reach within 3-5 times more than in the normal epidermis [18, 19]. Secondly, it was assumed that for the model to obtain a steady state, both P_0 and P_1 rates in the balanced state were 0.5, where there is an equal chance of a cell to divide to the same type as the parent and of a different type. The model used a concept similar to how wound healing occurs in the skin, with the difference that the immune cytokine stimulus pushes the model back to a proliferative (expanding) state.

The results showed that in the expanding state, both P_0 and P_1 values increased significantly as compared to the normal epidermis. This not only supports how a different set of division probabilities are required when modelling psoriasis and other inflammatory diseases, but also gives an insight on how we can trace proliferation in keratinocytes in clinical experiments.

7.3 Limitations

The 3D model is a simplification of how the epidermis develops in reality. The model takes into account the three main types of keratinocytes involved in the epidermis and their interactions with a single immune cytokine stimulus to progress to psoriasis. However, in reality, there are more than the three types of cells mentioned such as granular cells and corneocytes [115, 116, 50] and different, multiple immune cyotkine stimulus and T cell species [106, 117, 105] that may be involved in the development of psoriasis. The limitations are listed as follows:

- The model starts as an embryonic state which may have a different initial rate of growth and transition to psoriasis.
- The model has been simplified to include only the main three types of keratinocytes - stem, TA and differentiated cells. However, in reality, differentiated cells can be further subdivided and labelled according to where it is located in the epidermis. For example, TA cells will differentiate to growth arrest cells which will differentiate to a spinous cell in the stratum spinosum layer. The cell will go on to differentiate further into a granular cell in the stratum granulosum and corneocyte stratum corneum layer [115, 116, 50].
- Corneocytes are differentiated cell found in the upper most layer of the epidermis, the stratum corneum. Corneocytes are not spherical in shape but a flat cells which has excreted out its contents in preparation to be desquamated out of the epidermis. In this model, corneocytes have not been taken into account and the action of differentiated cells flattening is not modelled. Therefore, the turnover time in the model is slightly shorter than what is found in literature as shedding does not occur.
- The model does not include other cells that are present in the epidermis such as hair follicles and melanocytes. Hair follicles produce the hair on our skin [91], and melanocytes produce melanin (the pigment responsible for our skin colour) [118, 119, 120, 121].

- A single immune cytokine and T cell species are modelled. However, in reality, there are many different types of T cell and cytokine species which are known to cause psoriasis such as IL-22, IL-23, IL-17, TNFα and so on [3]. Each cytokine is known to affect a different inflammatory response that can cause different severity of the disease. Hence, they are important in biological treatment as they target specific cytokines [3, 105].

7.4 Future Work

The 3D computational model simulates how the normal epidermis forms and how it transitions to psoriasis using a single immune cytokine stimulus. This model provides the first step as a baseline model to dive further into how we can use the model to better understand the disease and to model various treatment options such as NB-UVB phototherapy or biological treatments. Some directions for future studies include modelling NB-UVB phototherapy treatments, exploring different doses and frequencies of NB-UVB treatments and using single or combination mechanisms of action for clearance, similar to the 2D model in Chapter 3. The 3D model outputs can also be fed into the same machine learning algorithm [19] used to make predictions of how each simulation can be clustered to emulate real life patients.

The 3D model can also be modified to investigate specific immune cytokine stimuli and T cell species or a combination of them to better understand how each cytokine affects the skin to cause different variations of psoriasis. This would allow us to explore how different biological treatments aid clearance of psoriasis by targeting specific cytokines or may be used in combination therapies.

Apart from modelling psoriasis treatments, some possible future work include tackling some of the limitations mentioned in the current 3D model. This includes modelling the upper epidermal layers where differentiated cells flatten out and eventually shed off to develop a model where all layers of the epidermis are included which can be used to explore other skin diseases apart from psoriasis. Next, the inclusion of other cell types such as melanocytes as they are known to affect UVB phototherapy treatments [118, 119, 122, 123, 120]. Melanocytes are a type of dendritic cells that produce melanin, the pigment responsible for skin colour, located in the stratum basale layer. Melanin is known to absorb UV, preventing DNA damage to keratinocytes. The amount of melanin in the body correlates to how much UV protection the skin gets, hence, patients of colour has a lower susceptibility of UV damage as it offers

more protection [124]. It has been suggested that phototherapy is effective in patients of colour and may require a higher dose [125, 126]. A disadvantage of phototherapy is the risk of post-inflammatory hyperpigmentation (i.e. darkening of the skin), which occurs due to exposure to NB-UVB phototherapy treatments, and may not be acceptable to all patients [127]. It will be interesting to investigate how different NB-UVB doses affect patients of colour and how we may use computational modelling to predict the minimal dose required.

In conclusion, the 3D computational model present insights on how the epidermis forms and how immune cytokines trigger psoriasis, altering not only the structure of the epidermis but also alters how proliferative cells, stem and TA, divide. Directions for future work include modelling psoriasis NB-UVB and biological treatments but also tackling some of the limitations in the current model so that it can be used hand-in-hand or as a predictive tool for future clinical studies as well.

Bibliography

[1] S. Mohamed, B. Q. Huang, and M.-T. Kechadi, "Prediction of NB-UVB phototherapy treatment response of psoriasis patients using data mining," in *2017 IEEE International Conference on Bioinformatics and Biomedicine (BIBM)*, pp. 1067–1071, Nov. 2017.

[2] A. Roshan, K. Murai, J. Fowler, B. D. Simons, V. Nikolaidou-Neokosmidou, and P. H. Jones, "Human keratinocytes have two interconvertible modes of proliferation," *Nature Cell Biology*, vol. 18, pp. 145–156, Feb. 2016.

[3] M. A. Lowes, A. M. Bowcock, and J. G. Krueger, "Pathogenesis and therapy of psoriasis," *Nature*, vol. 445, pp. 866–873, Feb. 2007.

[4] "Psoriasis Association." https://www.psoriasis-association.org.uk/.

[5] M. J. Bhosle, A. Kulkarni, S. R. Feldman, and R. Balkrishnan, "Quality of life in patients with psoriasis," *Health Qual Life Outcomes*, vol. 4, p. 35, June 2006.

[6] R. Sarkar, S. Chugh, and S. Bansal, "General measures and quality of life issues in psoriasis," *Indian Dermatol Online J*, vol. 7, no. 6, pp. 481–488, 2016.

[7] M. Lebwohl, "A clinician's paradigm in the treatment of psoriasis," *Journal of the American Academy of Dermatology*, vol. 53, pp. S59–S69, July 2005.

[8] B. Tami Wong, B. Leon Hsu, and M. Wilson Liao, "Phototherapy in Psoriasis: A Review of Mechanisms of Action," *J Cutan Med Surg*, vol. 17, no. 1, pp. 6–12, 2013.

[9] P. Zhang and M. X. Wu, "A clinical review of phototherapy for psoriasis," *Lasers Med Sci*, vol. 33, no. 1, pp. 173–180, 2018.

[10] M. Rodgers, D. Epstein, L. Bojke, H. Yang, D. Craig, T. Fonseca, L. Myers, I. Bruce, R. Chalmers, S. Bujkiewicz, M. Lai, N. Cooper, K. Abrams, D. Spiegelhalter, A. Sutton,

M. Sculpher, and N. Woolacott, *Impact of Psoriasis on Costs*. NIHR Journals Library, Feb. 2011.

[11] C. Bonifati and E. Berardesca, "Clinical Outcome Measures Of Psoriasis," *Reumatismo*, vol. 59, Sept. 2011.

[12] B. L. Diffey, "Towards optimal regimens for the UVB phototherapy of psoriasis: A mathematical model," *Acta Dermato-Venereologica*, 2004.

[13] Dawe, Wainwright, Cameron, and Ferguson, "Narrow-band (TL-01) ultraviolet B phototherapy for chronic plaque psoriasis: Three times or five times weekly treatment?," *British Journal of Dermatology*, vol. 138, pp. 833–839, May 1998.

[14] S. M. Kirke, S. Lowder, J. J. Lloyd, B. L. Diffey, J. N. S. Matthews, and P. M. Farr, "A Randomized Comparison of Selective Broadband UVB and Narrowband UVB in the Treatment of Psoriasis," *J Invest Dermatol*, vol. 127, pp. 1641–1646, July 2007.

[15] M. B. G. Koek, V. Sigurdsson, H. van Weelden, P. H. A. Steegmans, C. A. F. M. Bruijnzeel-Koomen, and E. Buskens, "Cost effectiveness of home ultraviolet B phototherapy for psoriasis: Economic evaluation of a randomised controlled trial (PLUTO study)," *BMJ*, vol. 340, p. c1490, Apr. 2010.

[16] S. M. Langan, A. Heerey, M. Barry, and L. Barnes, "Cost analysis of narrowband UVB phototherapy in psoriasis," *Journal of the American Academy of Dermatology*, vol. 50, pp. 623–626, Apr. 2004.

[17] E. Klipp, W. Liebermeister, C. Wierling, and A. Kowald, *Systems Biology*. Wiley VCH; 2nd edition (4 May 2016), second edition ed., May 2016.

[18] S. C. Weatherhead, P. M. Farr, D. Jamieson, J. S. Hallinan, J. J. Lloyd, A. Wipat, and N. J. Reynolds, "Keratinocyte Apoptosis in Epidermal Remodeling and Clearance of Psoriasis Induced by UV Radiation," *Journal of Investigative Dermatology*, vol. 131, pp. 1916–1926, Sept. 2011.

[19] F. Shmarov, G. R. Smith, S. C. Weatherhead, N. J. Reynolds, and P. Zuliani, "Individualised computational modelling of immune mediated disease onset, flare and clearance in psoriasis," *PLOS Computational Biology*, vol. 18, p. e1010267, Sept. 2022.

[20] F. M. Watt, C. L. Celso, and V. Silva-Vargas, "Epidermal stem cells: An update," *Current Opinion in Genetics & Development*, vol. 16, pp. 518–524, Oct. 2006.

[21] S. Weatherhead, *The Role of Apoptosis in UVB- Induced Clearance of Psoriasis*. PhD thesis, Newcastle University, Oct. 2010.

[22] L. M. Biga, S. Bronson, S. Dawson, A. Harwell, R. Hopkins, J. Kaufmann, M. LeMaster, P. Matern, K. Morrison-Graham, K. Oja, D. Quick, J. Runyeon, O. Oeru, and OpenStax, "5.1 Layers of the Skin," *Anatomy & Physiology*, Sept. 2019.

[23] P. M. Elias, B. E. Brown, D. Crumrine, K. R. Feingold, and S. K. Ahn, "Origin of the Epidermal Calcium Gradient: Regulation by Barrier Status and Role of Active vs Passive Mechanisms," *Journal of Investigative Dermatology*, vol. 119, pp. 1269–1274, Dec. 2002.

[24] Y. Kobayashi, Y. Sawabu, H. Kitahata, M. Denda, and M. Nagayama, "Mathematical model for calcium-assisted epidermal homeostasis," *Journal of Theoretical Biology*, vol. 397, pp. 52–60, May 2016.

[25] F. M. Watt, "23 - Human Epidermal Stem Cells," in *Handbook of Stem Cells* (R. Lanza, J. Gearhart, B. Hogan, D. Melton, R. Pedersen, J. Thomson, and M. West, eds.), pp. 245–256, Burlington: Academic Press, Jan. 2004.

[26] P. H. Jones, S. Harper, and F. M. Watt, "Stem cell patterning and fate in human epidermis," *Cell*, vol. 80, pp. 83–93, Jan. 1995.

[27] Z. Shen, L. Sun, Z. Liu, M. Li, Y. Cao, L. Han, J. Wang, X. Wu, and S. Sang, "Rete ridges: Morphogenesis, function, regulation, and reconstruction," *Acta Biomaterialia*, vol. 155, pp. 19–34, Jan. 2023.

[28] Z. Bata-Csorgo, C. Hammerberg, J. J. Voorhees, and K. D. Cooper, "Flow cytometric identification of proliferative subpopulations within normal human epidermis and the localization of the primary hyperproliferative population in psoriasis.," *Journal of Experimental Medicine*, vol. 178, pp. 1271–1281, Oct. 1993.

[29] C. S. Potten, "The epidermal proliferative unit: The possible role of the central basal cell," *Cell Proliferation*, vol. 7, pp. 77–88, Jan. 1974.

[30] G. D. Weinstein and P. Frost, "Abnormal Cell Proliferation in Psoriasis**From the Department of Dermatology, University of Miami School of Medicine, Miami, Florida.," *Journal of Investigative Dermatology*, vol. 50, pp. 254–259, Mar. 1968.

[31] G. D. Weinstein, J. L. McCullough, and P. Ross, "Cell Proliferation in Normal Epidermis," *Journal of Investigative Dermatology*, vol. 82, pp. 623–628, June 1984.

[32] D. D. Bikle, Z. Xie, and C.-L. Tu, "Calcium regulation of keratinocyte differentiation," *Expert Rev Endocrinol Metab*, vol. 7, pp. 461–472, July 2012.

[33] S. E. Lee and S. H. Lee, "Skin Barrier and Calcium," *Ann Dermatol*, vol. 30, pp. 265–275, June 2018.

[34] K. Leuner, M. Kraus, U. Woelfle, H. Beschmann, C. Harteneck, W.-H. Boehncke, C. M. Schempp, and W. E. Müller, "Reduced TRPC Channel Expression in Psoriatic Keratinocytes Is Associated with Impaired Differentiation and Enhanced Proliferation," *PLOS ONE*, vol. 6, p. e14716, Feb. 2011.

[35] H. Wang, X. Cheng, J. Tian, Y. Xiao, T. Tian, F. Xu, X. Hong, and M. X. Zhu, "TRPC channels: Structure, function, regulation and recent advances in small molecular probes," *Pharmacology & Therapeutics*, vol. 209, p. 107497, May 2020.

[36] G. Vazquez, B. J. Wedel, O. Aziz, M. Trebak, and J. W. Putney, "The mammalian TRPC cation channels," *Biochimica et Biophysica Acta (BBA) - Molecular Cell Research*, vol. 1742, pp. 21–36, Dec. 2004.

[37] J. Ovadia and Q. Nie, "Stem Cell Niche Structure as an Inherent Cause of Undulating Epithelial Morphologies," *Biophysical Journal*, vol. 104, pp. 237–246, Jan. 2013.

[38] H. Izuka, H. Honda, and A. Ishida-Yamamoto, "Epidermal Remodeling in Psoriasis (II): A Quantitative Analysis of the Epidermal Architecture," *Journal of Investigative Dermatology*, vol. 109, pp. 806–810, Dec. 1997.

[39] G. D. Weinstein and E. J. van Scott, "Autoradiographic Analysis of Turnover Times of Normal and Psoriatic Epidermis**From the Dermatology Branch, National Cancer Institute, National Institutes of Health, Bethesda, Maryland. Public Health Service, U.S. Department of Health, Education and Welfare.," *Journal of Investigative Dermatology*, vol. 45, pp. 257–262, Oct. 1965.

[40] H. Iizuka, H. Honda, and A. Ishida-Yamamoto, "Epidermal remodelling in psoriasis (III): A hexagonally-arranged cylindrical papilla model reveals the nature of psoriatic architecture," *Journal of Dermatological Science*, vol. 21, pp. 105–112, Oct. 1999.

[41] G. D. Weinstein, J. L. McCullough, and P. A. Ross, "Cell Kinetic Basis for Pathophysiology of Psoriasis," *Journal of Investigative Dermatology*, vol. 85, pp. 579–583, Dec. 1985.

[42] F. K. Doger, E. Dikicioglu, F. Ergin, E. Unal, N. Sendur, and M. Uslu, "Nature of cell kinetics in psoriatic epidermis," *Journal of Cutaneous Pathology*, vol. 34, no. 3, pp. 257–263, 2007.

[43] S.-L. Karvonen, T. Korkiamäki, H. Ylä-Outinen, M. Nissinen, H. Teerikangas, K. Pummi, J. Karvonen, and J. Peltonen, "Psoriasis and Altered Calcium Metabolism: Downregulated Capacitative Calcium Influx and Defective Calcium-Mediated Cell Signaling in Cultured Psoriatic Keratinocytes1," *J Invest Dermatol*, vol. 114, pp. 693–700, Apr. 2000.

[44] W. Lapolla, B. A. Yentzer, J. Bagel, C. R. Halvorson, and S. R. Feldman, "A review of phototherapy protocols for psoriasis treatment," *Journal of the American Academy of Dermatology*, vol. 64, pp. 936–949, May 2011.

[45] A. Tanew, S. Radakovic-Fijan, M. Schemper, and H. Hönigsmann, "Narrowband UV-B Phototherapy vs Photochemotherapy in the Treatment of Chronic Plaque-Type Psoriasis: A Paired Comparison Study," *Archives of Dermatology*, vol. 135, pp. 519–524, May 1999.

[46] H. B. Oza, R. Pandey, D. Roper, Y. Al-Nuaimi, S. K. Spurgeon, and M. Goodfellow, "Modelling and finite-time stability analysis of psoriasis pathogenesis," *International Journal of Control*, vol. 90, pp. 1664–1677, Aug. 2017.

[47] P. K. Roy, J. Bhadra, and B. Chattopadhyay, "Mathematical Modeling on Immunopathogenesis in Chronic Plaque of Psoriasis: A Theoretical Study," *Dendritic Cells*, p. 6, 2010.

[48] Z. C. Félix Garza, J. Liebmann, M. Born, P. A. J. Hilbers, and N. A. W. van Riel, "A Dynamic Model for Prediction of Psoriasis Management by Blue Light Irradiation," *Front Physiol*, vol. 8, Jan. 2017.

[49] T. Sun, P. McMinn, S. Coakley, M. Holcombe, R. Smallwood, and S. MacNeil, "An integrated systems biology approach to understanding the rules of keratinocyte colony formation," *J R Soc Interface*, vol. 4, pp. 1077–1092, Dec. 2007.

[50] H. Zhang, W. Hou, L. Henrot, S. Schnebert, M. Dumas, C. Heusèle, and J. Yang, "Modelling epidermis homoeostasis and psoriasis pathogenesis," *J R Soc Interface*, vol. 12, Feb. 2015.

[51] S. Adra, T. Sun, S. MacNeil, M. Holcombe, and R. Smallwood, "Development of a Three Dimensional Multiscale Computational Model of the Human Epidermis," *PLOS ONE*, vol. 5, p. e8511, Jan. 2010.

[52] E. Rognoni, A. O. Pisco, T. Hiratsuka, K. H. Sipilä, J. M. Belmonte, S. A. Mobasseri, C. Philippeos, R. Dilão, and F. M. Watt, "Fibroblast state switching orchestrates dermal maturation and wound healing," *Molecular Systems Biology*, vol. 14, p. e8174, Aug. 2018.

[53] G. Schaller and M. Meyer-Hermann, "A modelling approach towards epidermal homoeostasis control," *Journal of Theoretical Biology*, vol. 247, pp. 554–573, Aug. 2007.

[54] S. Hu and F. A. Cucinotta, "Epidermal homeostasis and radiation responses in a multiscale tissue modeling framework," *Integr. Biol.*, vol. 6, pp. 76–89, Dec. 2013.

[55] N. Grabe, T. Pommerencke, D. Müller, S. Huber, K. Neuber, and H. Dickhaus, "Modelling epidermal homeostasis as an approach for clinical bioinformatics," *Stud Health Technol Inform*, vol. 124, pp. 105–110, 2006.

[56] H. Iizuka, "Epidermal architecture that depends on turnover time," *Journal of Dermatological Science*, vol. 10, pp. 220–223, Nov. 1995.

[57] D. T. Gillespie, "Stochastic Simulation of Chemical Kinetics," *Annu. Rev. Phys. Chem.*, vol. 58, pp. 35–55, May 2007.

[58] L. Sordo Vieira and R. C. Laubenbacher, "Computational models in systems biology: Standards, dissemination, and best practices," *Current Opinion in Biotechnology*, vol. 75, p. 102702, June 2022.

[59] L. Michaelis and M. L. Menten, "Die Kinetik der Invertinwirkung," *Biochem Z*, vol. 49, pp. 333–369, 1913.

[60] B. Li, D. Taniguchi, J. P. Gedara, V. Gogulancea, R. Gonzalez-Cabaleiro, J. Chen, A. S. McGough, I. D. Ofiteru, T. P. Curtis, and P. Zuliani, "NUFEB: A massively parallel simulator for individual-based modelling of microbial communities," *PLOS Computational Biology*, vol. 15, p. e1007125, Dec. 2019.

[61] "BioDynaMo — The Biology Dynamics Modeller." https://biodynamo.web.cern.ch/.

[62] M. H. Swat, G. L. Thomas, J. M. Belmonte, A. Shirinifard, D. Hmeljak, and J. A. Glazier, "Chapter 13 - Multi-Scale Modeling of Tissues Using CompuCell3D," in *Methods in Cell Biology* (A. R. Asthagiri and A. P. Arkin, eds.), vol. 110 of *Computational Methods in Cell Biology*, pp. 325–366, Academic Press, Jan. 2012.

[63] "LAMMPS Molecular Dynamics Simulator." https://lammps.sandia.gov/.

[64] "Elasticity and Hooke's law," in *The Rock Physics Handbook: Tools for Seismic Analysis of Porous Media* (G. Mavko, J. Dvorkin, and T. Mukerji, eds.), pp. 21–80, Cambridge: Cambridge University Press, 2 ed., 2009.

[65] Y. Zhang, S. X. Zhang, J. Qiao, R. Zhao, S. Song, Y. Li, M. J. Chang, G. Y. Liu, P. F. He, and X. Li, "Pos0199 Time-Series Analysis in Moderate to Severe Plaque Psoriasis Under Different Biologics Treatments," *Annals of the Rheumatic Diseases*, vol. 80, pp. 315–316, June 2021.

[66] L. S. van der Schoot and J. M. P. A. van den Reek, "Data-driven prediction of biologic treatment responses in psoriasis: Steps towards precision medicine," *British Journal of Dermatology*, vol. 185, no. 4, pp. 698–699, 2021.

[67] A. X. Du, Z. Ali, K. K. Ajgeiy, M. G. Dalager, T. N. Dam, A. Egebjerg, C. V. S. Nissen, L. Skov, S. F. Thomsen, S. Emam, and R. Gniadecki, "Machine Learning Model for Predicting Outcomes of Biologic Therapy in Psoriasis," Dec. 2021.

[68] S. Emam, A. Du, P. Surmanowicz, S. Thomsen, R. Greiner, and R. Gniadecki, "Predicting the long-term outcomes of biologics in patients with psoriasis using machine learning," *British Journal of Dermatology*, vol. 182, no. 5, pp. 1305–1307, 2020.

[69] V. K. Shrivastava, N. D. Londhe, R. S. Sonawane, and J. S. Suri, "A novel and robust Bayesian approach for segmentation of psoriasis lesions and its risk stratification," *Computer Methods and Programs in Biomedicine*, vol. 150, pp. 9–22, Oct. 2017.

[70] Y. Liu, Y. Wang, and J. Zhang, "New Machine Learning Algorithm: Random Forest," in *Information Computing and Applications* (B. Liu, M. Ma, and J. Chang, eds.), Lecture Notes in Computer Science, (Berlin, Heidelberg), pp. 246–252, Springer, 2012.

[71] "What is Random Forest? — IBM." https://www.ibm.com/topics/random-forest.

[72] S.-C. Wang, "Artificial Neural Network," in *Interdisciplinary Computing in Java Programming* (S.-C. Wang, ed.), The Springer International Series in Engineering and Computer Science, pp. 81–100, Boston, MA: Springer US, 2003.

[73] R. Shouval, O. Bondi, H. Mishan, A. Shimoni, R. Unger, and A. Nagler, "Application of machine learning algorithms for clinical predictive modeling: A data-mining approach in SCT," *Bone Marrow Transplant*, vol. 49, pp. 332–337, Mar. 2014.

[74] W.-T. Wu, Y.-J. Li, A.-Z. Feng, L. Li, T. Huang, A.-D. Xu, and J. Lyu, "Data mining in clinical big data: The frequently used databases, steps, and methodological models," *Military Medical Research*, vol. 8, p. 44, Aug. 2021.

[75] O. Kramer, "K-Nearest Neighbors," in *Dimensionality Reduction with Unsupervised Nearest Neighbors* (O. Kramer, ed.), Intelligent Systems Reference Library, pp. 13–23, Berlin, Heidelberg: Springer, 2013.

[76] "What is the k-nearest neighbors algorithm? — IBM." https://www.ibm.com/topics/knn.

[77] C. Proust-Lima, V. Philipps, and B. Liquet, "Estimation of Extended Mixed Models Using Latent Classes and Latent Processes: The R Package lcmm," *Journal of Statistical Software*, vol. 78, pp. 1–56, June 2017.

[78] "NetLogo Home Page." https://ccl.northwestern.edu/netlogo/.

[79] E. Fuchs, "Skin stem cells: Rising to the surface," *The Journal of Cell Biology*, vol. 180, pp. 273–284, Jan. 2008.

[80] J. Bauer, F. A. Bahmer, J. Wörl, W. Neuhuber, G. Schuler, and M. Fartasch, "A Strikingly Constant Ratio Exists Between Langerhans Cells and Other Epidermal Cells in Human Skin. A Stereologic Study Using the Optical Disector Method and the Confocal Laser Scanning Microscope11Presented in part at the International Investigative Dermatology 1998, Cologne, Germany 1998.," *Journal of Investigative Dermatology*, vol. 116, pp. 313–318, Feb. 2001.

[81] J. Körver, M. Van Duijnhoven, M. Pasch, P. Van Erp, and P. Van De Kerkhof, "Assessment of epidermal subpopulations and proliferation in healthy skin, symptomless and

lesional skin of spreading psoriasis," *British Journal of Dermatology*, vol. 155, pp. 688–694, Oct. 2006.

[82] E. J. van Scott and T. M. Ekel, "Kinetics of Hyperplasia in Psoriasis," *Archives of Dermatology*, vol. 88, pp. 373–381, Oct. 1963.

[83] J. Krutmann and A. Morita, "Mechanisms of Ultraviolet (UV) B and UVA Phototherapy," *Journal of Investigative Dermatology Symposium Proceedings*, vol. 4, pp. 70–72, Sept. 1999.

[84] B. M. Aufiero, H. Talwar, C. Young, M. Krishnan, J. S. Hatfield, H. K. Lee, H. K. Wong, I. Hamzavi, and G. J. Murakawa, "Narrow-band UVB induces apoptosis in human keratinocytes," *Journal of Photochemistry and Photobiology B: Biology*, vol. 82, pp. 132–139, Feb. 2006.

[85] M. Athar, A. L. Kim, N. Ahmad, H. Mukhtar, J. Gautier, and D. R. Bickers, "Mechanism of Ultraviolet B-Induced Cell Cycle Arrest in G2/M Phase in Immortalized Skin Keratinocytes with Defective p53," *Biochemical and Biophysical Research Communications*, vol. 277, pp. 107–111, Oct. 2000.

[86] A. L. Kim, M. Athar, D. R. Bickers, and J. Gautier, "Ultraviolet-B-Induced G1 Arrest is Mediated by Downregulation of Cyclin-Dependent Kinase 4 in Transformed Keratinocytes Lacking Functional p53," *Journal of Investigative Dermatology*, vol. 118, pp. 818–824, May 2002.

[87] P. G. Jayathilake, P. Gupta, B. Li, C. Madsen, O. Oyebamiji, R. González-Cabaleiro, S. Rushton, B. Bridgens, D. Swailes, B. Allen, A. S. McGough, P. Zuliani, I. D. Ofiteru, D. Wilkinson, J. Chen, and T. Curtis, "A mechanistic Individual-based Model of microbial communities," *PLOS ONE*, vol. 12, p. e0181965, Aug. 2017.

[88] N. Watson, N. Wilson, F. Shmarov, P. Zuliani, N. Reynolds, and S. Weatherhead, "The use of psoriasis biomarkers, including trajectory of clinical response, to predict clearance and remission duration to UVB phototherapy," *Journal of the European Academy of Dermatology and Venereology*, vol. 35, no. 11, pp. 2250–2258, 2021.

[89] G. E. Briggs, "A Further Note on the Kinetics of Enzyme Action," *Biochemical Journal*, vol. 19, pp. 1037–1038, Jan. 1925.

[90] G. E. Briggs and J. B. S. Haldane, "A Note on the Kinetics of Enzyme Action," *Biochemical Journal*, vol. 19, pp. 338–339, Jan. 1925.

[91] F. M. Watt, "Stem cell fate and patterning in mammalian epidermis," *Current Opinion in Genetics & Development*, vol. 11, pp. 410–417, Aug. 2001.

[92] Y. A. Miroshnikova, H. Q. Le, D. Schneider, T. Thalheim, M. Rübsam, N. Bremicker, J. Polleux, N. Kamprad, M. Tarantola, I. Wang, M. Balland, C. M. Niessen, J. Galle, and S. A. Wickström, "Adhesion forces and cortical tension couple cell proliferation and differentiation to drive epidermal stratification," *Nature Cell Biology*, vol. 20, pp. 69–80, Jan. 2018.

[93] M. T. Niessen, J. Scott, J. G. Zielinski, S. Vorhagen, P. A. Sotiropoulou, C. Blanpain, M. Leitges, and C. M. Niessen, "aPKCλ controls epidermal homeostasis and stem cell fate through regulation of division orientation," *J Cell Biol*, vol. 202, pp. 887–900, Sept. 2013.

[94] N. V. Brilliantov, F. Spahn, J.-M. Hertzsch, and T. Pöschel, "Model for collisions in granular gases," *Phys. Rev. E*, vol. 53, pp. 5382–5392, May 1996.

[95] R. Sun, H. Xiao, and H. Sun, "Investigating the settling dynamics of cohesive silt particles with particle-resolving simulations," *Advances in Water Resources*, vol. 111, pp. 406–422, Jan. 2018.

[96] H. Du, Y. Wang, D. Haensel, B. Lee, X. Dai, and Q. Nie, "Multiscale modeling of layer formation in epidermis," *PLOS Computational Biology*, vol. 14, p. e1006006, Feb. 2018.

[97] X. Li, A. K. Upadhyay, A. J. Bullock, T. Dicolandrea, J. Xu, R. L. Binder, M. K. Robinson, D. R. Finlay, K. J. Mills, C. C. Bascom, C. K. Kelling, R. J. Isfort, J. W. Haycock, S. MacNeil, and R. H. Smallwood, "Skin Stem Cell Hypotheses and Long Term Clone Survival – Explored Using Agent-based Modelling," *Sci Rep*, vol. 3, May 2013.

[98] G. Mascré, S. Dekoninck, B. Drogat, K. K. Youssef, S. Brohée, P. A. Sotiropoulou, B. D. Simons, and C. Blanpain, "Distinct contribution of stem and progenitor cells to epidermal maintenance," *Nature*, vol. 489, pp. 257–262, Sept. 2012.

[99] R. M. Lavker and T.-T. Sun, "Epidermal Stem Cells," *Journal of Investigative Dermatology*, vol. 81, pp. S121–S127, July 1983.

[100] R. M. Lavker and T.-T. Sun, "Epidermal stem cells: Properties, markers, and location," *Proceedings of the National Academy of Sciences*, vol. 97, pp. 13473–13475, Dec. 2000.

[101] B. Alberts, A. Johnson, J. Lewis, M. Raff, K. Roberts, and P. Walter, "Epidermis and Its Renewal by Stem Cells," in *Molecular Biology of the Cell. 4th Edition*, Garland Science, 2002.

[102] M. P. Adams, D. G. Mallet, and G. J. Pettet, "Towards a Quantitative Theory of Epidermal Calcium Profile Formation in Unwounded Skin," *PLoS One*, vol. 10, Jan. 2015.

[103] C.-A. Peng and B. Ø. Palsson, "Cell growth and differentiation on feeder layers is predicted to be influenced by bioreactor geometry," *Biotechnology and Bioengineering*, vol. 50, no. 5, pp. 479–492, 1996.

[104] A.-K. Ekman, C. Bivik Eding, I. Rundquist, and C. Enerbäck, "IL-17 and IL-22 Promote Keratinocyte Stemness in the Germinative Compartment in Psoriasis," *Journal of Investigative Dermatology*, vol. 139, pp. 1564–1573.e8, July 2019.

[105] J. E. Gudjonsson, A. Johnston, H. Sigmundsdottir, and H. Valdimarsson, "Immunopathogenic mechanisms in psoriasis," *Clinical & Experimental Immunology*, vol. 135, no. 1, pp. 1–8, 2004.

[106] R. Joshi, "Immunopathogenesis of psoriasis," *Indian J Dermatol Venereol Leprol*, vol. 70, no. 1, pp. 10–12, 2004 Jan-Feb.

[107] T. Simonart, M. Heenen, and O. Lejeune, "Epidermal kinetic alterations required to generate the psoriatic phenotype: A reappraisal," *Cell Prolif*, vol. 43, pp. 321–325, Apr. 2010.

[108] M. Aragona, S. Dekoninck, S. Rulands, S. Lenglez, G. Mascré, B. D. Simons, and C. Blanpain, "Defining stem cell dynamics and migration during wound healing in mouse skin epidermis," *Nat Commun*, vol. 8, p. 14684, Mar. 2017.

[109] H. Valdimarsson, B. S. Baker, I. Jónsdóttir, A. Powles, and L. Fry, "Psoriasis: A T-cell-mediated autoimmune disease induced by streptococcal superantigens?," *Immunology Today*, vol. 16, pp. 145–149, Mar. 1995.

[110] J. E. Gudjonsson, A. M. Thorarinsson, B. Sigurgeirsson, K. G. Kristinsson, and H. Valdimarsson, "Streptococcal throat infections and exacerbation of chronic plaque psoriasis: A prospective study," *British Journal of Dermatology*, vol. 149, no. 3, pp. 530–534, 2003.

[111] X. Xiong, T. Wu, and S. He, "Physical forces make rete ridges in oral mucosa," *Medical Hypotheses*, vol. 81, pp. 883–886, Nov. 2013.

[112] S. Ipponjima, T. Hibi, and T. Nemoto, "Three-Dimensional Analysis of Cell Division Orientation in Epidermal Basal Layer Using Intravital Two-Photon Microscopy," *PLOS ONE*, vol. 11, p. e0163199, Sept. 2016.

[113] E. a. W. Wolberink, P. E. J. van Erp, M. M. Teussink, P. C. M. van de Kerkhof, and M. J. P. Gerritsen, "Cellular features of psoriatic skin: Imaging and quantification using in vivo reflectance confocal microscopy," *Cytometry Part B: Clinical Cytometry*, vol. 80B, no. 3, pp. 141–149, 2011.

[114] H.-Y. Jia, Y. Shi, L.-F. Luo, G. Jiang, Q. Zhou, S.-Z. Xu, and T.-C. Lei, "Asymmetric stem-cell division ensures sustained keratinocyte hyperproliferation in psoriatic skin lesions," *International Journal of Molecular Medicine*, vol. 37, pp. 359–368, Feb. 2016.

[115] J. A. McGrath, R. a. J. Eady, and F. M. Pope, "Anatomy and Organization of Human Skin," in *Rook's Textbook of Dermatology*, ch. 3, pp. 45–128, John Wiley & Sons, Ltd, 2004.

[116] P. A. J. Kolarsick, M. A. Kolarsick, and C. Goodwin, "Anatomy and Physiology of the Skin," *Journal of the Dermatology Nurses' Association*, vol. 3, p. 203, July 2011.

[117] J. Rajiv, "Immunopathogenesis of psoriasis," *Indian Journal of Dermatology, Venereology, and Leprology*, vol. 70, p. 10, Jan. 2004.

[118] Y. Yamaguchi and V. J. Hearing, "Melanocytes and Their Diseases," *Cold Spring Harb Perspect Med*, vol. 4, May 2014.

[119] T. Hirobe, "Keratinocytes regulate the function of melanocytes," *Dermatologica Sinica*, vol. 32, pp. 200–204, Dec. 2014.

[120] A. Arakawa, K. Siewert, J. Stöhr, P. Besgen, S.-M. Kim, G. Rühl, J. Nickel, S. Vollmer, P. Thomas, S. Krebs, S. Pinkert, M. Spannagl, K. Held, C. Kammerbauer, R. Besch, K. Dornmair, and J. C. Prinz, "Melanocyte antigen triggers autoimmunity in human psoriasis," *J Exp Med*, vol. 212, pp. 2203–2212, Dec. 2015.

[121] M. B. Abdel-Naser, A. I. Liakou, R. Elewa, S. Hippe, J. Knolle, and C. C. Zouboulis, "Increased Activity and Number of Epidermal Melanocytes in Lesional Psoriatic Skin," *Dermatology*, vol. 232, no. 4, pp. 425–430, 2016.

[122] J. X. Wang, M. Fukunaga-Kalabis, and M. Herlyn, "Crosstalk in skin: Melanocytes, keratinocytes, stem cells, and melanoma," *J Cell Commun Signal*, vol. 10, pp. 191–196, Sept. 2016.

[123] J. P. Strassner, M. Rashighi, and J. E. Harris, "Melanocytes in psoriasis: Convicted culprit or bullied bystander?," *Pigment Cell & Melanoma Research*, vol. 29, no. 3, pp. 261–263, 2016.

[124] A. F. Alexis and P. Blackcloud, "Psoriasis in Skin of Color: Epidemiology, Genetics, Clinical Presentation, and Treatment Nuances," *J Clin Aesthet Dermatol*, vol. 7, pp. 16–24, Nov. 2014.

[125] Z. U. Syed and I. H. Hamzavi, "Role of phototherapy in patients with skin of color," *Semin Cutan Med Surg*, vol. 30, pp. 184–189, Dec. 2011.

[126] Y. Wong, M. J.-A. Koh, and W.-S. Chong, "Role of Narrowband Ultraviolet B Phototherapy in the Treatment of Childhood Psoriasis in Asian Children," *Pediatric Dermatology*, vol. 32, no. 5, pp. e221–e223, 2015.

[127] Y. Lytvyn, M. Sachdeva, A. Mufti, and J. Yeung, "Dermatology: How to manage psoriasis and recognize differences in pathophysiology and presentation in patients with skin of colour," *Drugs Context*, vol. 11, pp. 2021–9–3, May 2022.

Appendix A

Appendix

A.1 2D Model

A.1.1 Netlogo code with automation

The code can be found on my GitHub repository, `https://github.com/dinikap/netlogo.git`, with the original base code from [18] and my modified version of the code.

A.2 3D Model

A.2.1 Code

The code can be found on my GitHub repository, `https://github.com/dinikap/NUFEB.git`, under the branch "psoriasis-remote". The source code for the psoriasis package can be found in "src/USER-PSORIASIS". The working examples can be found in "examples/epidermis-test" and "examples/psoriasis-test" for the normal and psoriatic epidermis, respectively. In "examples/epidermis-test/epidermis-1", runs the normal epidermal formation and in "examples/psoriasis-test/psoriasis-1" runs the transitional state to psoriasis using random seed 10. For the steady state model for the same random seed, run "examples/psoriasis-test-psoriasis-10".

A.2.2 Random seeds used in 3D model

Ten different random seeds were used in validating the model. These were generated using a random generator between a numbers 0 to 99999. Tables A.1, A.2, A.3 presents the random seeds used and the cell population numbers for stem, TA and differentiated cells, respectively.

Stem cell

Case	Random Seed	Normal Epidermis	Transition	Psoriasis
1	14564	715	3,046	2,104
2	56783	679	3,061	2,296
3	34670	676	2,965	2,087
4	79936	646	2,910	2,059
5	6831	673	3,051	2,266
6	48085	726	3,041	2,137
7	80294	699	2,888	2,968
8	9288	706	2,860	1,954
9	3715	667	3,089	2,108
10	53511	680	2,821	2,053

Table A.1: Summary of the stem cell population numbers in each state based on the 10 random seeds used in both normal and psoriatic epidermis development in the 3D model. Each random seed was randomly generated using a random seed generator.

TA cell

Case	Random Seed	Normal Epidermis	Transition	Psoriasis
1	14564	3,799	11,786	11,825
2	56783	3,659	13,402	13,752
3	34670	3,546	12,494	11,828
4	79936	3,649	10,984	11,334
5	6831	3,664	11,491	12,993
6	48085	3,832	13,088	12,243
7	80294	3,780	10,739	11,033
8	9288	3,871	11,868	11,130
9	3715	3,623	12,614	11,997
10	53511	3,746	11,181	11,447

Table A.2: Summary of the TA cell population numbers in each state based on the 10 random seeds used in both normal and psoriatic epidermis development in the 3D model. Each random seed was randomly generated using a random seed generator.

Differentiated cell

Case	Random Seed	Normal Epidermis	Transition	Psoriasis
1	14564	10,289	36,714	31,191
2	56783	10,009	39,888	38,091
3	34670	9,807	37,734	32,066
4	79936	9,782	34,442	31,047
5	6831	9,895	35,458	34,085
6	48085	10,448	38,392	31,545
7	80294	10,148	33,166	29,330
8	9288	10,064	35,654	29,449
9	3715	9,964	37,951	32,047
10	53511	10,090	35,025	32,031

Table A.3: Summary of the differentiated cell population numbers in each state based on the 10 random seeds used in both normal and psoriatic epidermis development in the 3D model. Each random seed was randomly generated using a random seed generator.